THE UNIVERSITY OF NOTTINGHAM

A Polymeric Protein-loaded Microsphere Delivery System for Use in Bone Tissue Engineering

Yamina Boukari, MPharm

Submitted in June 2016

Thesis submitted to the University of Nottingham in fulfilment of the requirements for the Degree of Doctor of Philosophy

Table of Contents

Abstract 1
Dedication 3
Acknowledgements 4
Publications 6
Conferences 7
Awards 8
Chapter 1: An introduction to tissue engineering with a specific focus on bone tissue engineering 9
1.1 A brief history of tissue engineering 10
1.2 Bone tissue engineering 11
1.3 The fundamentals of bone tissue 12
1.3.1 Bone function 12
1.3.2 Bone structure 13
1.3.3 Bone formation 13
1.3.4 Bone remodelling 15
1.4 Growth factors 16
1.4.1 Growth factors for bone tissue engineering 17
1.5 Biomaterials used for bone tissue engineering applications 21
1.5.1 Bioactive inorganic materials 21
1.5.2 Natural polymers 23
1.5.3 Synthetic Polymers 27
1.6 PLGA in bone tissue engineering 32
1.6.1 PLGA microspheres 32
1.6.2 Formulation methods 34
1.7 The use of stem cells 38
1.8 Project aims and overall plan 40
Chapter 2: Formulation of porous PLGA microspheres for bone tissue engineering 42
2.1 Introduction 43
2.2 Materials and methods 46
2.2.1 Materials 46
2.2.2 Preparation of PVA solution 46

2.2.3 General method for the preparation of porous microspheres....47
2.2.4 Variations to the general protocol....48
2.2.5 Effect of porogens....48
2.2.6 Effect of primary and secondary emulsion homogenization speed on the resultant microspheres....49
2.2.7 Characterization of microspheres....49
2.3 Results and Discussion....50
2.3.1 General procedure....50
2.3.2 Methods to increase porosity in microspheres prepared using a pH-controlled external aqueous phase....54
2.3.3 Degree of hydrolysis of PVA....55
2.3.4 Porosity of microspheres prepared with partially hydrolysed PVA....57
2.3.5 Effect of homogenization speed of the secondary emulsion on the size of microspheres....61
2.4 Conclusions....64
Chapter 3: Physico-mechanical properties of sintered scaffolds formed from porous and protein-loaded poly (DL-lactic-co-glycolic acid) microspheres....66
3.1 Introduction....67
3.2 Materials & Methods....68
3.2.1 Materials....68
3.2.2 Formulation of microspheres....68
3.2.3 SEM and size analysis....69
3.2.4 Differential Scanning Calorimetry (DSC)....69
3.2.5 Encapsulation efficiency of lysozyme within microspheres....69
3.2.6 Preparation of 3D scaffolds....70
3.2.7 Characterization of 3D scaffolds....70
3.2.8 Release of lysozyme from microspheres and scaffolds....71
3.3 Results and discussion....72
3.3.1 Microstructure and size analyses of porous and non-porous PLGA microspheres 72
3.3.2 Microstructure and porosity of scaffolds....75
3.3.3 Compressive strength of scaffolds....78
3.3.4 Distribution of lysozyme on and within the scaffolds....79
3.3.5 Release of lysozyme from non-porous microspheres and scaffolds....83
3.4 Conclusions....89

Chapter 4: Control of the burst release of protein from PLGA microspheres 91
4.1 Introduction 92
4.2 Materials & Methods 95
4.2.1 Materials 95
4.2.2 Preparation of lysozyme-loaded Pluronic F127-coated microspheres 95
4.2.3 Preparation of lysozyme-loaded PLO/heparin-coated microspheres 95
4.2.4 Preparation of lysozyme-loaded PLGA/pectin and PLGA/κ-carrageenan microspheres 96
4.2.5 Preparation of protein-loaded PLGA/chitosan microspheres 96
4.2.6 Characterization of coated microspheres 96
4.2.7 Release studies 97
4.3 Results and Discussion 97
4.3.1 Pluronic F127-coated PLGA microspheres 97
4.3.2 PLO/heparin-coated PLGA microspheres 104
4.3.3 Pectin/κ-carrageenan coated- PLGA microspheres 107
4.3.4 Protein-loaded PLGA/chitosan microspheres 110
4.4 Conclusions 116
Chapter 5: Further characterisation and *in vitro* testing of PLGA/chitosan composite microspheres and scaffolds 117
5.1 Introduction 118
5.2 Materials & Methods 119
5.2.1 Materials 119
5.2.2 Preparation of non-porous and porous microspheres 120
5.2.3 Fourier transform infrared (FTIR) spectroscopy analysis of PLGA/chitosan non-porous microspheres 120
5.2.4 Preparation of 3D scaffolds 120
5.2.5 Encapsulation efficiency of the scaffolds 120
5.2.6 ToF-SIMS analysis 121
5.2.7 Release of BSA from the scaffolds 123
5.2.8 Preparation of 3D scaffolds after injection through a needle 123
5.2.9 Compressive strength of scaffolds 124
5.2.10 Cell culture and seeding onto scaffolds 124
5.2.11 Cell viability assay 125
5.2.12 Assessment of mineralization 125

5.2.13 Osteocalcin immunostaining....126
5.3 Results and Discussion....126
5.3.1 FTIR....127
5.3.2 Encapsulation Efficiency....128
5.3.3 ToF-SIMS analyses of the scaffold surfaces....129
5.3.4 Release of BSA from scaffolds....131
5.3.5 Sintering and compressive strength....132
5.3.6 Cell proliferation on scaffolds....134
5.3.7 Osteogenic differentiation....137
5.3.8 Effect of chitosan processing on the toxicity of scaffolds....141
5.4 Conclusions....146
Chapter 6: Final conclusions and future work....148
6.1 Final conclusions....149
6.2 Future work....149
References....152

List of Figures and Tables

Figure 1.1: Chemical structure and formation of poly (lactic-co-glycolic acid). 30

Figure 1.2: Schematic diagram of the double emulsion solvent evaporation method. 36

Figure 1.3: Overview of the experimental work carried out in the project. 41

Figure 2.1: SEM images of PLGA microspheres prepared using the double emulsion solvent evaporation method following the general protocol with 5 minutes (A) and 2 minutes (B) of stirring followed by sieving (aperture size of 63 µm). Insert images represent close-up images of individual microspheres. 51

Figure 2.2: SEM image of PLGA microspheres prepared with a pH-controlled aqueous phase, using PBS as a porogen. 53

Figure 2.3: SEM images of PLGA microspheres prepared with a pH controlled aqueous phase using sodium chloride solution as a porogen. 54

Figure 2.4: SEM images of PLGA microspheres prepared with 250 µL (A), 500 µL (B) and 750 µL (C) of sodium chloride solution (10 % w/v) as a porogen in a pH-controlled environment. 55

Figure 2.5: SEM images of PLGA microspheres prepared using partially hydrolyzed (87–89%) poly (vinyl alcohol). 56

Figure 2.6: SEM images of PLGA microspheres prepared with partially hydrolyzed PVA using PBS (A) and sodium chloride solution (B) as pore forming agents. 57

Figure 2.7: SEM images of PLGA microspheres prepared using the double emulsion solvent evaporation method using PBS as a pore-forming agent with varying primary emulsion homogenization speeds (A = 1000 rpm, B = 2000 rpm, C = 3000 rpm, D = 4000 rpm, E = 5000 rpm, F= 6000 rpm, G = 7000 rpm, H = 8000 rpm and I = 9000 rpm). 59

Figure 2.8: SEM images of PLGA microspheres prepared using the double emulsion solvent evaporation method, with PBS as a pore forming agent before (A) and after (B) treatment with 30% 0.5 M sodium hydroxide. 60

Figure 2.9: SEM images of PLGA microspheres prepared using the double emulsion solvent evaporation method using sodium chloride as a pore-forming agent with varying primary emulsion homogenization speeds (A = 1000 rpm, B = 2000 rpm, C = 3000 rpm, D = 4000 rpm, E = 5000 rpm, F = 6000 rpm, G = 7000 rpm, H = 8000 rpm and I = 9000 rpm).....61

Figure 2.10: SEM images of PLGA microspheres produced using the double emulsion solvent evaporation method using PBS as a porogen with varying secondary emulsion homogenization speeds (A= 3000 rpm, B = 2500 rpm, C = 2000 rpm, D = 1500 rpm, E =1000 rpm).....63

Figure 2.11: The effect of homogenization speed (rpm) of the secondary emulsion on mean microsphere diameter (μm).....63

Figure 3.1: SEM images of porous (A-C) and non-porous microsphere (D-F) microspheres formulated with LMW (A, D), IMW (B, E) and HMW (C, F) PLGA. 73

Figure 3.2: Size distribution for porous (A) and non-porous (B) microspheres as a function of PLGA molecular weight. 74

Figure 3.3: SEM images of sintered scaffolds with various lysozyme loadings (A-C = LMW, D-F = IMW and G-I = HMW; 1 mg/g, 2 mg/g and 3 mg/g, from left to right).....75

Figure 3.4: DSC thermal profiles of (A) LMW, (B) IMW and (C) HMW porous microspheres pre- and post-ethanolic NaOH treatment. 77

Figure 3.5: Percentage porosity of porous PLGA scaffolds loaded with various lysozyme concentrations. 78

Figure 3.6: Compressive strengths of scaffolds with various lysozyme loadings (ns = statistically not significant, *$p < 0.05$ and **$p < 0.01$).....79

Figure 3.7: Overlay images of ToF-SIMS scans from scaffold surfaces with various lysozyme loadings (A-D = LMW, E-H = IMW and I-L = HMW, 0, 1, 2 and 3 mg/g of lysozyme from left to right respectively). PLGA/green= $C_3H_3O_2^-$, $C_3H_5O_2^-$, $C_2H_3O_3^-$; red/lysozyme = CN^- and CNO^-. 80

Figure 3.8: Overlay images of ToF-SIMS scans from scaffold cross-sections with various lysozyme loadings (PLGA/green= $C_3H_3O_2^-$, $C_3H_5O_2^-$, $C_2H_3O_3^-$; red/lysozyme = CN^- and CNO^-). 82

Figure 3.9: In vitro lysozyme release from microspheres as a function of PLGA molecular weight (LMW, IMW and HMW).....83

Figure 3.10: In vitro lysozyme release from sintered scaffolds as a function of the PLGA molecular weight (A= 1 mg, B = 2 mg and C = 3 mg of lysozyme per gram of scaffold).....85

Figure 3.11. In vitro lysozyme release from scaffolds over 30 days. (A) LMW, (B) IMW and (C) HMW PLGA scaffolds. 88

Figure 4.1: SEM images of lysozyme-loaded PLGA microspheres coated with varying concentrations of Pluronic F127 solution. 98

Figure 4.2: DSC thermal profiles of lysozyme-loaded PLGA microspheres coated with Pluronic F127.....99

Figure 4.3: Chemical structure of Pluronic.....101

Figure 4.4: Areas of diagnostic peaks identified by TofSIMS in lysozyme-loaded PLGA microspheres. (A) Diagnostic peaks indicative of Pluronic F127 (m/z = 59), lysozyme (m/z = 26 and 42) and PLGA (m/z = 71, 73, 87 and 89). (B) Pluronic F127 diagnostic peak (m/z = 59). 102

Figure 4.5: Cumulative % release of lysozyme from Pluronic F127-coated microspheres...104

Figure 4.6: SEM images of lysozyme-loaded PLGA microspheres coated with (A) poly-L-ornithine and (B) a poly-L-ornithine/heparin complex.....105

Figure 4.7: DSC thermal profiles of lysozyme-loaded PLGA microspheres coated with poly-L-ornithine or a poly-L-ornithine/heparin polyelectrolyte complex.....106

Figure 4.8: Cumulative % lysozyme release from poly-L-ornithine- and poly-L-ornithine/heparin-coated PLGA microspheres 107

Figure 4.9: Cumulative % lysozyme release from pectin and carrageenan composite microspheres. 109

Figure 4.10: Cumulative % lysozyme release from PLGA microspheres prepared with a variety of concentrations of carrageenan and pectin.....110

Figure 4.11: Protein-loaded PLGA/chitosan microspheres. SEM images of (A) PLGA microspheres, (B) PLGA/low chitosan microspheres and (C) PLGA/high chitosan microspheres. (C) Size analysis of the microspheres.....111

Figure 4.12: DSC thermal profiles of microspheres and their constituents. 113

Figure 4.13: DSC thermal profiles indicating the Tg of microspheres. 114

Figure 4.14: Cumulative % BSA release from the PLGA/chitosan microspheres. 115

Figure 5.1: ToF-SIMS (A) negative and (B) positive spectra of BSA-loaded and blank PLGA/chitosan scaffolds. 122

Figure 5.2: ToF-SIMS (A) negative and (B) positive spectra of PLGA and PLGA/chitosan scaffolds. 123

Figure 5.3: FTIR spectroscopy of PLGA and PLGA/chitosan microspheres and their constituents. 128

Figure 5.4: ToF-SIMS analysis of PLGA and PLGA/chitosan scaffolds. Areas of diagnostic ion peaks for (A) chitosan and (B) PLGA. Data points represent the mean ± standard deviation; * $p < 0.05$, - $p > 0.05$.....130

Figure 5.5: Secondary ion intensity maps of (A) PLGA and (B) PLGA/chitosan scaffolds. 131

Figure 5.6: Release of BSA from PLGA/chitosan composite and PLGA scaffolds. (A) Cumulative percentage release and (B) cumulative release (µg of protein/mg of scaffold). 132

Figure 5.7: Morphology and compressive strength of PLGA and PLGA/chitosan scaffolds. (A) Images of PLGA and PLGA/chitosan scaffolds sintered as a suspension, post-injection through a 19 G needle and as a paste. (B) Compressive strength of scaffolds sintered post-

injection through a 19 G needle and as a paste. Data points represent the mean ± standard deviation. 133

Figure 5.8: Biocompatibility of MG-63 osteosarcoma cells with PLGA and PLGA/chitosan scaffolds. Data points represent the mean ± standard deviation. Live cells were stained with calcein-AM on day 3. 135

Figure 5.9: Biocompatibility of primary hMSCs with PLGA and PLGA/chitosan composite scaffolds. (A) Cell viability of hMSCs on scaffolds at various time points. Data points represent the mean ± standard deviation. SEM images of hMSCs on (B) PLGA and (C) PLGA/chitosan composite scaffolds on day 8. 136

Figure 5.10: Von Kossa staining of (A) PLGA and (B) PLGA/chitosan composite scaffold-cell constructs 21 days after seeding. Arrow indicates the presence of a nodule. 138

Figure 5.11: Osteocalcin presence on (A) PLGA and (B) PLGA/chitosan composite scaffolds seeded with hMSCs. Green = osteocalcin, blue = Hoechst staining of the cell DNA. 139

Figure 5.12: ImageJ processing of osteocalcin images. (1) Original image, (2) original image adjusted for brightness and contrast, (3) converted to binary format and (4) total area in pixels exported. 140

Figure 5.13: Comparison of osteocalcin staining on PLGA and PLGA/chitosan scaffolds in basal and osteogenic media. 140

Figure 5.14: SEM images of PLGA/chitosan microspheres prepared with 0.25% w/v chitosan solution in 2% v/v acetic acid adjusted with (A) 0.5 M, (B) 1 M and (C) 2 M sodium hydroxide. 142

Figure 5.15: Size distribution of PLGA/chitosan microspheres prepared with 0.25% w/v chitosan solution adjusted with different molarities of sodium hydroxide solution. 143

Figure 5.16: Cell proliferation on scaffolds prepared with 2 M and 1 M-adjusted PLGA/chitosan microspheres in combination with porous PLGA microspheres. 144

Figure 5.17: SEM images of primary hMSCs on porous PLGA/chitosan composite scaffolds after 8 days in culture prepared with 0.25% w/v chitosan solution in 2% acetic acid adjusted with (A) 1 M and (B) 2 M sodium hydroxide solution. 145

Figure 5.18: Osteocalcin staining on PLGA/chitosan scaffolds prepared with (A) 1 M-adjusted and (B) 2 M-adjusted chitosan solution. 146

Table 3.1: PLGA scaffold formulations 70

Table 3.2. Glass transition temperatures (Tg) of porous PLGA microspheres pre- and post-ethanolic-NaOH treatment. 76

Table 3.3: Subsequent lysozyme release after the initial burst release at day 1. 89

Table 4.1: Atomic concentrations of components of the C-1s peak derived from XPS spectra data 100

Table 4.2: Effect of the Pluronic F127 coating on the lysozyme content of PLGA microspheres. 103

Table 4.3: Effect of poly-L-ornithine and poly-L-ornithine/heparin polyelectrolyte complex on the lysozyme content of the PLGA microspheres 107

Abstract

The bone graft procedure is the gold standard therapy for large bone defects and usually involves implanting autologous bone into the defect site. The need to find more patient-friendly alternatives to the bone graft procedure is a driving force behind recent advances in bone tissue engineering. Different synthetic and natural biomaterials are being investigated for their use in the repair of large bone defects. However, there is still a need for scaffold materials that are able to sinter *in situ* with the capability of delivering growth factors that promote the bone repair process with minimal invasion.

In this study, our main aim was to develop a porous, protein-loaded microsphere delivery system with the capability of sintering *in situ* and with injectable potential. Poly (lactic-co-glycolic acid) (PLGA) was used for this formulation due to its biodegradability, biocompatibility, controllable mechanical properties and good processing capabilities. An optimised procedure for formulating porous and non-porous (protein-loaded) microspheres was established and the microspheres were extensively characterised. There was an inverse relationship between the molecular weight of the PLGA and both the protein release and compressive strength. An intermediate molecular weight (53 kDa) variety of PLGA was chosen for further work based on balancing the need for retaining sufficient compressive strength and a slower protein release profile.

The burst release of protein was addressed by investigating various coatings. The combination of chitosan and PLGA to form composite PLGA/chitosan microspheres resulted in the desired reduction in the burst release. The protein-loaded and porous microspheres were combined as a paste and found to sinter at body temperature (37°C) into scaffolds. Whilst previous investigations have focused primarily on a single type of PLGA microsphere

(with or without an additional biomaterial), in this study we combined both porous and protein-loaded microspheres into a single delivery system. Furthermore, successful sintering was confirmed when a suspension of the microspheres was injected through a 19 G needle.

The biocompatibility and osteogenic potential of the scaffolds were investigated. The composite PLGA/chitosan scaffolds supported the growth of MG-63 osteosarcoma cells and a primary human stem cell line. Furthermore, the scaffolds also supported the osteogenesis of the stem cells, as demonstrated by the presence of the late protein marker of osteogenesis, osteocalcin, and positive von Kossa staining, which is indicative of mineralization.

The composite PLGA/chitosan and porous microspheres combine both porosity and the ability to load and sustain the release of protein into one system. Moreover, their ability to sinter at body temperature when injected or applied as a paste demonstrates the dual functionality of the system. This represents a novel approach to delivering protein for tissue regeneration as presently, there has been no report of the combination of PLGA/chitosan microspheres with porous PLGA microspheres as a system that is able to sinter, both post-injection and when packed as a paste, at 37°C. Therefore, the formulation presented in this thesis shows potential for further *in vitro* and *in vivo* testing to determine its suitability for bone tissue engineering applications.

Dedication

"Recite and your Lord is most Generous- Who taught by the pen- taught man that which he knew not"

Surah Al-'Alaq (96:3-5)

In the name of Allah, the most Beneficent, the most Merciful, I dedicate this PhD thesis to

Maristella Boukari,

Abdelkader Boukari,

Mohammad Dasseh,

Khaled Boukari

and Hassiba Boukari.

Acknowledgements

I would like to first and foremost thank and praise Allah for allowing me to carry out this research, which without His assistance and guidance, would have been impossible.

My huge thanks and appreciation go to my supervisor, Professor Nashiru Billa, who was always patient and supportive throughout the whole process. I thank him for always being available to answer my questions, even when he was very busy. I would also like to thank my co-supervisors, Professor Andrew Morris, Professor Stephen Doughty and Professor Kevin Shakesheff, for their help and support. I would like to sincerely thank Dr Cheryl Rahman for her encouragement, motivation, invaluable help and friendship. My appreciation goes to Dr Manish Gupta, Dr Adeyinka Aina, Dr Helen Cox and Dr Omar Qutachi for all their help and technical expertise throughout this project. I would also like to acknowledge the EU FP7 Biodesign project for funding this work.

I am especially thankful to my amazing family for supporting me throughout this journey. To my mum (Maristella) and my dad (Abdelkader) – I thank you both for your unwavering support throughout my life, endless encouragement and love; I am forever grateful to you both. Thank you to my brother (Khaled) and sister (Hassiba) for being the best siblings I could hope for. My deep appreciation also goes to my mother-in-law (Huda) and late father-in-law (Yousef – May Allah have mercy on his soul) for their acceptance and support. Finally, to the best life partner I could ask for – my husband Mohammad Dasseh – thank you for your patience, love, guidance and encouragement, all of which were invaluable throughout this PhD journey.

My huge appreciation goes to my lab-mates for their friendship and assistance, especially Enas Alkhader, Hilda Amekyeh, Shi Ting Lee, Abdulrahman Baki, Noura Alom,

and Mahetab Amer. To my lab-mate, desk-mate and close friend, Yivonn Khoo, I would like to express my immense gratitude for the cell culture training and for always being around for a chat.

Finally, I ask Allah to guide us all to the Straight Path and allow the truth to light up our lives.

Publications

Boukari Y, Qutachi O, Scurr DJ, Morris AP, Doughty SW, Billa, N. **Dual-function porous PLGA/chitosan composite scaffolds for potential use in bone tissue engineering** (2016). Submitted to Journal of Pharmaceutical Sciences.

Aina A, Gupta M, **Boukari Y**, Morris A, Billa N, Doughty S (2016). **Monitoring model drug microencapsulation in PLGA scaffolds using X-ray powder diffraction**. Saudi Pharmaceutical Journal. Vol 24, issue 2. 227–231.

Boukari Y, Scurr DJ, Qutachi O, Morris AP, Doughty SW, Rahman CV and Billa N (2015). **Physico mechanical properties of sintered scaffolds formed from porous and protein-loaded poly ($_{DL}$-lactic-co-glycolic acid) microspheres for potential use in bone tissue engineering**. Journal of Biomaterials Science, Polymer Edition. Vol 26, issue 12. 796–781.

Aina A, Morris A, Gupta M, Billa N, Madhvani N, Sharma R, Doughty S, Shah V and **Boukari Y** (2014). **Dissolution behaviour of poly (vinyl alcohol) in water and its effect on the physical morphology of PLGA scaffolds**. UK Journal of Pharmaceutical and Biosciences. Vol 2(1), 1–6.

Conferences

Boukari Y, Billa N, Morris AP, Doughty SW (2015). **Poly (DL-Lactic-Co-Glycolic Acid)/chitosan composite microspheres for potential use in bone regeneration** *In:* 6th APS International PharmSci 2015, The University of Nottingham, UK.

Boukari Y, Billa N, Doughty S, Morris A, Shakesheff K (2015). **Poly (lactic-co-glycolic acid) microparticles for use in tissue engineering** *In:* International Conference on Biomedical Engineering 2015, Kuala Lumpur.

Boukari Y, Billa N, Morris A, Doughty S, Qutachi O, Scurr D, Shakesheff K, Rahman CV (2014). **The effect of molecular weight on poly (lactic-co-glycolic acid) microparticles and scaffolds in tissue engineering** *In:* International Post Graduate Research Award Seminar 2014, University of Malaya.

Gupta M, Aina A, **Boukari Y**, Doughty SW, Morris AP and Billa N (2013). **Strategic Approaches To The Formulation of Porous And Non-porous Microparticulate Scaffolds** *In:* TERMIS-AP 2013 Annual Conference.

Aina A, Morris A, Billa N, Gupta M, **Boukari Y** and Doughty S (2013). **Synthesis and characterization of porous poly (DL-lactide-co-glycolide) scaffolds** *In:* Biodesign Consortium Meeting.

Awards

Judges Choice and Overall Winner of the Postgraduate Research Showcase 2015. **Repair bones with one prick of a needle.**

Second Prize for Best Oral Presentation at the International Conference on Pharmaceutical Sciences (Dubai, 2015). **The effect of polymer molecular weight on poly (lactic-co-glycolic acid) microparticles and scaffolds for use in tissue engineering.**

Best Oral Presentation at the International Post Graduate Research Award Seminar (University of Malaya, 2014). **The effect of polymer molecular weight on poly (lactic-co-glycolic acid) microparticles and scaffolds for use in tissue engineering.**

Chapter 1: An introduction to tissue engineering with a specific focus on bone tissue engineering

1.1 A brief history of tissue engineering

Although the field of tissue engineering began to flourish in the late 1980s, there were concerted efforts prior to this that led up to its establishment. In the early 1960s, researchers had begun investigating both artificial skin [1] and synthetic fibres [2] for the potential treatment of burn victims. By the late 1960s and early 1970s, scientists were coating implant devices with a heparin complex in order to induce thromboresistance [3], and there were studies investigating the biocompatibility and toxicity of organic polymers for use in the body [4]. The investigation into the use of collagen as the basis for artificial skin for the treatment of oral mucosal injury was started in the late 1970s [5]. A major breakthrough in 1981 was the successful use of an artificial skin construct composed of a porous collagen-chrondroitin dermal layer and a silastic epidermal layer in patients with extensive burns injuries [6].

The science of tissue engineering began to take shape as a distinct research field in the late 1980s. One of the key events that led to this is thought to be the collaboration between Dr Joseph Vacanti (Massachusetts General Hospital) and Dr Robert Langer (MIT). This collaboration led to the development of cells seeded onto synthetic biocompatible/biodegradable polymers formulated into scaffolds, as reported in 1988 [7]. The field was defined as "the application of the principles and methods of engineering and life sciences toward the fundamental understanding of structure-function relationships in normal and pathologic mammalian tissue, and the development of biological substitutes to restore, maintain or improve function"[8].

The regeneration of new tissue was split into three broad categories by Langer and Vacanti, (i) the replacement of the cells or cell substitutes, which are required for the specific function that has been lost, (i) the use of tissue inducing agents such as growth factors in order to promote the new tissue formation and (i) the placement of cells on a scaffold structure made from either natural or synthetic materials [9]. The cells would be the basis of

the new tissue and as they grow, they would deposit their own extracellular matrix (ECM) [10]. In effect, the scaffold acts as an exogenous form of the ECM, which provides a structural support for the cells, binds them into the surrounding tissue, as well as providing them with signals that aid in their development and morphogenesis [11]. It is, therefore, important that the degradation rate of the scaffold closely ties in with the rate at which the ECM is deposited, and the rate at which new tissue is formed [12].

One approach that has been explored in the field of tissue engineering involves combining exogenous solid scaffolds with cells [13]. These scaffolds can then be implanted into the body at the required site [13]. However, damage to the host tissue can be a possible complication of this approach, as the implant does not mould to the architecture of the host tissue and must be surgically implanted [13]. A more desirable approach involves the use of systems that can be injected into the patient, hence, preventing the need for invasive surgical procedures. In addition to this, the system should be non-toxic to the body, so as not to cause or create any additional reactions [14].

1.2 Bone tissue engineering

The treatment of bone damage following a fracture or orthopaedic damage, which may be associated with traumatic, surgical or degenerative events, is a key application of the tissue engineering approach [15]. The current ‘gold standard’ therapy is the bone graft procedure, which involves taking autologous bone, usually harvested from the iliac crest of the patient, and implanting it into their defect site [16, 17]. Alternatively, allograft bone from donors or cadavers is sometimes used in the same manner and is extracted from femoral heads or the extremities of other long bones [18]. The implanted tissue then acts as a scaffold for the existing bone tissue to infiltrate and deposit ECM, leading to the remodelling of the bone [19]. It is a relatively common procedure, with an estimated 2.2 million operations being carried out per year [20] and with the demand set to increase over the coming years due to an

increasingly aging population [17]. However, there are numerous drawbacks to this approach, including the limited supply of autologous bone, the usage of which can result in complications at the donor site. Issues arising from graft resorption are also common in the case of large defects, with resorption sometimes occurring before osteogenesis is complete [21]. Allograft bone is associated with issues such as incompatibility with the host and the transmission of disease and infections such as hepatitis and HIV [15, 19, 22, 23]. Conversely, the processing or devitalization of allograft bone, via freeze-drying or irradiation, in order to reduce the risk of infections, may cause a loss of bone inductive factors leading to a reduction in osteoinductivity and the mechanical strength [17–19]. Furthermore, both autograft and allograft bone present with high surgical costs [16], in particular autografts, due to the necessity of two operations required on the same patient. Other options aside from bone grafts include the usage of bone morphogenetic proteins, distraction osteogenesis and bone cement; however, these are also not ideal [17]. Pitfalls in the clinically available treatments have, therefore, led to efforts in the field of bone tissue engineering as a potentially attractive strategy for the repair of bone.

1.3 The fundamentals of bone tissue

1.3.1 Bone function

Bone plays a key role in our bodies and has a variety of different functions. Adequate knowledge of the structure and functions of bone is required in order to develop suitable biomaterials as scaffolds for use in bone tissue engineering. Bones form the basis of our body's ability to move and possess some of the following key functions such as the ability to bear loads and protect the delicate internal organs, homeostasis of electrolytes such as calcium and phosphate via storage in bone tissue, storage of substances required for haematopoiesis and the ability to confine dangerous metals such as lead. Bone is an

anisotropic tissue, which means that the mechanical properties change depending on the axis on which the load is applied [24]. Generated bone must be able to integrate with the original bone tissue and carry out the functions listed above in order for bone tissue engineering to be successful.

1.3.2 Bone structure

There are more than 200 bones in the human body, the macroscopic structure and mechanical properties of which are greatly influenced by the loading environment that is distinct to each type. Bones possess different skeletal structures such as long, short, flat and irregular varieties. Furthermore the pattern arrangement may take the form of either trabecular (cancellous) or compact (cortical) bone. At the microscopic architectural level bone is much simpler, with its ECM comprising two main elements; an inorganic mineralized component (hydroxyapatite crystals) and an organic non-mineralized component (type-1 collagen fibres). It has a largely interconnected porous structure to allow the inflow of bodily fluids.

The two varieties of bone (cancellous and compact) are found in different locations [25] . Cancellous bone is more porous in nature and is highly vascularized in comparison to compact bone. It is in this bone that yellow and red bone marrow is found for the storage of fat and erythropoiesis, respectively. Alternatively, compact bone has a higher density and is important for load bearing and is found in the shafts of long bones.

1.3.3 Bone formation

There are two main ways in which bone is formed that involve the transformation of existing mesenchymal tissue into bone tissue. Bone may be formed by intramembranous ossification, which directly involves the conversion of mesenchymal tissue into bone tissue. This route is primarily for the formation of bones that form the skull structure. Bone may also

be formed by endochondral ossification, and first involves the formation of cartilage from mesenchymal cells, which are then later replaced by bone tissue [26].

1.3.3.1 Intramembranous ossification

Intramembranous ossification involves the proliferation and subsequent condensation of neural crest-derived mesenchymal stem cells into compact nodules. Some of these cells differentiate into capillaries, whilst others become specific bone precursor cells known as osteoblasts. The osteoblasts then secrete a matrix material comprising collagen and proteoglycans, known as the osteoid matrix. This matrix is able to bind with salts of calcium, which enables the calcification of the tissue. Osteoblasts are generally separated from the calcified matrix by the osteoid matrix, but in some instances they may become engulfed in the calcified matrix and become bone cells, known as osteocytes. During this process spicules emanate out from the area in which the calcification began. The entire area is eventually surrounded with a layer of compact mesenchymal cells, which form what is known as the periosteum [26], [27].

1.3.3.2 Endochondral ossification

Endochondral ossification first involves the condensation and differentiation of mesenchymal cells into chondrocytes [28]. The chondrocytes proliferate and lay down a cartilage-specific ECM in order to form the template of the bone. They then undergo both hypertrophy and apoptosis. The hypertrophic chondrocytes secrete an altered ECM consisting of fibronectin and collagen X, which allows the binding of calcium carbonate. The cell death allows blood vessels to enter, which in turn brings osteoblasts to the area. These osteoblasts bind to the cartilage matrix as it degenerates and then lay down bone matrix [26]. A structure known as a growth plate emerges from the top of forming bones, which comprises distinct phases; a) a resting zone, b) a proliferating zone consisting of several layers of chondrocytes, c) a hypertrophic zone and d) a zone of vascular in growth [29].

1.3.4 Bone remodelling

Bone remodelling is the process by which old bone is continuously replaced by new bone in order to maintain the quality, size and shape of the skeleton. It involves the repair of any fractures that may occur and also modifications in the structure that take place in response to biomechanical stresses [30]. The process of repair after damage closely resembles skeleton formation, i.e. intramembranous and endochondral ossification; however, there is an inflammation aspect associated with fracture repair [29].

1.3.3.3 Normal bone remodelling

Osteoclasts and osteoblasts play a key role in the bone-remodelling process. Osteoblasts are involved in the formation of bone and deposition of bone matrix, whereas osteoclasts are responsible for the resorption of bone. Resorption occurs via the acidification and proteolysis of the matrix. Bone remodelling follows a three stage process, which includes resorption, reversal and formation. The first resorption phase begins with partially differentiated mononuclear pre-osteoclasts attaching to the surface of the bone where they then become multinucleated osteoclasts. After resorption has taken place, the reversal phase ensues, in which mononuclear cells are present on the bone surface in order to prepare for the formation of bone by osteoblasts. One of the ways in which they do this is by facilitating signals for the migration and differentiation of osteoblasts. In the final formation phase the osteoblasts lay down new bone matrix in order to replace the bone that was previously resorbed. Following the completion of this phase, a period of rest takes place until the bone is ready for the next cycle of bone remodelling [30].

The process of bone remodelling is controlled by a variety of different hormones, the most important of which is parathyroid hormone. Parathyroid hormone is able to stimulate bone resorption, in addition to the reabsorption of renal tubular calcium and the production of calcitriol by the kidney [30]. It has also been found that when it is administered

intermittently, it results in an increase in bone formation, whereas when it is given continuously bone resorption occurs [31, 32]. Growth factors are also key players in the bone remodelling process and will be discussed in detail in section 1.4.

1.3.3.4 Bone repair following fracture

There are two main types of fracture repair; secondary/indirect bone healing and primary/direct bone healing. In secondary/indirect bone healing, simple fractures are immobilized using a plaster cast, and involves the formation of a callus and has a number of distinct phases. The first phase involves the formation of a haematoma due to bleeding originating from the bone and surrounding tissue. The next phase is an inflammation phase in which granulation tissue replaces the haematoma with a hard callus (mineralized, new woven bone) forming via intramembranous ossification [24]. Next, in the repair phase, the gap between the bones is filled with soft callus or cartilage, which is then replaced with bone via endochondral ossification. The final remodelling stage is just a continuation of normal bone remodelling, with any excess callus being removed and the remodelling of woven bone into lamellar bone [24].

Primary/direct bone healing occurs when the ends of the fracture are completely immobilized and there is complete stability when a functional load is applied [24]. In these cases the bone formation follows the normal bone formation and remodelling processes, without evidence of a callus formation [24].

1.4 Growth factors

Growth factors are biological molecules that promote or prevent cell processes such as proliferation, differentiation, migration, motility and adhesion [11]. They often work in a concentration-dependent manner, which in turn determines whether there will be an up or down regulation in the synthesis of various components, e.g. proteins, other growth factors

and receptors. They undergo a rapid turnover and their half-life can be as little as a few minutes [11].

The use of growth factors to mimic the body's normal physiological patterns, both spatially and temporally [33], is a technique that is showing promise in the field of regenerative medicine, including bone defect repair due to fractures, diseases or surgical procedures [34]. The formation of functional tissue requires coordinated cell processes; for example, proliferation, differentiation and angiogenesis [11]; which is achieved by the release of a complex series of growth factors. This allows the transfer of information between the ECM and the cells [22]. The type of growth factor varies between different tissues; however, it is apparent that in order to facilitate tissue regeneration, the controlled release of growth factors must play a part in any cell-scaffold system [11].

1.4.1 Growth factors for bone tissue engineering

1.4.1.1 Bone morphogenetic proteins and their delivery systems

Bone morphogenetic proteins (BMPs) have been widely studied for use in non-union bone defects, spinal fusion and open tibial fractures [35–37]. They are a type of growth factor belonging to the transforming growth factor β (TGFβ) protein superfamily and can be used to simulate natural repair processes with great specificity and effectiveness. However, the disadvantages to using them include their short half-life *in vivo*, high cost and the requirement for high doses to elicit a response [38]. These problems can potentially be reduced by using a sustained/targeted delivery approach to control both the rate and location of growth factor delivery [39].

It has been found that BMP-2 is present at the initial phase of fracture repair and during chondrogenesis and osteogenesis[40]. It is produced in recombinant forms and the short half-life necessitates the need to use recombinant BMP-2 (rhBMP-2) above its

physiological range (1–30 nM). As a result of this, various issues have been associated with rhBMP-2 usage, which, in 2008, led to the issue of a Public Health Notification of life threatening complications by the US Food and Drug Administration (FDA) [35, 41]. Swelling of the neck and throat tissue was found to be an issue in anterior cervical discectomy and fusion ACDF procedures, as well as problems associated with high doses [35]. BMP-4 has also been found to induce osteogenic differentiation of both osteoblasts and osteoprogenitors [42].

The BMP-2 signalling pathway is initiated with the binding of BMP-2 to its membrane receptor. Following the membrane receptor's phosphorylation, subsequent phosphorylation of Smad proteins [43] and various other downstream transcription factors ensues [38].

Controlled delivery of BMP-2, and the subsequently reduced concentrations that this entails, may help to circumvent the toxicity issues mentioned above. It can be delivered to the target site by a number of different techniques [44]. It can be entrapped non-covalently in reservoir devices (A), microspheres (B), or coatings (C); as well as being adsorbed into sponges (D) or hydrogels (E), or subjected to ionic complexation (F). Furthermore covalent methods are also available, which include functionalization with a linker or the attachment of an oligopeptide derived from the growth factor to a carrier (G,H) [44].

BMP-2 has been formulated into numerous scaffold systems for use in bone tissue engineering, including fibrous scaffolds composed of silk fibroin [45] and chitosan [46], gels comprising gelatin nanospheres [47], a combination of chitosan and gelatin [48], hydrogels [44, 45] and PLGA microspheres (as discussed in later sections). INFUSE® is a commercially available BMP-2 formulation in which rhBMP-2 is adsorbed onto a collagen sponge, which is

then implanted at the defect site [51]. It was licensed for use in anterior lumbar interbody fusion spinal surgery in 2002 by the FDA [51].

Nano systems have also been investigated for the delivery of BMP-2 in bone tissue engineering. Moore et al. [52] loaded BMP-2 onto detonation nanodiamonds via physisorption. The stable colloidal solution of nanodiamonds and BMP-2 was able to release the loaded BMP-2 in slightly acidic conditions and promoted osteoblast differentiation in C2C12 cells [52]. Another formulation that has been investigated for the delivery of BMP-2 comprises poly (Ɛ-caprolactone)-co-poly (ethylene glycol), dexamethasone and bovine serum albumin (BSA) nanoparticles containing BMP-2 [53]. These components were electrospun to form nanofibres, which released BMP-2 and dexamethasone in a sequential manner and promoted repair in a rat calvarial defect model [53]. Nie et al. [54] also used the electrospinning technique to formulate BMP-2-loaded nanofibrous scaffolds from hydroxyapatite and PLGA. The authors reported a sustained release of BMP-2 over 2 to 8 weeks, with a faster rate of release when the hydroxyapatite content was higher.

Keratose, a biomaterial obtained from hair, was used to prepare a BMP-2 delivery system via the formation of a freeze-dried implant [55]. This implant released BMP-2 at a rate that correlated with keratose degradation, and the authors suggested that it indirectly enhanced bone regeneration via the suppression of adipose tissue formation. Yang at al. [56] also combined BMP-2 with a biomaterial, heparin-conjugated fibrin, and reported more favourable osteogenic activity than the clinically available BMP-2-loaded collagen sponge in a mouse calvarial defect model.

Recombinant forms of BMP-7 (OP-1 putty and implant) have been approved by the FDA for use in revision posterolateral lumbar spine fusion and long bone non-union fractures; as in the case of INFUSE®, BMP-7 is combined with collagen (purified Type I

collagen) [57]. Delivery systems that combine BMP-2 and BMP-7 have been developed by researchers. Yilgor et al. [46], [58] combined PLGA nanocapsules loaded with BMP-2 with poly (2-hydroxybutyrate-co-3-hydroxyvalerate) nanocapsules loaded with BMP-7. They reported that sequential delivery of BMP-2 and BMP-7 resulted in slightly lower stem cell proliferation, but higher alkaline phosphatase activity, indicative of osteogenic differentiation, when compared to simultaneous delivery of the two growth factors.

1.4.1.2 Vascular endothelial growth factor

Angiogenesis is also an important process in tissue regeneration as it involves the formation of new vessels from the already-present vascular network [59]. It is crucial for the delivery of nutrients and oxygen to cells, the removal of their waste products and also for the recruitment of specialized cells such as osteoprogenitors and haemopoietc stem cells to the area, which can aid in tissue regeneration [60]. A key growth factor involved in both the normal and pathological process of angiogenesis is vascular endothelial growth factor (VEGF) [61]. VEGF and its receptors, VEGFR1 and VEGFR2, have been reported to be pivotal regulators of angiogenesis during endochondral ossification [62]. Some studies carried out *in-vitro* have shown that VEGF, along with BMPs, play a key role in signalling between the cells during both angiogenesis and osteogenesis [59]. Street et al. [63] found that when VEGF activity was inhibited in a mouse model, there was a decrease in angiogenesis, and the formation of bone and callus mineralization in femoral fractures, hence emphasising the importance of this growth factor. Studies have shown that for angiogenesis to be effective, i.e. for new vessels to be stable, VEGF levels need to be sustained for approximately four weeks. However it has a very short half-life *in*-vivo; therefore, its incorporation into a delivery system is very important [60].

VEGF has been combined with BMP-2 in a single delivery system and investigated for its usefulness in bone tissue engineering. Young et al. [64] encapsulated VEGF and BMP-

2, separately, into gelatin microspheres. The microspheres were then combined to give formulations containing different doses of VEGF and BMP-2, and then incorporated into porous poly (propylene fumarate) scaffolds. They observed a decrease in the percentage of bone fill at lower doses of BMP-2, which could not be reversed by simultaneously delivering VEGF. The authors concluded that in this rat cranial critical-size defect model, the addition of VEGF to BMP-2 does not increase the formation of bone when compared with BMP-2 alone.

1.5 Biomaterials used for bone tissue engineering applications

Biomaterials are a crucial component of the bone tissue engineering approach as they provide the means to form scaffolds. Scaffolds, as mentioned previously, are needed in order to provide multidimensional support to growing cells and, furthermore, to encourage their attachment, proliferation and differentiation [65]. The chosen biomaterials must meet certain criteria, which include mechanical and physical properties that are suitable for the particular area, the ability to undergo sterilization without a loss in structure, biocompatibility and the appropriate degradation time [21]. Materials used at the defect sites must be specifically capable of withstanding compressive loads that are common in this type of tissue [66]. A variety of materials are being investigated in this field and there is an increasing demand for them to be bioactive rather than inert. The material should be osteoconductive, osteoinductive and capable of undergoing osseointegration [67]. Biomaterials for bone tissue engineering can be split into the following groups; bioactive inorganic materials, natural and synthetic polymers and composite materials, which often combine the two.

1.5.1 Bioactive inorganic materials

Biomaterials whose compositions share similarity with the mineral phase of bone, possess clinical relevance in the field. This subclass of biomaterials include hydroxyapatite,

tricalcium phosphate and bioactive glasses [67]. These materials are often capable of reacting with bodily fluids to form a layer of hydroxy carbonate apatite, which is then able to act as an interface between the material and tissue [68–70]. Furthermore, another advantage is that some of these materials; such as 45S5 Bioglass®, which is a silicate bioactive glass; are able to promote the release and exchange of soluble silicon, calcium, phosphate and sodium ions, which leads to intracellular and extracellular responses that promote bone formation [38, 40].

Bioactive glasses are amongst the oldest of the bioactive inorganic materials used and were discovered by Hench et al. [72] in 1969. The initial formulation comprised a silicate network containing 45% SiO_2 with the addition of 24.5% Na_2O, 24.5% CaO and 6% P_2O_5 [73]. In 1985 the first Bioglass® product was approved for use in the USA for the treatment of conductive hearing loss, involving the replacement of the middle ear bone with the material [73]. However, the low fracture toughness and high elastic modulus, when compared to cortical bone, mean that for load bearing joints, their solitary use is limited [68].

Hydroxyapatite ceramics have also been widely investigated and used for bone regeneration. Their structure is similar to that of the natural mineral phase of bone, which is predominantly composed of hydroxyapatite, and they possess osteoconductive properties [43, 44]. They are available in a number of forms, including granules, blocks and injectable materials, but a significant drawback is their slow degradation time, with particles of such materials being found inside patients years after their treatment [75]. The process of degradation may occur by fragmentation or dissolution, which would then be followed by phagocytosis by macrophages. However, another route may also involve resorption by osteoclasts, which would be more favourable as this process is closer to the natural physiological bone processing; therefore, it may result in surfaces that would be more attractive to osteoblasts [75]. Degradation by the osteoclast route may be encouraged via

changing the various properties of the hydroxyapatite scaffolds, e.g. the crystal size and surface roughness [75].

Calcium phosphate-based cements (CPC) are biomaterials that comprise a solid and a liquid phase. The solid phase is composed of one or more calcium phosphate-containing compounds and the liquid phase comprises water or a phosphate or calcium-containing solution. Upon combining the two phases, the solid phase dissolves in the liquid phase until it supersaturates and begins to re-precipitate. The cement hardens via the entanglement of the crystals. The end product is usually brushite or apatite [76]. Issues that still need to be resolved include the lack of osteoinduction and angiogenesis, which are crucial for bone regeneration, the lack of suitability for load-bearing joints due to low mechanical strength, the challenge in delivering the CPC to complex injuries [76] and the slow degradation times [77].

Metals also have the potential to be used in bone tissue engineering and it has been reported by Kokubo et al. [68] that following heat or sodium hydroxide treatment, metals such as titanium became bioactive and formed an apatite layer soon after implantation into a rabbit tibia. Sodium hydroxide and heat treatment of tantalum have also been investigated. However, the potential drawbacks could include the lack of biodegradability and difficulties with the incorporation of biomolecules [78]. The issue of biodegradability has been investigated extensively, with researchers taking advantage of the corrosion process as a means of allowing the metal to slowly degrade *in-vivo*, followed by the metabolism of the metal elements by the body [79]. Various metals are being studied such as magnesium, iron and their alloys.

1.5.2 Natural polymers

Natural polymers include materials such as collagen, chitosan and silk fibroin.

Collagen is a natural protein that is found in the ECM of many tissues and provides structural and mechanical support to tissues [23]. It is biocompatible, has low antigenicity and is able to bind cells [80]. A collagen sponge has been shown to promote the attachment and growth of cells and tissues [81]. Furthermore, it has also been combined with other materials such as bioactive ceramics [82] and hydroxyapatite [83–85]. The FDA have approved the use of a collagen sponge impregnated with a recombinant form of BMP-2, known as INFUSE®, for use in anterior lumbar inter-body fusions [86]. However, there are also negative aspects related to the use of collagen, for example, its degradation rate is very high, leading to the rapid loss of its mechanical strength [87], and it has low biomechanical stiffness [23]. In an attempt to combat these problems, collagen has been combined with PLGA, which combines the good mechanical strength of the synthetic polymer with the benefits conferred by collagen [88]. A PLGA-knitted mesh was combined with collagen to provide the mechanical strength for its application in cartilage regeneration [89]. Although it has low antigenicity, there are still some immune-mediated reactions that can be triggered through the telopeptide regions, which are the non-helical portions of tropocollagen, the molecular subunit of collagen [90]. The telopeptide region is susceptible to protease cleavage, which has led to the formation of atelocollagen [90].

Chitosan, a linear cationic polysaccharide, is a natural polymer that is derived from the N-deacetylation of chitin and has a similar structure to hyaluronic acid, a component of the ECM [91, 92]. It is a popular choice in the field of regenerative medicine as it is biocompatible, non-cytotoxic to living cells, does not illicit an immune response and is easy to functionalise [92, 93]. Its surface is hydrophilic, which promotes the adhesion, differentiation and proliferation of cells [23]. Chitosan has been applied in various forms, including porous film-like structures (either pure chitosan or composite materials), films, fibres [94] and gels [93]. It has been shown to promote the differentiation and mineralization

of osteoblasts via the up-regulation of genes that are responsible for controlling these processes [91] and, therefore, has promising applications in bone tissue engineering. Chitosan has also been used for protein delivery. Yilgor et al. [46] formulated a chitosan-based mesh using the wet spinning technique, which was seeded with BMP-2- and BMP-7-loaded polyester nanocapsules. Another study reported the formulation of alginate/chitosan/PLGA composite microspheres containing bovine serum albumin as a model protein, which displayed a reduced protein burst release when compared to PLGA microspheres [95].

The silk from the silkworm comprises a fibrous protein called silk fibroin (SF), along with a glue-like protein called sericin that holds the fibroins together [23]. SF meets many of the requirements of a scaffold biomaterial; it has a slow degradation rate, a high degree of strength and flexibility and is permeable to both water and oxygen [23]. Via an aqueous solution, it can be used to form gels, powders, membranes and sponges with it also being possible to modify its surface due to the presence of acid and amino groups [23]. A major issue with SF is biocompatibility, as sericin can elicit an immune response at the implantation site [23]. It is, therefore, extremely important that it is purified thoroughly prior to use. SF has also been used in conjunction with other biomaterials, for example, Wenk et al. [96] created a microporous SF scaffold embedded with PLGA microspheres pre-loaded with insulin-like growth factor 1 (IGF-1), which they found to give a more sustained, albeit lower, release of IGF-1 in comparison with free PLGA microspheres.

Pectins are a group of natural polymers that are composed of covalently linked polysaccharides rich in D-galacturonic acid, which are found in plant cell walls [97]. They are commonly used as thickeners and gelling agents in the food industry [97]; the ability of pectin to gel and form films is affected by the degree of esterification of the galacturonic acid residues [98]. Pectin has also be investigated for use in bone tissue engineering, with freeze-dried chitosan/pectin polyelectrolyte complexes shown to be non-toxic to human osteoblast

cells [97]. Kim et al. [99] investigated the release of albumin from pectin beads coated with chitosan; calcium chloride was used in combination with pectin to form a gel. They found that the protein release was pH dependent and affected by the concentration of calcium chloride and molecular weight of chitosan that were used [99].

Carrageenans are high-molecular-weight polysaccharides that are extracted from red seaweed [100]. They are copolymers of 1,4-linked 3,6-anhydro-α-$_D$-galactose and 1,3-linked β-$_D$-galactose [100]. Various carrageenan subtypes are available (kappa, lambda and iota), which form as a result of the type of seaweed that they are extracted from and the technique used [100]. Carrageenan is ionic in nature and has been combined with chitosan to form polyelectrolyte complexes encapsulated with bovine serum albumin [101]. These complexes were pH sensitive such that the protein was released at pH 7.5, but release was retarded at pH 1.2. Grenha et al. [102] also combined chitosan and carrageenan, forming chitosan/carrageenan nanoparticles loaded with a model protein, ovalbumin, the release of which was sustained over three weeks. Carrageenan has also been used to prepare hydrogel beads encapsulated with albumin, a model protein for platelet-derived growth factor. This growth factor is thought to be involved in angiogenesis via stimulating smooth muscle cells to produce VEGF. The protein release profile showed an initial burst release within the first 4 days, followed by a slower period of release thereafter [103].

Heparin is a sulphated polysaccharide, which has been reported to enhance the biological activity of BMPs, as shown by the increase in osteoblast differentiation in C2C12 cells. It has been used to functionalise various different materials in order to enhance and stabilise BMP-2 activity, which include a heparin-conjugated hyaluronic acid-based hydrogel [49] and heparin-conjugated PLGA scaffolds [104]. Additionally, when heparin was immobilised onto demineralized bone matrix, a collagen-based scaffold, the material's mechanical strength and ability to bind to BMP-2 were enhanced [105].

Overall, natural organic polymers have a range of useful attributes; however, they lack the mechanical strength exhibited by natural bone tissue, which along with organic materials also contains an inorganic component [66].

1.5.3 Synthetic Polymers

Poly (ε-caprolactone) (PCL) is a widely available synthetic polymer, which has been extensively studied for use in bone tissue engineering applications. It is bioresorbable, exhibits stability in ambient conditions, is economical in comparison to other polymers and is widely available [106]. It possesses a hydrophobic structure, hence, leading to a relatively slow degradation rate, but a good degree of ductility, which is a useful attribute in a biomaterial [107]. PCL has been utilised in a variety of formulations including microspheres [106], porous scaffolds prepared from a combination of polymer/salt leaching [108] and cryomilling combined with compression moulding/salt leaching [109].

Poly (hydroxyalkanoates) are polyesters that are produced when microorganisms are exposed to unbalanced conditions [110]. They generally possess properties such as biodegradability and biocompatibility and, hence, are considered to be useful materials for tissue engineering applications [110]. A co-polymer of 3-hydroxbutyrate and 3-hydroxvalerate, known as PHBV, has been used in various tissue engineering applications, including in combination with poly (lactic-co-glycolic acid) (PLGA) [46, 58]. It has a slow degradation rate, with just 15–43% being degraded over a 6 month period [111].

Poly (lactic acid) (PLA) is another biosynthetic polymer that is often employed in the field of regenerative medicine due to its good biodegradability and biocompatibility [112]. It is a poly (α-hydroxyacid) and can exist in three different forms, P_DLA, P_LLA and a racemic mixture, $P_{DL}LA$ [23]. It is degraded by hydrolysis of the ester linkage to form lactic acid, a normal metabolic breakdown product [23]; however, the increase in acidity than can ensue

following the degradation of PLA can lead to inflammation and swelling [113]. PLA also suffers from high hydrophobicity due to the lack of hydrophilic groups on its surface, which lends to its poor affinity to cells [113]. PLA is often modified with other compounds or combined with other bioactive materials in order to tackle some of the issues above. One such example of this was carried out by Niu et al. [113] in which they functionalized $P_{DL}LA$ with an aliphatic diamine and a peptide RGDS (Arg-Gly-Asp-Ser). The addition of the aliphatic diamine led to a reduction in the degree of acidity during the degradation of the polymer, and the additional functionalization with RGDS enhanced the surface attachment and viability of osteoblasts [113]. The alkaline phosphate (ALP) activity was also monitored to determine the differentiated function and was found to be higher on the modified PLA when compared with the unmodified polymer [113]. Composite materials have also been produced, such as the electrospinning of hydroxyapatite (HA) nanoparticles, in a dispersion of P_LLA to produce a P_LLA/HA hybrid membrane by Sui et al. [114]. HA is often used due to its osteoconductivity and bioactivity [115]. The composite membrane showed enhanced osteoblast cell growth in comparison with a membrane composed of P_LLA alone, a higher elastic modulus and lower strain at failure; in addition to slowing down the degradation rate of the membrane [114]. Jaiswal et al. [115] blended P_LLA with gelatin to form nanofibrous scaffolds and then mineralized the scaffolds with HA. They found that the mineralized scaffolds exhibited higher ALP activity, leading them to conclude that HA increased the osteogenic capacity of the scaffold. The inclusion of HA also leads to increased surface roughness, which is important for protein absorption, cell attachment and proliferation. With regards to the degradation rate, the addition of gelatin appeared to increase the degradation rate of the scaffolds, and the HA switched the mechanism from bulk to gradual degradation.

Pluronic is an amphiphilic tri-block copolymer that exhibits thermoreversible behaviour when it is in an aqueous solution, resulting in the formation of a gel at certain

temperatures and pH values [116]. Rahman et al. [117] combined a Pluronic F127 hydrogel with thermosensitive PLGA/PEG microspheres. They found that the formulation was able to solidify at 37°C over time, resulting in scaffolds with favourable compressive strength. Pluronic has also been used to modify the surfaces of micro-/nano-fibre PLGA meshes in order to reduce the hydrophobicity [118]. The modification increased the hydrophilicity of the mesh surface, without affected the bulk properties of the scaffolds.

1.5.3.1 PLGA

PLGA is an FDA-approved biosynthetic polymer that belongs to the poly (α-hydroxy acid) group. It is a linear copolymer that is formed from lactic and glycolic acid monomers and its structure is shown in **Figure 1.1**. It can be injected into the body [119] and finds many applications in drug delivery and tissue engineering [120]. Its biodegradability, biocompatibility, tuneable degradation rate (via varying the molecular weight and glycolic to lactic acid ratio) and its favourable mechanical properties are amongst some of the reasons that PLGA is so widely used [120–124].

PLGA can be formed via a number of different methods. Low-molecular-weight varieties (<10 kDa) can be obtained via the solution poly-condensation of monomers at temperatures above 120°C in a de-hydrating environment [125, 126]. High-molecular-weight varieties have been prepared by the ring opening co-polymerisation of its constituents, lactic acid and glycolic acid, in the presence of high temperatures and metal catalysts such as aluminium isopropoxide ($Al[OCH(CH_3)_2]_3$), tin (II) alkoxides ($Sn(OR)_2$) and tin (II) 2-ethylhexanoate ($[CH_3(CH_2)_3CH(C_2H_5)CO_2]_2Sn$) [123, 127]. Polymerization can also be undertaken in the presence of enzymes under mild reaction conditions. This technique reduces contamination with potentially toxic metallic residues; however, is slower and results in PLGA of lower molecular weights [127].

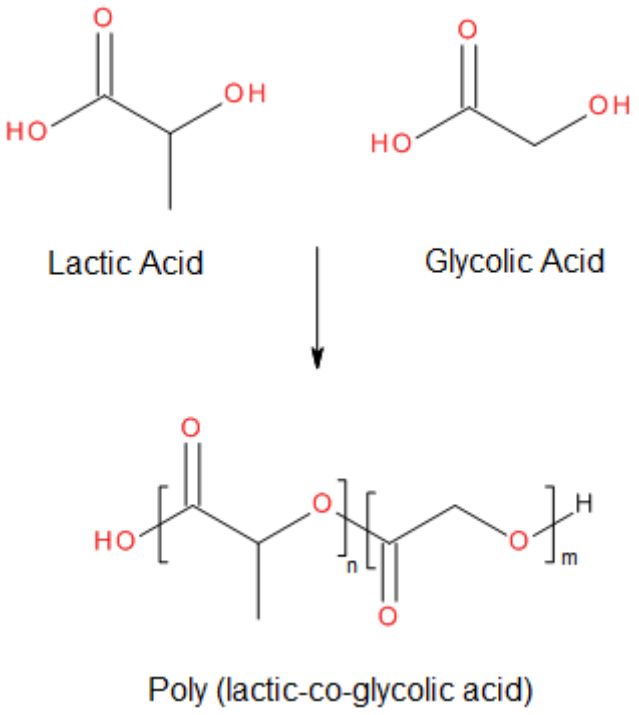


Figure 1.1: Chemical structure and formation of poly (lactic-co-glycolic acid).

It is possible to dissolve PLGA in a range of readily available solvents such as acetone, ethyl acetate, tetrahydrofuran and chlorinated solvents, which enables relatively easy processing of the polymer for a range of applications [124]. The lactic acid component can take the form of two different enantiomers, D and L, due to the presence of an alpha carbon atom in the methyl group. However, the glycolic acid monomer does not possess a methyl side chain, hence, resulting in a structure that is highly crystalline in nature. The two enantiomers of lactic acid result in PLGA taking an amorphous morphology [127].

A four-step process is involved in the biodegradation of PLGA, which comprises hydration, initial degradation, further degradation and solubilisation [128]. The aqueous media first penetrates the polymer and relaxes the structure, reducing its glass transition temperature (T_g). It is in these hydrated regions that the initial degradation begins, with the hydrolysis of the ester bonds within the polymer backbone structure. As the backbone is

degraded, the molecular weight of the polymer is reduced and the PLGA maintains its integrity but loses its mechanical strength. With the progression onto the next degradation step, the molecular weight is reduced to such an extent that the polymer loses its integrity. Finally, the smaller fragments are broken down into the monomers, leading to the solubilization of the PLGA [129]. PLGA degradation is also known to auto-accelerate due to the formation of acidic breakdown products, which is a phenomenon known as autocatalysis [130].

Various factors can influence the degradation rate of PLGA, which include the molecular weight of the polymer, the lactic acid to glycolic acid ratio, the stereochemistry and the functionalisation of the end group. The lactic acid to glycolic acid ratio has a large impact on the hydrophilicity of the resulting PLGA, with varieties containing a higher proportion of glycolic acid being more hydrophilic in nature due to the lack of a methyl group side chain. The lack of the side chains leads to increased water absorption, followed by a higher rate of degradation in comparison with the varieties containing a lower proportion of glycolic acid monomers. However, there is an exception to this rule, which comes from the 50:50 glycolic acid to lactic acid ratio PLGA, which exhibits the quickest degradation rate [124]. The stereochemistry also has an effect on the degradation rate, as an increase in D-L amorphous regions, which are formed as a result of a mixture of D and L enantiomers of lactic acid, leads to greater penetration of water in these areas and, hence, an increase in the degradation rate. Capping the end group with an ester decreases the degradation rate in comparison with the presence of free carboxylic acid end groups [128].

The T_g of PLGA has been reported to be over 37 °C, which means that at room temperature (25°C) and physiological conditions it generally takes a brittle, glassy form [131]. Factors that can reduce the T_g include a reduction in the lactic acid concentration, in addition to a reduction in the molecular weight [124].

1.5.3.2 Removal of PLGA waste products

The waste products that result from the breakdown of PLGA are lactic acid and glycolic acid. Lactic acid can enter the tricarboxylic acid cycle and is subsequently excreted as carbon dioxide and water. Additionally, glycolic acid can enter the cycle, or alternatively can be excreted unchanged by the kidney [124].

1.6 PLGA in bone tissue engineering

PLGA is a versatile polymer that has been widely used in bone tissue engineering applications in a variety of different forms. PLGA fibres have been prepared via the electrospinning technique, which is useful for producing fibrous scaffolds that are characteristic of the ECM [132–134]. Other studies report the fabrication of PLGA scaffolds using freeze-fixation and freeze-gelation methods, in which a porous scaffold was formed via freezing the polymer solution, following the removal of the solvent using a non-solvent, or gelation of the polymer [135]. Lu et al. [136] were able to prepare PLGA foams of different porosities and pore sizes using a solvent-casting, particulate-leaching technique. PLGA/PEG composite microspheres have also been incorporated into hydrogels comprising fibrin, Pluronic F127 or hyaluronic acid, which were able to solidify at 37°C, resulting in scaffolds of good mechanical strength and porosity [117].

1.6.1 PLGA microspheres

PLGA can also be formulated into microspheres, which, due to their size, offer the advantage of allowing the potential injectable delivery to defect sites. It is also possible to load the microspheres with useful agents, such as growth factors or other proteins. There are various examples of PLGA microspheres being investigated for use in bone tissue engineering. Microspheres loaded with dexamethasone were conjugated with BMP-2 and the RGD (Arg-Gly-Asp) peptide. These conjugated microspheres were found to promote the

adhesion of stem cells in addition to encouraging the proliferation and differentiation of the cells into a bone lineage [137].

Other groups have combined PLGA with poly (ethylene glycol) (PEG) in order to prepare temperature-sensitive microspheres with the ability to control the release of BMP-2 [138]. Furthermore, microspheres made of a PLGA/PEG copolymer, which has a lower T_g than PLGA alone, allows the fusion of microspheres at body temperature. These microspheres were then further combined with PLGA microspheres with amine-modified surfaces in order to promote cell differentiation [139]. Similarly, PLGA/PEG microspheres mixed with a BMP-2 solution were sintered to form scaffolds and were found to control the release of BMP-2, in addition to eliciting a 55% new bone volume in a mouse calvarial defect model [140]. Furthermore it has been found that the inclusion of PEG leads to the decoupling of the protein release kinetics (via the generation of quasi-zero-order protein release) from the PLGA degradation rate [35]. Another way in which PLGA microspheres have been utilized is for the encapsulation of plasmid DNA into microspheres. This PLGA formulation facilitated the sustained release of DNA [141].

Porous PLGA microspheres have also been formulated, with an ethanolic sodium hydroxide treatment step, which enabled the microspheres to sinter at body temperature, resulting in highly porous scaffolds [142]. Shen et al. [143] prepared composite PLGA/hydroxyapatite microspheres that were also treated with ethanolic sodium hydroxide. The surface treatment of these microspheres promoted the attachment, proliferation and alkaline phosphatase activity of mouse OCT-1 osteoblast-like cells.

1.6.2 Formulation methods

Various methods have been used to produce PLGA microspheres, including the double emulsion and solvent evaporation method, spray-drying, phase separation, the 'syringe infusion pump' method, electrospraying and electrospinning.

The spray-drying technique involves the homogenization of a solid, often lyophilized protein, with PLGA dissolved in a volatile organic solvent [33]. The mixture is then atomized by subjecting it to heated air, which leads to the rapid evaporation of the organic solvent and the formation of microspheres [33].

In the electrospraying method the polymer is dissolved, along with the agent to be incorporated (e.g. drug or growth factor), in a solvent and then forced through a nozzle, which has a voltage applied across it [144]. This method was used by Nath et al. [144] to formulate simvastatin encapsulated microspheres with a size range of 2–8 μm, which when tested on human MG-63 osteoblast cells, were non-cytotoxic and facilitated cell proliferation.

Phase separation is another technique, which involves the addition of silcone oil to the polymer-organic solvent with the protein dispersed within it. This reduces the solubility of the polymer within the organic solvent, resulting in the encapsulation of protein within a polymeric microsphere [33].

The 'syringe infusion pump' method involves the polymer solution, e.g. PLGA in dichloromethane (DCM), being pushed through a syringe into a perpendicular flow of poly vinyl alcohol (PVA) solution acting as the continuous phase [121]. The size of the microspheres can be reduced by reducing the size of the needle used to inject the polymer solution and also by increasing the speed at which the continuous phase is pumped in [121].

1.6.2.1 Double emulsion solvent evaporation method

The double emulsion solvent evaporation technique is a common method used to produce microspheres and is particularly appropriate for the encapsulation of water soluble proteins or macromolecules [145]. A water in oil in water (w/o/w) emulsion, a solid in oil in water (s/o/w) emulsion, or an oil in oil in water (o/o/w) are all forms that a double emulsion can take [146].

A schematic diagram illustrating the main stages involved in this technique is shown in **Figure 1.2**. For a w/o/w double emulsion PLGA polymer is first dissolved in an organic solvent, often DCM, and then emulsified with an aqueous phase to produce a w/o primary emulsion [142]. It is in this first aqueous phase that proteins or drugs can be incorporated, if required. This primary emulsion is then transferred to a second aqueous phase, often containing PVA functioning as a surfactant, to create a w/o/w double emulsion. The DCM acts as a barrier between the two aqueous phases in order to prevent the escape of any drug/protein that was dissolved in the first aqueous phase [145]. The removal of DCM is then the next step and occurs by either the application of heat, vacuum or extraction [33]. The resultant microspheres are then centrifuged, washed to remove any remaining porogen or surfactant, and then freeze dried [147].

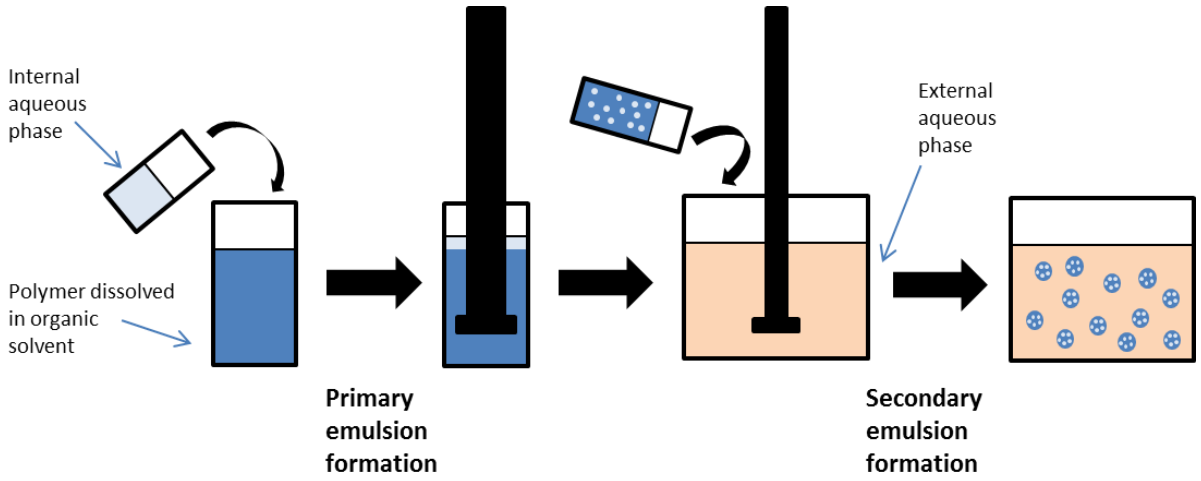


Figure 1.2: Schematic diagram of the double emulsion solvent evaporation method.

The s/o/w method is similar but involves dispersing the drug/growth factor directly into the polymer solution and then adding this to the aqueous continuous phase, whereas for the o/o/w double emulsion the drug/growth factor is dissolved in an organic solvent and then dispersed in a different organic solvent [146].

The advantages of this method include the simplicity of the procedure, the lack of complicated equipment and the ability to manipulate the processing parameters. It is also possible to incorporate proteins into the microspheres with good encapsulation efficiencies; in addition to maintaining their biological activity [148]. For these reasons, this method was adapted in the present study [147].

1.6.2.2 Release profiles of PLGA microspheres

As the end goal is to use the PLGA microspheres as a scaffold system within the body, the release of any bioactive agents should ensue in a manner that is similar to the *in-vivo* release kinetics. It is important to study how the encapsulated agents, such as proteins, are released from PLGA microspheres and the characteristics of their release profiles. PLGA microspheres have been reported to follow a tri-phasic release profile involving both erosion

and diffusion [149], which consists of an initial burst release, followed by a lag phase and then ending with a linear phase [149, 150].

The initial burst release is caused by the release of any surface-bound agent; whereas, the lag phase is a result of the inability of the entrapped agent to escape from the hydrophobic PLGA matrix [148]. This lag phase remains until the PLGA backbone has significantly eroded via ester hydrolysis, which allows the encapsulated agent to escape [151].

The type of release profile required depends on the agent that is being encapsulated. In this work, BMP-2 is the protein of interest. Cho et al. [152] reported the early induction of BMP-2 on day 1 of normal fracture healing, suggesting that an initial release of protein would be favourable. It has also been reported that the genes encoding BMP-2 are upregulated for four weeks in uncomplicated fracture healing, which demonstrates that a sustained release profile is also desirable [153].

Previous studies have utilised other agents in combination with PLGA in order to tailor the release profile of proteins from the microspheres. The addition of a PEG triblock polymer resulted in a release profile that was decoupled from the matrix degradation, which followed a quasi-zero order profile over 4 weeks [35].

1.6.2.3 Sintering of microspheres

The sintering of microspheres is crucial as it is the means by which the individual discrete microspheres bond/stick together to become intact scaffolds. This can either happen *in situ* (i.e. in the body at 37°C) or in the laboratory. Various methods have been investigated for the sintering of microspheres. Strategies include the incorporation of plasticizers in order to reduce the polymer T_g [154], the application of heat [106, 120, 155] and the addition of

organic solvents such as DCM [156, 157]. Although the use of high temperatures and organic solvents result in scaffolds of high mechanical strength, these techniques are not preferential for sintering *in-situ,* as such conditions would be detrimental to the body.

1.7 The use of stem cells

Stem cells are not committed to a specific lineage, as other cells in the body are. Multipotent and pluripotent stem cells are types of undifferentiated cells that are extremely useful in the field of tissue engineering due to their ability to differentiate in multiple tissue types. Mesenchymal stem cells (MSCs) and progenitor cells that can be found in adult connective tissue are multipotent cells meaning that they are able to differentiate into a variety of different mesenchymal tissues, one of which being bone, making them a good choice in bone tissue engineering [158–161] . In adults they can be isolated from the bone marrow and adipose tissue, or from the umbilical cord blood and placenta [158]. They are able to undergo extensive proliferation in culture conditions due to the presence of the telomerase enzyme, which enables the duplication of telomere DNA (which usually loses 50–100 base pairs during telophase), hence, ensuring that the cells are able to divide and replicate for an extended period of time [162]. This feature makes MSCs an attractive choice for use in the present application [163]. Interestingly, cultured MSCs have been found to have an immunosuppressive effect both *in vivo* and *in vitro*, which is thought to be mediated by various soluble factors such as; prostaglandin E2, interleukin-10 and transforming growth factor ß [164].

The use of stem cells alongside the scaffold material is an important component of bone tissue engineering. There are numerous factors to consider when deciding upon the source of the stem cells, which include autologous (the patient's own) cells or allogenic cells (from another person). The availability of tissue with minimal morbidity at the donor site and the

use of cells with a limited potential for proliferation (e.g. primary osteogenic cells), or stem cells that are self-renewing, are other factors that need to be considered [165–167].

1.8 Project aims and overall plan

From the literature, it is apparent that bone tissue engineering has the potential to have a significant clinical impact on patients with defective bone growth. Various materials have been investigated, as described above, including natural and synthetic polymers. The injectable delivery route is an attractive strategy in bone tissue engineering as it would circumvent the need for invasive bone graft procedures. Therefore, the overall aim of this project was to develop a porous, protein-loaded microparticulate scaffold system for potential use in bone regeneration.

The project is described in four chapters, each with specific objectives, as highlighted below.

Chapter 2:

- To successfully produce a protocol for the production of porous microspheres, including the investigation of methods to increase their porosity.

Chapter 3:

- To study the release profiles of a model protein from microspheres prepared with various molecular weights of PLGA.
- To formulate sintered scaffolds from porous and non-porous protein-loaded microspheres.
- To determine the release profiles of a model protein from the above scaffolds.

Chapter 4:

- To determine the effects of various coatings on the release of protein from PLGA microspheres.

Chapter 5:

- To characterize a PLGA/chitosan microsphere system and determine its injectable potential.
- To investigate the attachment, proliferation and differentiation of primary bone marrow derived MSCs on PLGA/chitosan microsphere sintered scaffolds.

A summary of the experimental work carried out in this project is shown in **Figure 1.3.**

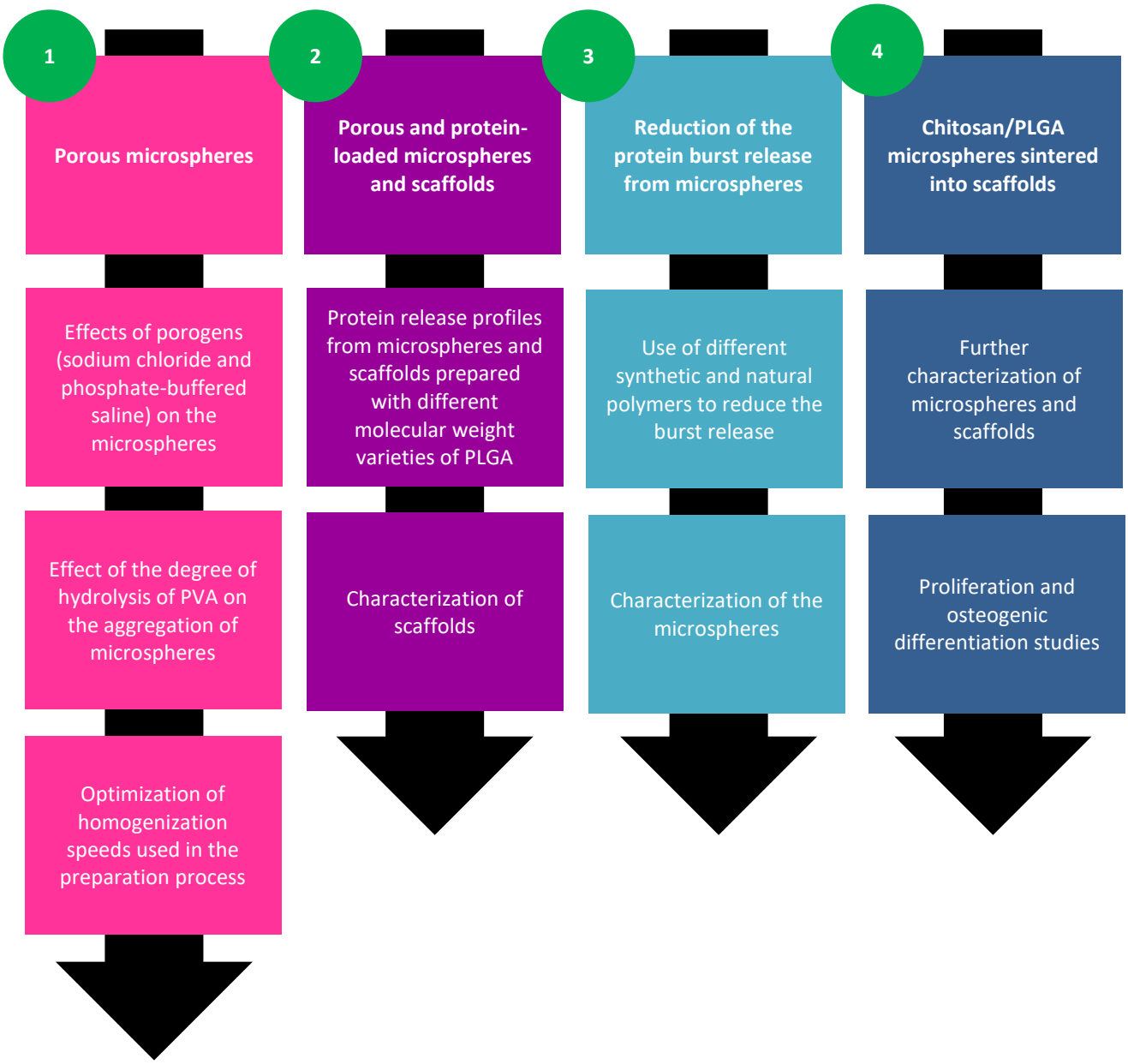


Figure 1.3: Overview of the experimental work carried out in the project.

Chapter 2: Formulation of porous PLGA microspheres for bone tissue engineering

2.1 Introduction

Scaffolds for use in bone tissue engineering must be sufficiently porous in order to allow proliferating cells access to nutrients, whilst at the same time, maintaining a suitable degree of mechanical strength that matches with the requirement of the specific tissue in question [14, 16, 23, 123]. Porous microspheres have been found to promote cell proliferation during cartilage regeneration, in addition to enhancing the deposition of collagen and glycosaminoglycan in comparison with non-porous microparticulate systems [168]. Porosity may be increased in scaffolds via the introduction of pores within microspheres. This was previously demonstrated by Qutachi et al. [142] via the formulation of porous PLGA microspheres using the double emulsion solvent evaporation method that form solid porous scaffolds at body temperature. Variations of this method have also been investigated in an attempt to induce porosity using various porogens such as ammonium bicarbonate [120, 169–172], phosphate-buffered saline (PBS) [142], hydrogen peroxide [173], sodium oleate [174], sodium chloride [175] and Pluronic F127 [176, 177].

The kinetics of the polymer precipitation step during formulation is important such that if the polymer precipitates rapidly, then it will harden while there are still solvent droplets present, leading to a porous structure [178]. On the other hand, at a slower rate of polymer precipitation, the solvent is more likely to have been removed, resulting in denser (less porous) microspheres [178].

The mechanism via which ammonium bicarbonate works involves the liberation of carbon dioxide and ammonia gas, which forms pores when the primary water in oil emulsion comes into contact with the second water phase. Gas is liberated throughout the early stage of formation of the PLGA microspheres, leading to droplet volume expansion and the stabilisation of enlarged inner phase aqueous droplets from coalescence during the phase of

solvent evaporation. This maintains a macroporous structure until the microspheres solidify [179].

A study by Wang et al. [120] looked at the effect of various concentrations of ammonium bicarbonate in the production of PLGA microsphere-sintered scaffolds. They found that the porosity increased with higher concentrations of ammonium bicarbonate and that its presence led to higher cell viability after 14 days. Enhanced cell proliferation of synovium-derived MSCs was also observed. They concluded that of the two types of pores present within the scaffold, the pores between microspheres and the smaller pores on the surface of the microspheres, the ammonium bicarbonate had an effect on the surface pores. It is thought that these small pores lead to a rough surface that subsequently enhanced cell attachment and proliferation [120].

Another study carried out by Mittal et al [172] examined the porosity of microspheres produced by varying the amount of ammonium bicarbonate. As the concentration of ammonium bicarbonate increased from 0 to 15% the microsphere size increased from 200 to 357 μm, with the maximum porosity of 81.2% attained when 15% of ammonium bicarbonate was used [172]. Another observation was that the microspheres containing less ammonium bicarbonate degraded more rapidly. This was attributed to the degradation products being entrapped within the microsphere structure, as there were more closed pores (rather than uniformly distributed, open, interconnected pores), which then served as autocatalysts for further degradation [172].

Sodium chloride functions as a porogen by leaching during various aqueous washing steps [180]. An example of its use was in the formation of microspheres loaded with oligonucleotides by Ahmed et al. [175]. Varying amounts of sodium chloride were added, from 0–100 mg/ml of water, to PLGA solutions of varying molecular weights and lactic acid

content. The resulting microspheres were porous and it was observed that as the sodium chloride concentration increased the microspheres became larger in size. Porosity was seen to increase as the molecular weight and lactic acid content increased. This was attributed to the more rapid precipitation of the polymer [175]. The same group also used glycerol monooleate as a pore forming agent; however, the resulting microspheres were much less spherical and more irregular in shape [175]. Bae et al. [173] also reported that as they increased the molecular weight of PLGA used to prepare their microspheres, they observed an increase in the porosity, which they attributed to the intrinsically poor mechanical and physical properties of the low molecular weight PLGA.

Sun et al. [174] produced spherical PLGA microspheres using sodium oleate, a salt of the fatty acid oleic acid, as a porogen to create interconnected pores. They used the w/o/w double emulsion solvent evaporation method described previously, and found that as the weight ratio between sodium oleate and PLGA increased, the size of the microspheres and the pore size increased. The maximum microparticle diameter that they attained was 12.91 ± 2.10 µm, with a maximum pore size of 1.53 ± 0.62 µm [174].

The focus of this chapter was to successfully formulate a reproducible protocol for preparing porous PLGA microspheres using the double emulsion solvent evaporation method. The reproducibility is important as it is one of the major constraints in the formulation of microspheres. Furthermore, different methods of controlling the porosity were explored and the effect of the degree of PVA hydrolysis on microsphere aggregation was also investigated.

2.2 Materials and methods

2.2.1 Materials

PVA (CAS: 9002-89-5), fully hydrolysed and 87–89% hydrolysed, was obtained from Sigma-Aldrich (USA). PLGA (CAS: 26780-50-7) 85:15 ratio was obtained from Lakeshore Biomaterials (manufactured by Evonik Degussa Corporation, Birmingham Laboratories, USA). Sodium chloride (CAS:7647-14-5), AR grade, was obtained from QRëc (Malaysia) and Fisher Scientific (USA). DCM, HPLC and AR grade, was obtained from Fisher Scientific. Sodium dodecyl sulphate PhEur was obtained from Merck (USA). PBS tablets (0.01 M phosphate buffer, 0.0027 M potassium chloride and 0.137 M sodium chloride, pH 7.4 at 25°C) were obtained from Sigma-Aldrich, in addition to PBS tablets (1 tablet to be dissolved in 100 ml of water) from Fisher Scientific. Sodium hydroxide (CAS: 1310-73-2) was obtained from Sigma-Aldrich.

2.2.2 Preparation of PVA solution

PVA solution (0.3% w/v) was prepared using the two methods described in sections 2.2.2.1 and 2.2.2.2. The use of PVA at a concentration of 0.3% w/v was based on previous work by Kirby et al. [138].

2.2.2.1 Preparation of PVA solution from water

Distilled water (400 ml) was heated on a magnetic stirrer (LMS Harmony Hotplate Stirrer HTS1003) at 180 rpm until the temperature reached 70°C. PVA (1.2 g) was added, with the temperature and stirring speed maintained until the PVA dissolved. The resulting solution was then cooled and filtered under vacuum.

2.2.2.2 Preparation of PVA solution in PBS

PBS (pH 7.4) was prepared by dissolving 2 tablets in 400 ml of distilled water and stirring on a magnetic stirrer at 180 rpm until both tablets were fully dissolved. The PBS was

then heated and once a temperature of 70°C was reached, 1.2 g of PVA was added. Temperature and constant stirring were maintained until the PVA was fully dissolved. The resulting solution was then cooled and filtered under vacuum.

2.2.3 General method for the preparation of porous microspheres

PLGA (1 g) was dissolved in 5 ml of DCM in a polytetrafluoroethylene (PTFE) jar (Fisher brand; 60 ml capacity, 46 mm height, 60 mm diameter; or 30 ml capacity, 62 mm height, 34 mm diameter) and placed on an orbital shaker (Yih Der TS 520, Taiwan; or IKA Sonuttler MTS-4) for 30 minutes (or until the PLGA was fully dissolved). The required volume of porogen (sodium chloride solution, ammonium chloride solution or PBS) was added to the PLGA/DCM solution and homogenized (Silverson high shear laboratory mixer L5M-A, Silverson, UK) at 9000 rpm for 2 minutes in order to form the primary emulsion. The primary emulsion was transferred in a single addition to 200 ml of the previously prepared PVA solution, which was then homogenized at 3000 rpm for 2 minutes using the same Silverson homogenizer in order to form the secondary emulsion.

The secondary emulsion was stirred using a glass stirrer bar (50 mm length, 8 mm diameter) on a multi-plate magnetic stirrer (RO 15 power IKA-WERKE or Thermo Scientific Variomag Poly Stirrer, USA), at 300 rpm for varying times (2 minutes, 3 minutes or 4 hours) to allow the evaporation of the DCM. In the case of some preparations, aggregation was observed after 2 or 3 minutes. The microspheres in these formulations were immediately sieved (Wheaton & WS Tyler Sieve, no. 230, 63 μm, USA) after this short stirring time in order to remove any remaining DCM and the microspheres were collected with distilled water.

Microspheres were washed and centrifuged (Eppendorf Centrifuge, Germany; or MSE Mistral 1000, UK) at 4500 rpm at 21°C for three sets of 5 minutes and then frozen using

liquid nitrogen prior to freeze-drying at -20°C and 1.0 mbar for 48 hours (Freeze Dryer Alpha 1-2 LD Plus or Thermo fisher Scientific FR-Drying Digital Unit Modulyod-230).

2.2.4 Variations to the general protocol

2.2.4.1 Alternative procedure for the production of microspheres

Microspheres were produced using the general procedure outlined above, and stirred for 2 minutes, as detailed in section 2.2.3. The double emulsion was then transferred into 600 ml of distilled water, stirred for 1 hour at 300 rpm and allowed to stand before carrying out the processes of centrifugation and freeze-drying.

2.2.4.2 Effect of temperature

The effect of temperature on the outcome of the obtained material was studied at 25, 27, 30, and 40°C using an electric, temperature-controlled water bath. The lower temperature range (25–30°C) was chosen as it represented possible temperature fluctuations in the laboratory. The upper limit of 40°C was chosen as it is just above the boiling point of DCM (39.75°C) [181].

2.2.4.3 Effect of maintaining pH at 7.4

The pH of the preparation procedure was maintained at 7.4 by preparing PVA solution in PBS instead of distilled water, as described in section 2.2.2.2. Aside from the alteration to the PVA solution, the method remained as detailed above.

2.2.5 Effect of porogens

2.2.5.1 Sodium hydroxide

Microspheres were prepared using sieving to accelerate the DCM extraction step and were treated with sodium hydroxide to further open up any pores present. A 0.5 M sodium hydroxide and 96% ethanol solution was prepared at a ratio of 30:70, respectively. A 10-ml

aliquot of this solution was added rapidly to 300–350 mg of sample, whilst on a vortex mixer and vortexed for 7 minutes. The sample was then poured into a 40-µm cell strainer (BD Falcon, 40 µm, nylon) and washed with water for 2 minutes. The excess water was removed from the cell strainer using blue roll and the microspheres were then freeze-dried in the cell strainer.

2.2.5.2 Sodium chloride

Microspheres were prepared using PBS/PVA, as detailed in section 2.2.2.2. Aliquots of a 1.71 M aqueous solution of sodium chloride were added to the PLGA DCM solution to create the primary emulsion as a substitution for PBS as a porogen. This primary emulsion was then added into the PVA aqueous phase and homogenized at 3000 rpm for 2 minutes, stirred for 4 hours at 300 rpm, centrifuged and freeze-dried as detailed in section 2.2.3.

2.2.6 Effect of primary and secondary emulsion homogenization speed on the resultant microspheres

The stirring speeds during the formation of the primary and secondary emulsions were varied from 1000 to 9000 rpm and 1000 to 3000 rpm, respectively. These investigations were carried out when PBS and sodium chloride were used as porogens. All formulations were stirred for 2 minutes at both the primary and secondary emulsion formation stages.

2.2.7 Characterization of microspheres

2.2.7.1 Scanning electron microscopy (SEM)

Samples were mounted on metal stubs and viewed under the electron microscope (FE-SEM, Quanta 400F, FEI, USA). For a more detailed view, the samples were mounted on metal stubs, coated in gold and viewed under the electron microscope (LEO 1450- LEO Company Ltd, UK) with the accelerating voltage set between 5 and 20 kV. The samples were also viewed under a variable pressure electron microscope (JEOL 6060LV, Jeol UK Ltd,

UK); however, these samples were coated in gold for 6 minutes (Leica EM SCD005 Sputter Coater, Leica Microsystems) prior to viewing.

2.3 Results and Discussion

2.3.1 General procedure

Aggregation of the microspheres ensued at the solvent extraction stage after 3–5 minutes of stirring the secondary emulsion. This aggregation prevented any microspheres from being collected. Various approaches were investigated in order to overcome this problem, including the use of a sieve (Wheaton & WS Tyler sieve No. 230; 63 µm) in order to accelerate the removal of DCM and the formation of microspheres. The sieving of the secondary emulsion prevented the aggregation of microspheres. The microspheres prepared using this method are presented in **Figure 2.1**. **Figure 2.1A** shows the microspheres prepared with 5 minutes of stirring, followed by sieving. The mean microsphere diameter was calculated using the ImageJ software and was found to be 93.3594 ± 19.4340 µm. The high magnification image presents a representation of the pores present in one of the microspheres, with a mean pore diameter of 1.7689 ± 0.7577 µm (also determined using ImageJ). **Figure 2.1B** shows microspheres prepared with 2 minutes of stirring in the hardening bath, followed by sieving. The mean microsphere diameter was found to be 70.8196 ± 20.7531 µm, with a mean pore diameter of 2.0498 ± 0.8140 µm. The relatively smaller size of the microspheres obtained after stirring for 2 minutes compared to those stirred for 5 minutes prior to sieving may be attributed to the fact that longer stirring times induce aggregation.

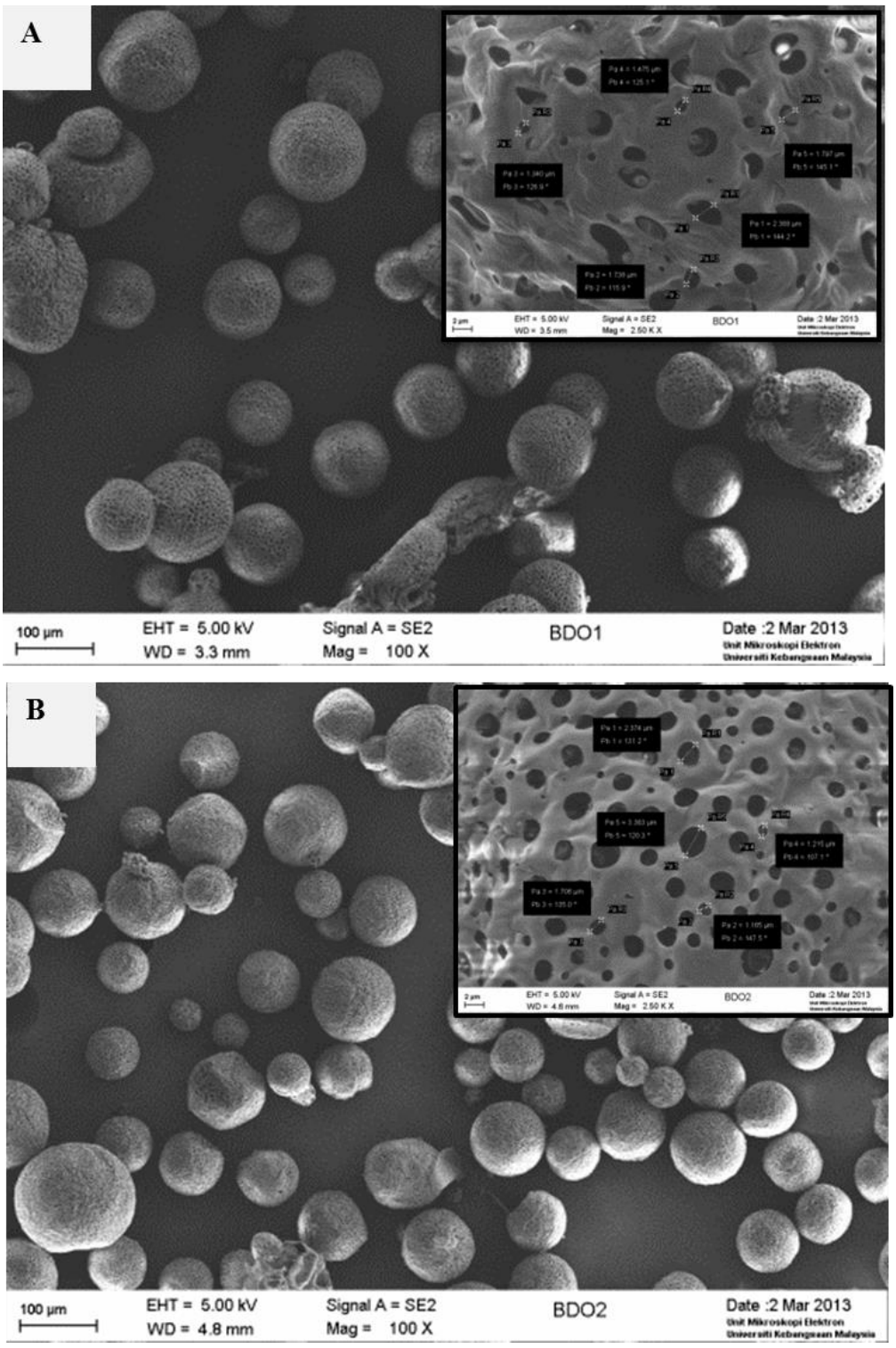


Figure 2.1: SEM images of PLGA microspheres prepared using the double emulsion solvent evaporation method following the general protocol with 5 minutes (A) and 2 minutes (B) of stirring followed by sieving (aperture size of 63 µm). Insert images represent close-up images of individual microspheres.

2.3.1.1 Control of temperature

Microspheres were prepared in a controlled temperature environment via the use of a water bath set at a range of temperatures; 25, 27, 30 and 40°C. After the formation of the secondary emulsion, the DCM dissolves in the PVA solution (solvent extraction) and then evaporates at the liquid-air interface (solvent evaporation) [182]. Mehta et al. [183] reported that the preparation temperature influences the rate of solvent removal during the solvent evaporation phase, which can also have an effect on the microsphere morphology. However, the results showed that, even when the solvent evaporation step was accelerated, the microspheres still aggregated and, hence, it was not possible to collect them. This indicates that the aggregation was not caused by slow solvent removal. The effects of the maintenance of the pH at 7.4, and the degree of hydrolysis of the PVA in the external aqueous phase on the microsphere aggregation are discussed in section 2.3.1.2 and 2.3.3.

2.3.1.2 Maintenance of pH at 7.4

The next parameter that was tested in order to identify the root cause of the aggregation was the effect of maintaining the pH of the external aqueous phase at 7.4. In order to test the effect of pH on the aggregated microspheres, the PVA solution was prepared in PBS, which maintained the pH at 7.4. However, this resulted in a dramatic change in the microsphere morphology, with the resulting microspheres losing their surface porosity, as shown in **Figure 2.2.** It has been reported that aqueous porogens create an osmotic effect that is crucial for their mechanism of action, in which water is driven into the internal phase from the external aqueous phase [170]. Nasr et al. [184] hypothesised that the porogen then escapes into the external aqueous phase during the solvent extraction/microsphere hardening step. The lack of an osmotic concentration gradient between the internal and external aqueous phases, which both contained PBS, may account for the lack of surface porosity observed in

the case of the microspheres prepared with PVA/PBS solution. Alternatively, when the porogen, PBS, was substituted with sodium chloride solution, porous microspheres were formed, as shown in **Figure 2.3.** The inclusion of the sodium chloride into the internal aqueous phase creates an osmotic gradient for water from the external aqueous phase to enter the internal phase. Nasr et al. [185] varied the concentration of sodium chloride in both the internal and external aqueous phases. The use of high concentrations of sodium chloride exceeding 5% as an internal porogen resulted in the rapid movement of water from the external to the internal aqueous phase, resulting in the burst of the microspheres. When the sodium chloride concentration was equilibrated between both phases only a few pores were visible [185].

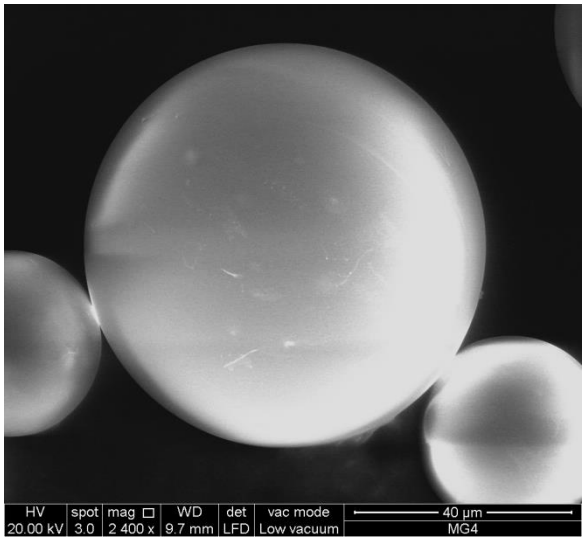


Figure 2.2: SEM image of PLGA microspheres prepared with a pH-controlled aqueous phase, using PBS as a porogen.

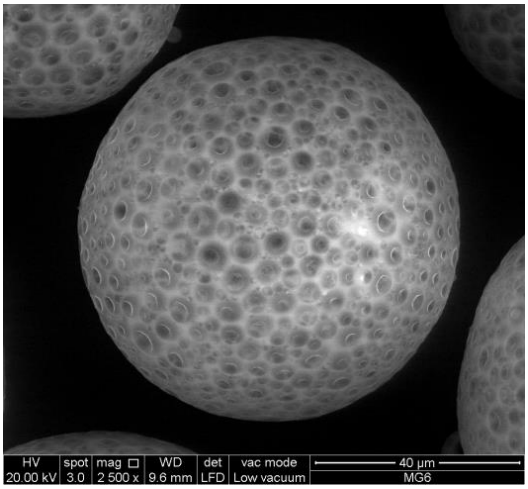


Figure 2.3: SEM images of PLGA microspheres prepared with a pH controlled aqueous phase using sodium chloride solution as a porogen.

2.3.2 Methods to increase porosity in microspheres prepared using a pH-controlled external aqueous phase

2.3.2.1 Sodium chloride as a porogen

The volume of sodium chloride solution (10 % w/v) added to the primary emulsion to act as a porogen was varied from 250 to 750 µL in a pH 7.4-maintained environment (as detailed above) in order to determine if the change in volume affected the porosity. It was thought that a higher internal aqueous phase volume would result in a more porous structure due to the larger initial pore volume. It has been previously reported that the internal volume can affect the shell-layer morphology [186]. Other researchers have reported the effect of a change in concentration of sodium chloride [185]; however, variation in the internal volume has not previously been investigated. **Figure 2.4** shows the results of varying the sodium chloride volume. From the SEM images, there is not much difference between microspheres prepared with 250 and 500 µL of sodium chloride solution. When 750 µL of sodium chloride solution was added, the size distribution became wider, with more polymer debris present between the microspheres. As the internal aqueous phase gets larger there may be larger porogen-filled spaces dispersed within the polymer solution for water in the external aqueous

phase to enter. This could lead to weaker, thinner microspheres, which may account for the presence of polymer debris.

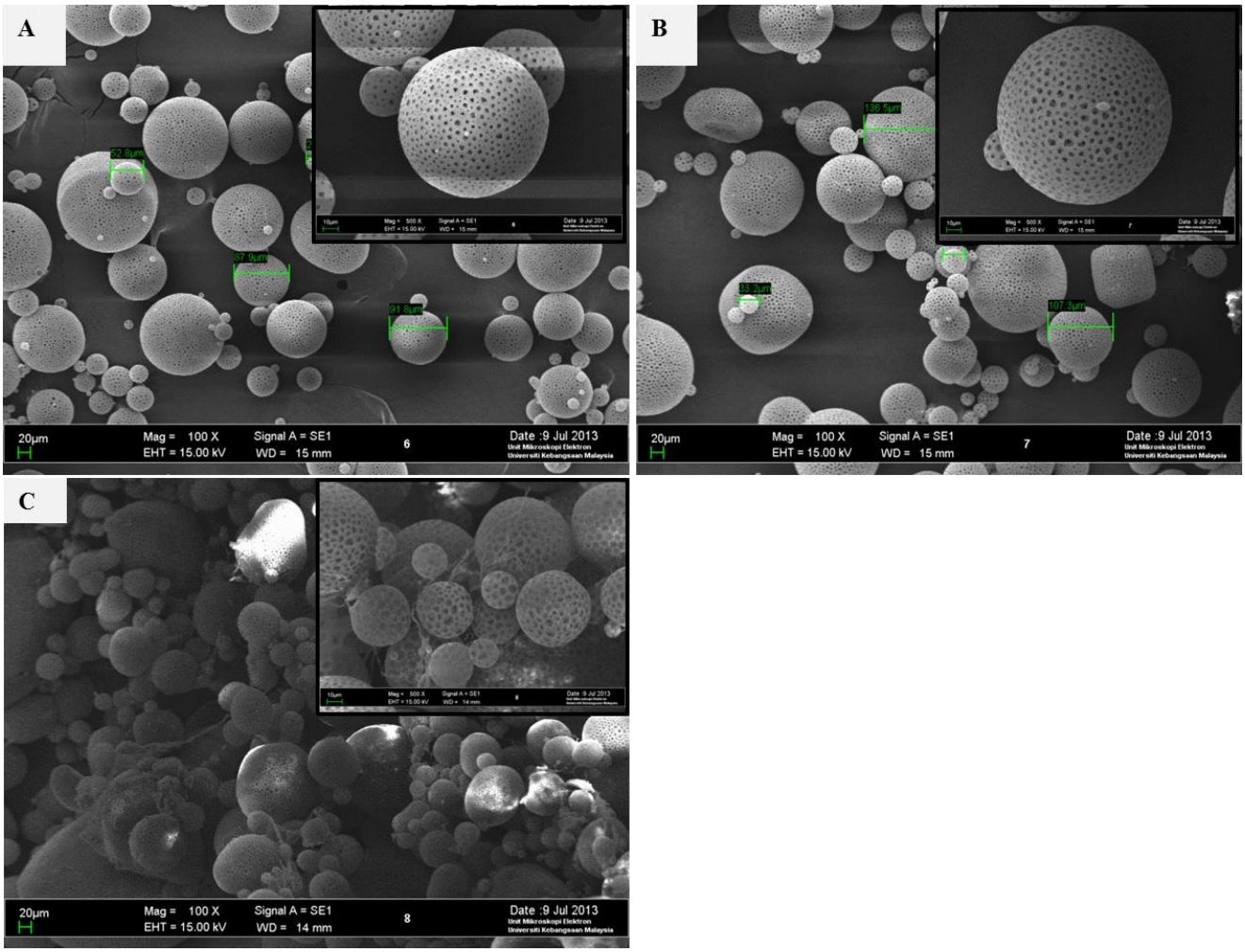


Figure 2.4: SEM images of PLGA microspheres prepared with 250 µL (A), 500 µL (B) and 750 µL (C) of sodium chloride solution (10 % w/v) as a porogen in a pH-controlled environment.

2.3.3 Degree of hydrolysis of PVA

The effect of the degree of hydrolysis of the PVA on the propensity of the microspheres to aggregate was examined by studying their resultant morphology. Microspheres prepared using fully hydrolysed PVA exhibited aggregation after just a few minutes of stirring the secondary emulsion. Conversely, when the degree of hydrolysis was 87–89% this aggregation was not observed, as shown in **Figure 2.5.**

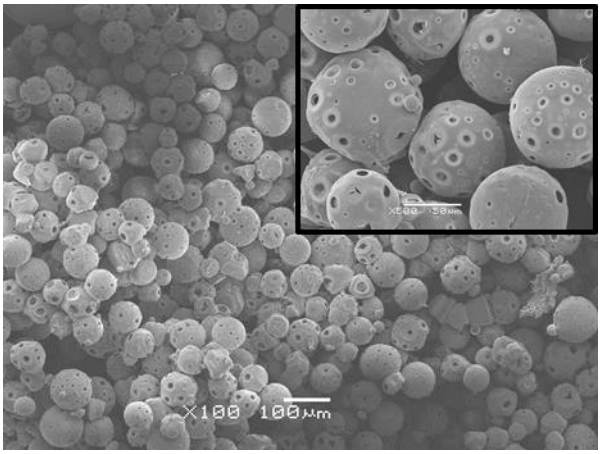


Figure 2.5: SEM images of PLGA microspheres prepared using partially hydrolyzed (87–89%) poly (vinyl alcohol).

Therefore, it appears that the PVA itself plays a role in the aggregation of the microspheres. The reasoning behind PVA's role in the aggregation of the microspheres is due to the fact PVA is moderately soluble in water due to weaker hydrogen bonding between PVA's hydroxyl groups and water when compared to intra-hydrogen bonding within PVA molecules [187]. Therefore, with a higher degree of PVA hydrolysis, the hydrophilicity decreases. A study into the effect of the degree of PVA hydrolysis on the formation of PLGA nanoparticles by Murakami et al. [188] postulated that hydrophobic portions of the PVA molecule are adsorbed onto the surface of the nanoparticles. The hydration of the PVA molecules on the surface of the nanoparticles, which results in a stable dispersion, are more likely to be hindered when the level of PVA hydrolysis is high as there is a greater inclination for hydrogen bonds to form inter- and intra-molecularly rather than with water molecules. This in turn leads to the aggregation of the particles. When the degree of hydrolysis is lower, the acetoxyl group provides steric hindrance, which reduces the amount of intra- and inter-molecular hydrogen bonding, hence, creating a dispersion that is more stable [188]. The lack of aggregation observed when the sieving method was used could also support this theory. In this amended method the microspheres were washed and collected to prevent the adsorption

of the PVA on the surface of the microspheres. It was, therefore, decided that the partially hydrolysed PVA would be used for all future studies.

2.3.4 Porosity of microspheres prepared with partially hydrolysed PVA

2.3.4.1 Porogens

Sodium chloride solution (10% w/v) and PBS were investigated as possible porogens with the use of partially hydrolysed PVA in the external aqueous phase. The morphology of the microspheres prepared using sodium chloride solution was less spherical, with larger, but more irregular pores and an overall larger size, as shown in **Figure 2.6**. The change in pore size could be attributed to the wider osmotic gradient created between the PVA and the inner aqueous phase for the microspheres prepared using sodium chloride, when compared with those prepared with PBS. Hence, an increased amount of water would have been encouraged to penetrate through the polymer, causing the internal droplets to swell to a greater degree and create larger pores, possibly leading to a more irregular shape. The irregular shape may be due to the formation of thinner microsphere walls as a result of a larger amount of pores, which makes the microspheres more prone to collapse.

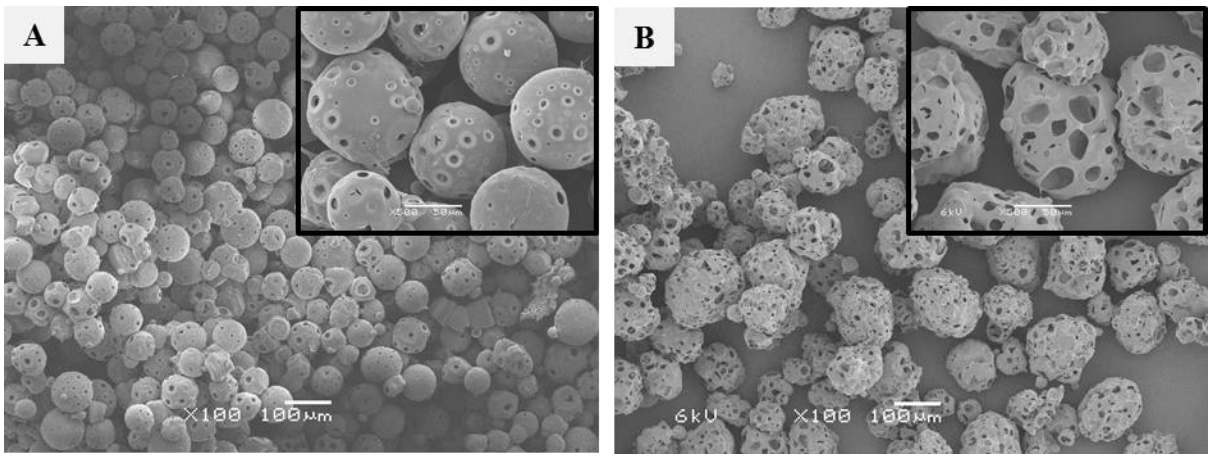


Figure 2.6: SEM images of PLGA microspheres prepared with partially hydrolyzed PVA using PBS (A) and sodium chloride solution (B) as pore forming agents.

2.3.4.2 Effect of homogenization speeds on microsphere morphology

The speed at which the primary emulsion was homogenized was varied from 1000 to 9000 rpm in order to see if this affected the porosity of the microspheres. Both PBS and sodium chloride were used as pore-forming agents in order to determine if there was variation between the porosity induced by the two agents and homogenization speeds. The results of this series of PBS preparations are shown in **Figure 2.7**. The figure shows a clear difference in the pores within the microspheres prepared at speeds from 1000 to 3000 rpm. There appears to be fewer pores within the microspheres and then from 4000 rpm onwards, a higher number of pores begin to present.

With the primary emulsion homogenization speed set at 1000 rpm, the resulting microspheres possessed no surface porosity, possibly because the energy put into the system to create the emulsion at this stage was not strong enough to disperse the internal aqueous phase, hence, leaving microspheres without pores. As the speed was increased to 2000 rpm and 3000 rpm a small number of pores began to emerge in the microspheres. However, at speeds of 4000 rpm and above, the microspheres gained more substantial porosity. At a speed of 9000 rpm the resultant microspheres appeared most porous after a qualitative examination of the SEM images.

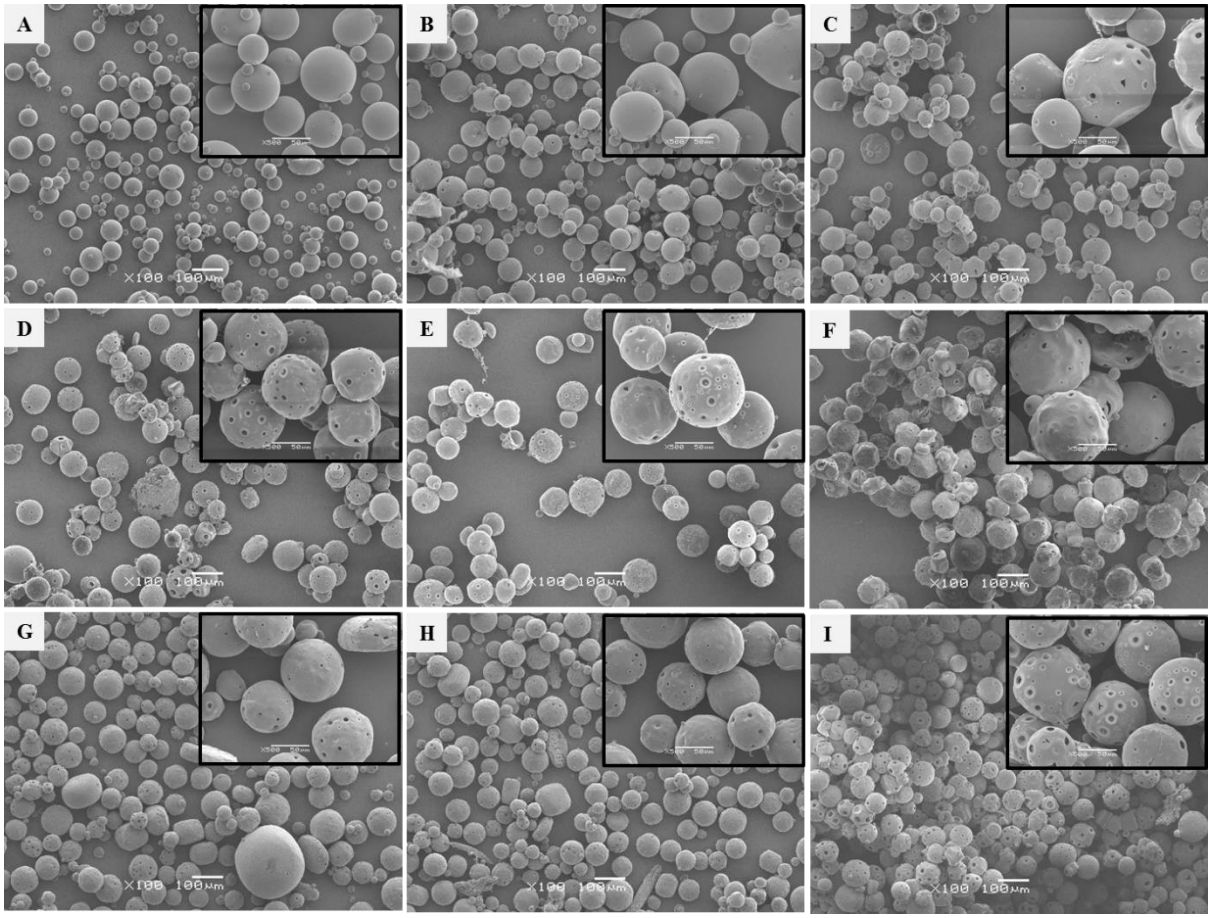


Figure 2.7: SEM images of PLGA microspheres prepared using the double emulsion solvent evaporation method using PBS as a pore-forming agent with varying primary emulsion homogenization speeds (A = 1000 rpm, B = 2000 rpm, C = 3000 rpm, D = 4000 rpm, E = 5000 rpm, F= 6000 rpm, G = 7000 rpm, H = 8000 rpm and I = 9000 rpm).

Microspheres prepared at a primary homogenisation speed of 9000 rpm (**Figure 2.7I**) were selected for further treatment due to the greater amount of surface porosity observed from the SEM images. They were treated with 30% 0.5 M sodium hydroxide: 70% absolute ethanol solution to observe if the pores could be effectively opened up, and the resultant microspheres are shown in **Figure 2.8**. After a qualitative assessment, the microspheres that were treated with sodium hydroxide (**Figure 2.8B**) appeared to have significantly larger pores than they did pre-treatment (**Figure 2.8A**).

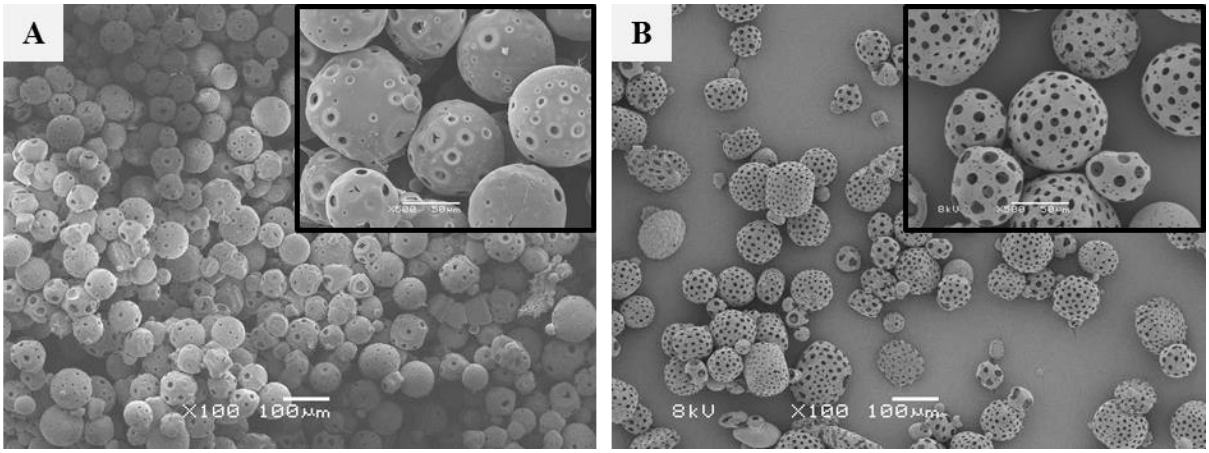


Figure 2.8: SEM images of PLGA microspheres prepared using the double emulsion solvent evaporation method, with PBS as a pore forming agent before (A) and after (B) treatment with 30% 0.5 M sodium hydroxide.

Preparations using sodium chloride as a porogen are shown in **Figure 2.9** and, again, show that when the primary emulsion was homogenized at 1000 rpm, the microspheres did not exhibit surface porosity. At 2000 and 3000 rpm there appears to be a loss of the spherical morphology with smaller microspheres mixed along with a few larger microspheres. From 4000 rpm onwards, the microspheres lost their spherical shape and developed a more irregular shape with a slightly rougher surface. This highly irregular and variable non-spherical shape is not desirable for their subsequent sintering with protein-loaded microspheres to form scaffolds as the protein release may, consequently, be more irregular. For this reason this formulation was not selected for further investigation.

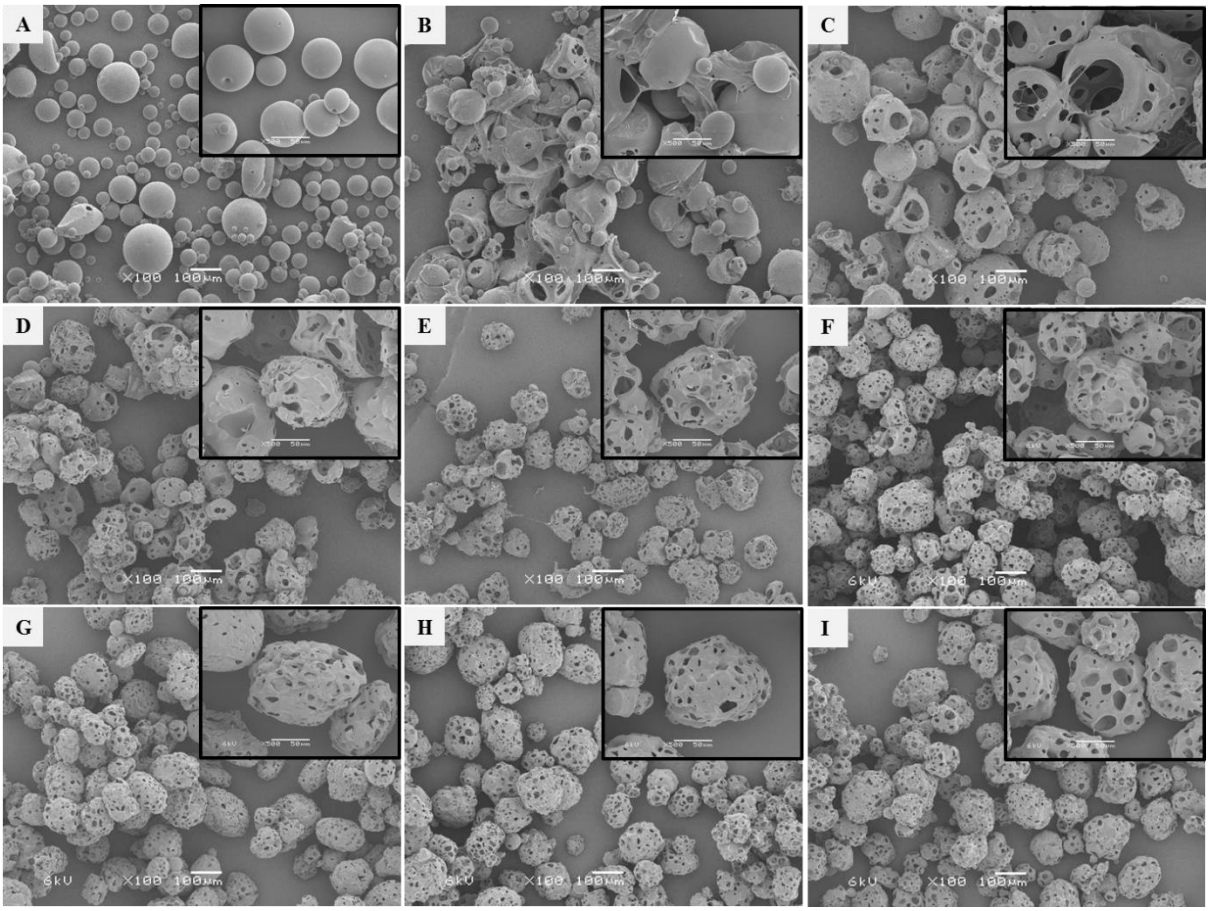


Figure 2.9: SEM images of PLGA microspheres prepared using the double emulsion solvent evaporation method using sodium chloride as a pore-forming agent with varying primary emulsion homogenization speeds (A = 1000 rpm, B = 2000 rpm, C = 3000 rpm, D = 4000 rpm, E = 5000 rpm, F = 6000 rpm, G = 7000 rpm, H = 8000 rpm and I = 9000 rpm).

2.3.5 Effect of homogenization speed of the secondary emulsion on the size of microspheres

The secondary emulsion homogenization speed is one of the parameters that has been reported to have an effect on the microsphere size. It provides the energy required to break up the droplets, with a higher homogenization speed decreasing the size of the microspheres due to more energy being provided to break up the droplets [189]. In this study the speed was decreased in order to investigate and confirm this effect. The speed at which the secondary emulsion was homogenized was varied from 3000 to 1000 rpm, the results of which are

shown in **Figure 2.10**. From the mean microsphere diameters presented in **Figure 2.11,** it is possible to see an emerging trend of increasing microsphere diameter with the decreasing homogenization speed, which agrees with previous reports [190].

The mean diameters of microspheres prepared using 3000 and 2500 rpm were very close, with approximately a 10 µm increase when the speed was reduced to 2000 rpm, followed by a 45 µm increase when the speed was decreased further to 1500 rpm. At the highest homogenization speed shown in **Figure 2.10**, the microspheres displayed more surface porosity, which may be due to the increased energy input associated with high speeds. Additionally, there is a narrower size distribution (**Figure 2.11**), which indicated better control over their size at this speed. This is due to the increased energy being applied to the polymer solution, which results in better dispersion of the polymer solution into droplets of a smaller size [191]. For these reasons, 3000 rpm was chosen as the secondary emulsion speed for all further work. Other factors that also affect the microsphere diameter include the viscosity of the polymer solution and the internal water phase and the PVA concentration [189].

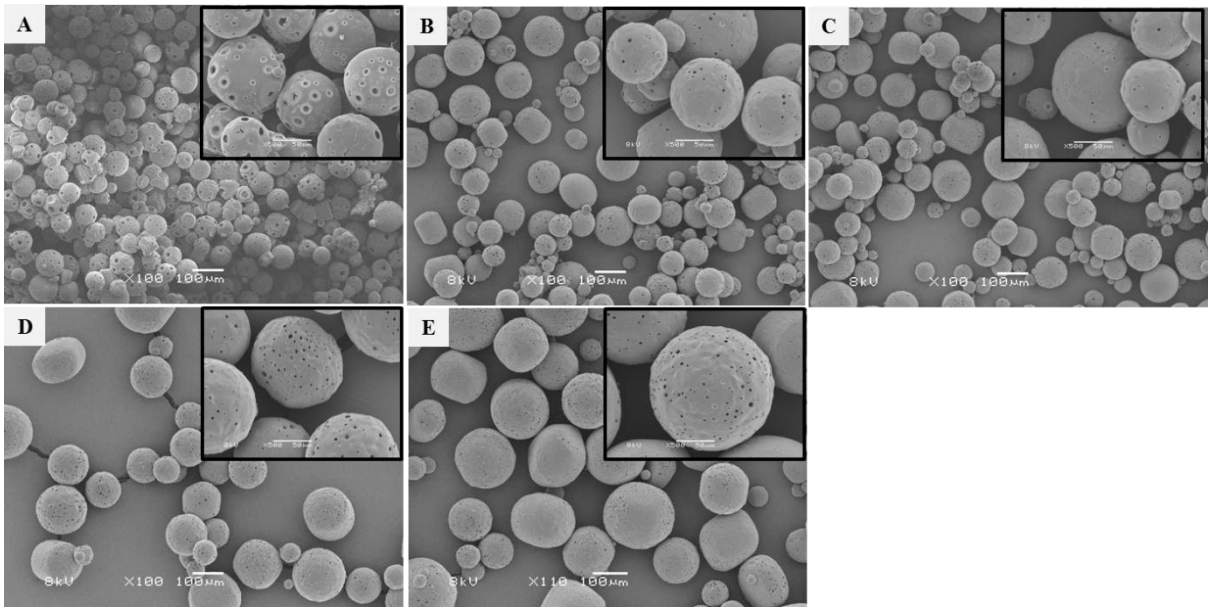


Figure 2.10: SEM images of PLGA microspheres produced using the double emulsion solvent evaporation method using PBS as a porogen with varying secondary emulsion homogenization speeds (A= 3000 rpm, B = 2500 rpm, C = 2000 rpm, D = 1500 rpm, E =1000 rpm).

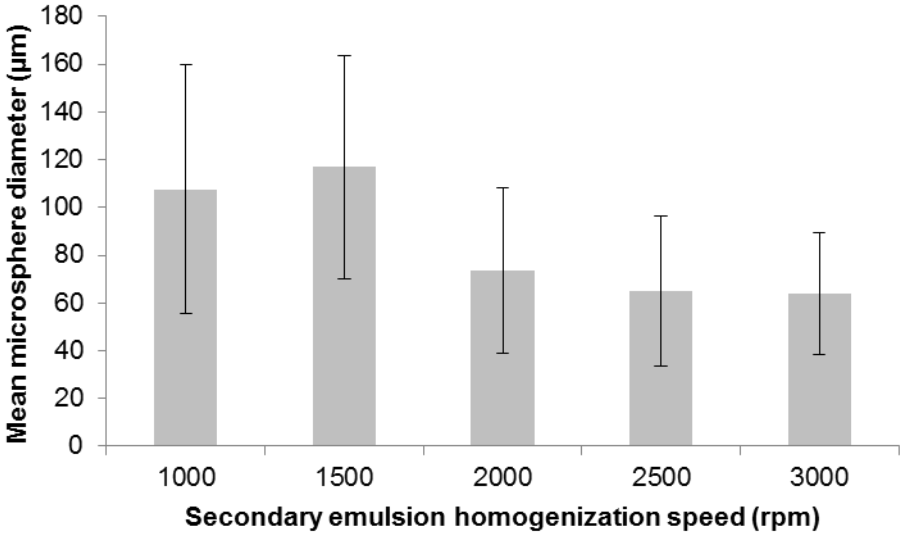


Figure 2.11: The effect of homogenization speed (rpm) of the secondary emulsion on mean microsphere diameter (µm).

2.4 Conclusions

In this chapter, preliminary work was carried out to investigate a porous microsphere preparation method. The degree of PVA hydrolysis was found to have a major impact on the feasibility of the microsphere production, with a fully hydrolysed variant eliciting aggregation of the microspheres during their formation. This resulted in the need to adapt the method in several ways, which included sieving the microspheres after just several minutes of stirring and preparing them in a pH-controlled environment. The use of a partially hydrolysed variant of PVA resolved this issue, which is thought to be due to the reduction in the hydrogen bonding between adjacent PVA molecules absorbed on the surface of the microspheres, and an increase in the hydrogen bonding between PVA molecules and water.

The primary emulsion homogenization speed was varied in order to determine the effect that this had on the porosity of the microspheres. Two distinct groups emerged; low levels of porosity from 1000 to 3000 rpm, and then moderate porosity from 4000 to 9000 rpm. The microspheres prepared with a primary homogenisation speed of 9000 rpm were selected for further work due to the observable higher levels of porosity. The secondary emulsion homogenization speed was also varied to determine its effect on the microsphere size; the results showed that the lower speeds resulted in larger microspheres. However, the highest speed, 3000 rpm, resulted in a smaller size distribution and more surface porosity. Based on these results, the parameters were set at 9000 rpm for the primary emulsion and 3000 rpm for the secondary emulsion for all further porous microsphere formulations.

The porogens sodium chloride and PBS were compared with sodium chloride, when prepared in the absence of a pH-controlled environment. The microspheres prepared with sodium chloride had larger pores, but a more irregular microsphere shape. The latter characteristic may not be ideal for regenerative medicine applications due to the lack of

control of the microsphere shape. Therefore, PBS was chosen for use in the future porous microsphere preparations.

Chapter 3: Physico-mechanical properties of sintered scaffolds formed from porous and protein-loaded poly (DL-lactic-co-glycolic acid) microspheres

3.1 Introduction

In Chapter 2, we described the successful development of a preparation procedure for porous microspheres. The delivery of growth factors is a key requirement in bone tissue engineering. BMPs can be used to simulate natural repair processes in injured bone tissue with good specificity and effectiveness. However, the disadvantages associated with using these proteins include their low stability, high cost and the requirement for high doses to elicit responses [38]. These constraints can potentially be minimised by adopting a sustained/targeted delivery approach to controlling both the rate and location of the growth factor delivery [39]. Such sustained delivery strategies have been explored by several research teams and include the encapsulation of growth factors within biodegradable PLGA microspheres prepared using the double emulsion solvent evaporation method [35, 138, 192]. Other methods such as phase separation [193] and spray drying [194] have also been employed for the encapsulation of proteins within microspheres.

In this chapter, we explore the formulation of protein-loaded microspheres to be used in conjunction with the porous microspheres described in Chapter 2. Due to cost constraints, lysozyme was used as a model protein for BMP-2. Lysozyme has been used previously as a model protein for BMP-2 due to their similar molecular weights (lysozyme, 14 kDa; BMP-2, 26 kDa) and isoelectric points (lysozyme, 9; BMP-2, >8.5) [35]. The lysozyme-loaded microspheres (non-porous) were similarly formulated using the double emulsion solvent evaporation method. This technique has been reported to yield good encapsulation efficiencies and retains lysozyme's biological activity [39, 148]. The capability of a microsphere-based delivery system to sinter into scaffolds is another key consideration, and this attribute has been investigated previously with the application of various strategies. These include the incorporation of plasticizers in order to reduce the polymer T_g [154], the

application of heat [106, 120, 155] and the addition of organic solvents such as DCM [156, 157]. Although the use of high temperatures and organic solvents result in scaffolds with high mechanical strength, these techniques are not practical for sintering *in-situ.* Therefore, a system that is able to sinter at 37°C would be desirable.

In this chapter, we aimed to formulate a lysozyme-loaded microsphere delivery system with injectable potential for possible use in bone regeneration. Whilst previous work has focused primarily on a single type of PLGA microsphere (with or without an additional biomaterial [156, 195]), this chapter reports the combination of porous and protein-loaded microspheres as a single delivery system. The effects of the PLGA molecular weight on the scaffold microstructure, mechanical properties and protein release were assessed.

3.2 Materials & Methods

3.2.1 Materials

PLGA (lactic acid: glycolic acid ratio, 85:15) of low (22–34 kDa), intermediate (53 kDa) and high (92–109 kDa) molecular weight was purchased from Evonik (USA). DCM, PBS, PVA and NaOH were acquired as detailed in Chapter 2 (section 2.2.1). Dimethyl sulfoxide (DMSO) and SDS were purchased from Fisher (UK). A micro BCA protein assay kit was purchased from Thermo Fisher Scientific (USA).

3.2.2 Formulation of microspheres

Porous PLGA microspheres of low (LMW), intermediate (IMW) and high molecular weight (HMW) were prepared using the double emulsion solvent evaporation method as described in the previous chapter (section 2.2.3) [142]. After the centrifugation step the microspheres were then suspended in 10 ml of ethanolic-NaOH solution (70% ethanol: 30% 0.5 M NaOH, pH 13.62) to enhance their porosity. The above suspension was vortex-mixed at 1400 rpm for varying durations, sieved (40 µm) and washed using distilled water.

Protein-loaded and blank non-porous microspheres were prepared in a similar way. Briefly, 100 µl of 100 mg/ml lysozyme solution or 100 µl of distilled water was added to a 20% w/v PLGA solution in DCM and homogenized at 4000 rpm using a Silverson L5M homogeniser to form the primary emulsion. This was then added to 200 ml of 0.3 % w/v PVA solution and homogenized at 2000 rpm to form the secondary emulsion. This was then stirred at 300 rpm for 4 hours to allow the DCM to evaporate and the microspheres to precipitate. The microspheres were washed with distilled water by centrifugation. All microspheres were freeze-dried using a Thermo Fisher Scientific FR-Drying Digital Unit (UK) for 48 hours and stored in a freezer until further use.

3.2.3 SEM and size analysis

The freeze-dried samples were gold-coated and viewed under the SEM as detailed in section 2.2.7.1 (Chapter 2). The average diameters of the microspheres were ascertained using a Coulter LS230 particle size analyser (Beckman, UK).

3.2.4 Differential Scanning Calorimetry (DSC)

The T_g of the porous PLGA microspheres pre- and post-treatment with ethanolic-NaOH was determined using a DSC (TA Q2000 and cooler RCS40- TA Instruments Delaware, USA) with a standard aluminium pan as the reference. Both the sample and the reference pan were heated from 0 to 250°C at 10°C/min using nitrogen as the purging gas at 50 ml/min. The first heating cycle was used for the assessment.

3.2.5 Encapsulation efficiency of lysozyme within microspheres

The encapsulation efficiency of lysozyme within the non-porous PLGA microspheres was determined by gently stirring of 10 mg of the freeze-dried microspheres in 750 µl of DMSO for 1 hour. This was followed by the addition of 2150 µl of 0.02% (w/v) SDS in 0.2 M NaOH. The solution was left to stand at room temperature for 1 hour. Standard

concentrations of lysozyme were calibrated with a BCA reagent so that the sample absorbance could be matched with standard concentrations on an Infinite 200 plate reader (Tecan, Switzerland) at 562 nm. The encapsulation efficiency (%EE) of lysozyme within the microspheres was then calculated using Equation 1.

$$\%\mathbf{EE} = \frac{\textbf{Actual mass of lysozyme in 10 mg of microspheres}}{\textbf{Mass of lysozyme used for 10 mg of microspheres}} \times \mathbf{100} \qquad \textbf{Equation 1}$$

3.2.6 Preparation of 3D scaffolds

PLGA scaffolds made from LMW, IMW and HMW PLGA were formed by mixing a 1:1 mass ratio of porous to non-porous microspheres in a weighing boat. Each of the three types of scaffolds contained an equivalent of 1, 2 or 3 mg of lysozyme per gram of total mixture. PBS (pH 7.4) was added to the microsphere mixtures at a ratio of 0.25:1 (v/w) and manually mixed to form a paste. The paste was packed into a 6-mm-diameter and 12-mm-height PTFE mould using a spatula and then stored in a sealed de-humidifying chamber for 17 hours at 37°C.

Table 3.1: PLGA scaffold formulations

Scaffold formulation	PLGA molecular weight[a]	Lysozyme loading (mg/ g of scaffold)
1	LMW	1
2	LMW	2
3	LMW	3
4	IMW	1
5	IMW	2
6	IMW	3
7	HMW	1
8	HMW	2
9	HMW	3

[a]LMW=22–34 kDa; IMW=53 kDa; HMW=92–109 kDa

3.2.7 Characterization of 3D scaffolds

The compressive strength of the scaffolds was assessed using a TA.HD+ texture analyser (Stable Microsystems, UK) equipped with a Peltier heating unit operated at 37°C and a 50 kg load cell. The test speed was set at 0.04 mm/second and the contact area of the

scaffold was 28.27 mm^2. Dry LMW, IMW and HMW PLGA scaffolds for all three loadings of lysozyme along with a lysozyme-free control were analysed in triplicate. The compressive strength was measured as the stress at the maximum strain.

The distribution of lysozyme on the surface of the scaffolds was assessed using a ToF-SIMS IV instrument (ION-TOF GmbH, Munster, Germany). Scaffolds were mounted on double-sided tape and attached to aluminium blocks, which were then secured on the ToF-SIMS stage. The surfaces of the scaffolds were bombarded with 25 keV of Bi^{3+} primary ions within a 256 × 256 pixel raster, while simultaneously not exceeding the limit of static, as previously described [196]. The resulting spectra were analysed and the secondary ions of fragments from lysozyme (CN^- and CNO^-) were added together and overlaid with those from the PLGA ($C_3H_3O_2^-$, $C_3H_5O_2^-$ or $C_2H_3O_3^-$), which were also combined together.

The porosity of the scaffolds was calculated based on the relative density (ρ) of the scaffold to PLGA using Equation 2 [108, 109].

$$\text{Porosity}(\%) = \left(1 - \frac{\boldsymbol{\rho}_{\text{scaffold}}}{\boldsymbol{\rho}_{\text{PLGA}}}\right) \times 100 \qquad \textbf{Equation 2}$$

3.2.8 Release of lysozyme from microspheres and scaffolds

The release profiles of lysozyme from the microspheres were studied using 50 mg of the non-porous lysozyme-loaded microspheres in 1.5 ml of PBS within a micro-centrifuge tube. The tubes were incubated at 37°C. At predetermined time intervals, all the PBS was removed and replaced with fresh buffer. Aliquots (150 µl) were withdrawn from the removed supernatant and assayed for their lysozyme content at 562 nm on the microplate reader using the BCA assay kit. Lysozyme release from the scaffolds were studied in 4 ml of PBS and assayed as described above.

3.3 Results and discussion

3.3.1 Microstructure and size analyses of porous and non-porous PLGA microspheres

Figure 3.1 shows SEM images of the porous microspheres treated with ethanolic-NaOH (A-C), and non-porous microspheres (D-F) loaded with lysozyme at various PLGA molecular weights. Longer treatment times with ethanolic-NaOH enhanced the porosity of the microspheres, but also compromised their structural integrity. The SEM images shown in **Figure 3.1(A-C)** represent the optimal ethanolic-NaOH exposure times for the LMW, IMW and HMW, which were 30 seconds, 1 minute and 1 minute 30 seconds, respectively. These optimal exposure times were based on a qualitative examination of the microspheres, such that they retained their integrity and imposed maximum observable porosity. There was a slight degree of fragmentation within the LMW microspheres, as shown in **Figure 3.1A** at this optimal treatment time; however, shorter treatment times did not yield sufficient porosity within the microspheres. From a qualitative inspection of the microspheres, the pore size distribution within the LMW microspheres appeared to be wider in comparison to those within the IMW (**Figure 3.1B**) and HMW (**Figure 3.1C**) microspheres, which were more uniform in size. The surface topography of the lysozyme-containing microspheres (**Figure 3.1D-F**) shows a relatively smooth surface, with no visible surface pores present. Furthermore, there was no apparent difference in the surface topographies of the microspheres in this series.

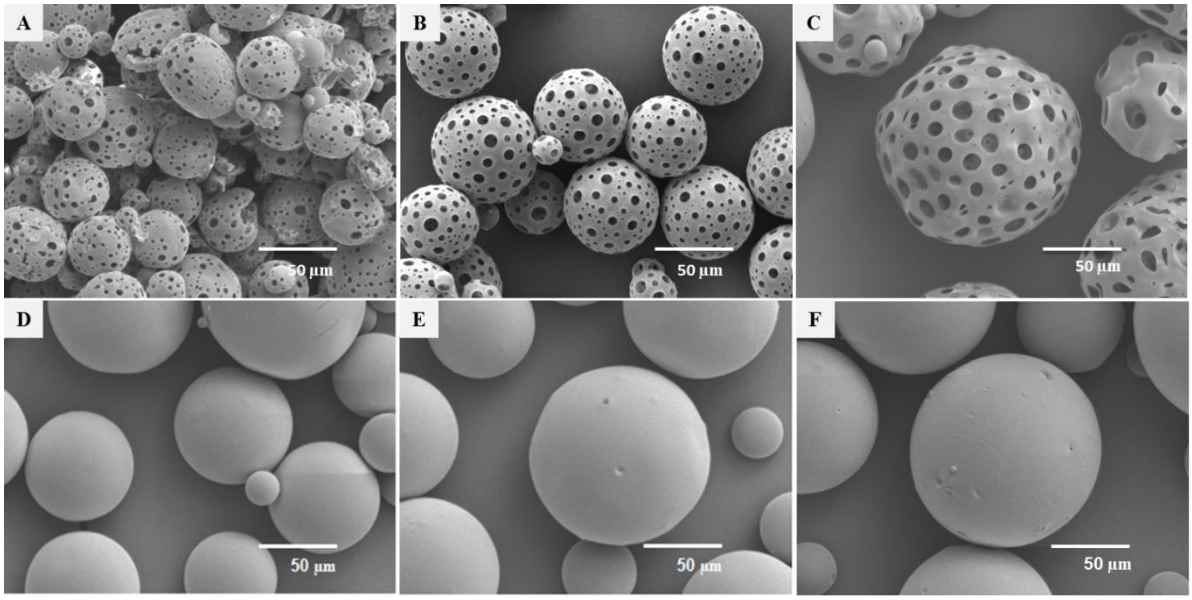


Figure 3.1: SEM images of porous (A-C) and non-porous microsphere (D-F) microspheres formulated with LMW (A, D), IMW (B, E) and HMW (C, F) PLGA [197]

The size distribution for both types of microspheres (porous and non-porous) is shown in **Figure 3.2**. The average diameters of the LMW, IMW and HMW microspheres were 32.69 ± 19.66, 56.67 ± 19.07 and 74.31 ± 26.84 µm, respectively. The average diameters of the non-porous microspheres were 46.87 ±, 16.28, 58.98 ± 18.23 and 88.91 ± 25.05 µm for the LMW, IMW and HMW, respectively. Thus, there was an increase in the respective average diameters amongst both the porous and non-porous microspheres. The comparatively larger average diameter observed amongst the non-porous microspheres can be attributed to the lower homogenisation speed of 2000 rpm used during the formation of the secondary emulsion, as opposed to 4000 rpm used during the formation of the porous microspheres [190]. Furthermore, the incorporation of lysozyme within the non-porous microspheres may also have contributed to the larger size observed amongst this series [198, 199]. Finally, surface erosion arising from the use of the ethanolic-NaOH on the porous microspheres will also contribute to the observed size reduction.

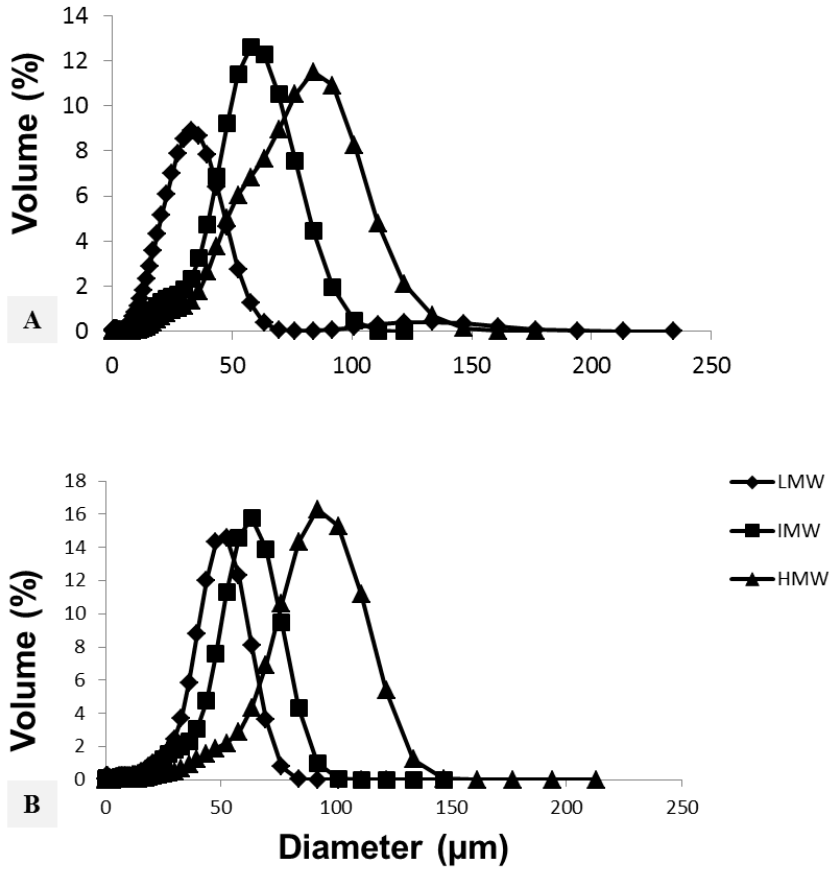


Figure 3.2: Size distribution for porous (A) and non-porous (B) microspheres as a function of PLGA molecular weight [197]

For both the porous and non-porous microspheres, there was a direct relationship between the molecular weight of the PLGA and the average diameter of the microspheres, as shown in **Figure 3.2**. This relationship is attributed to the viscosity of the polymer solutions, which increases with increase in the polymer molecular weight [200]. A more viscous solution would present a greater barrier to the breakdown of droplets during the homogenisation of the primary emulsion and, hence, result in the formation of larger microspheres [200] .The size range of both porous and non-porous microspheres fell between 30 to 100 µm, which has been shown previously to be compatible with injection through a 22-G needle [13, 142].

3.3.2 Microstructure and porosity of scaffolds

The microstructures of the three types of scaffolds sintered at 37°C after treatment with ethanolic-NaOH are shown in **Figure 3.3**. It has been shown that the NaOH-treatment of PLGA surfaces enhances the functionality of osteoblasts [94], which is advantageous in bone-regenerating scaffolds. The surface of the LMW scaffold appears to be extensively fused (**Figure 3.3A–C**), in contrast with the IMW (**Figure 3.3D–F**) and HMW scaffolds (**Figure 3.3G-I**).

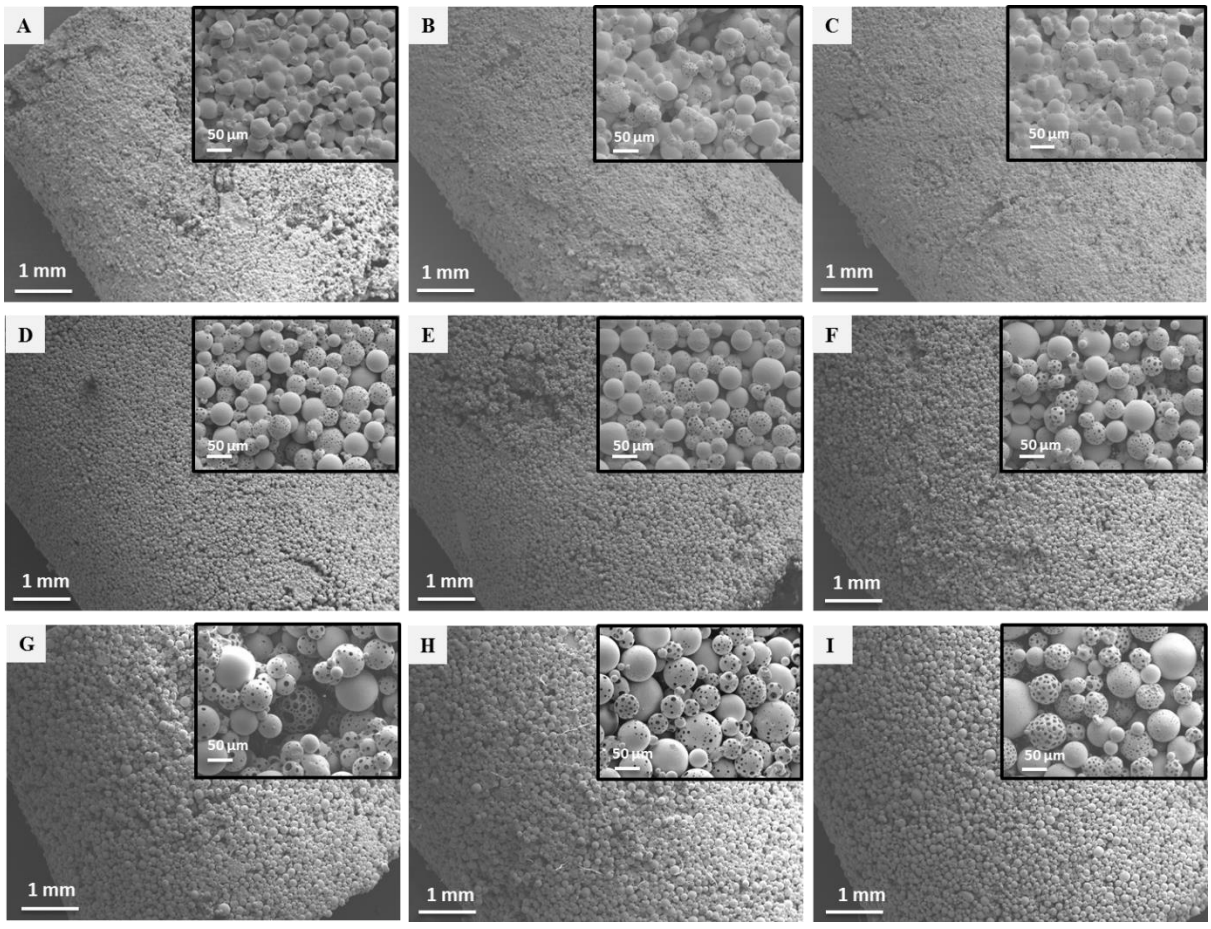


Figure 3.3: SEM images of sintered scaffolds with various lysozyme loadings (A-C = LMW, D-F = IMW and G-I = HMW; 1 mg/g, 2 mg/g and 3 mg/g, from left to right) [197]

A previous study reported that the ability of microspheres to sinter into scaffolds at body temperature may be due to the local degradation of the polymer following treatment

with ethanolic-NaOH [142]. In this regard, the degradation of the polymer is thought to result in a reduction in the T_g of the PLGA at the surface of the microspheres, which allows the surface to fuse more readily with neighbouring microspheres [142]. This hypothesis is supported in the present study, where the reduction in the T_g following the treatment with ethanolic-NaOH was 5.8, 1.8 and 0.2°C for the LMW, IMW and HMW scaffolds, respectively, as shown in **Table 3.2** and **Figure 3.4.** It is apparent that the higher the molecular weight of the PLGA, the less compliant the resulting microspheres are to the reduction in T_g following treatment with ethanolic NaOH.

Table 3.2. Glass transition temperatures (Tg) of porous PLGA microspheres pre- and post-ethanolic-NaOH treatment.

Molecular wt. of PLGA	**LMW**	**IMW**	**HMW**
T_g porous microspheres (°C)	51.4	53.2	51.7
T_g porous microspheres ethanolic-NaOH treated (°C)	45.6	51.4	51.5

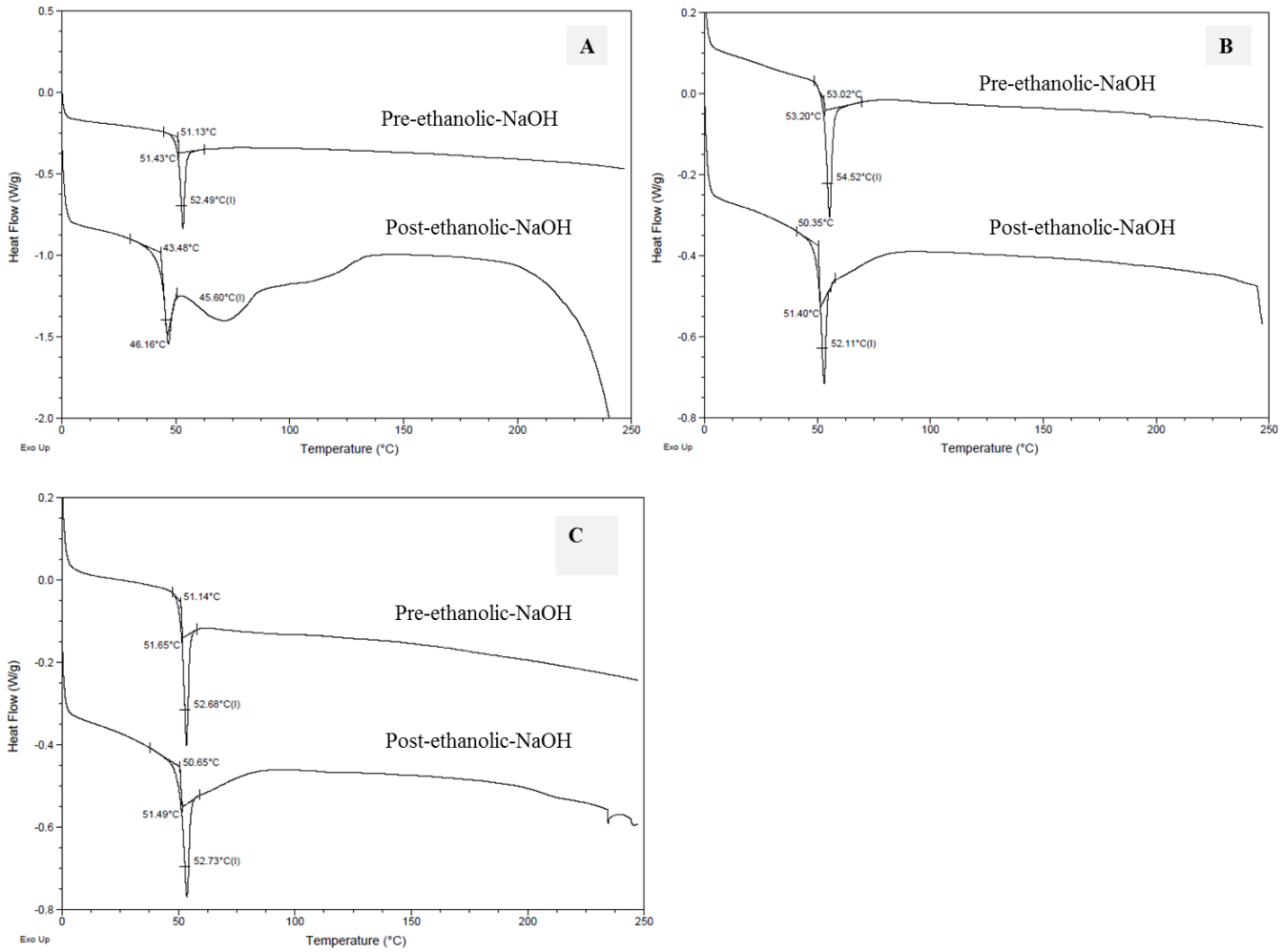


Figure 3.4: DSC thermal profiles of (A) LMW, (B) IMW and (C) HMW porous microspheres pre- and post-ethanolic NaOH treatment.

The DSC data are consistent with the SEM images of the scaffolds depicted in **Figure 3.3** which show that the LMW scaffolds have a more fused appearance compared with the HMW scaffolds. As shown in **Figure 3.5**, the porosity of the scaffolds ranged from 75 to 90%, which is preferential as it has been previously shown *in vivo* that higher porosity results in a higher degree of bone tissue ingrowth [201]. The HMW scaffolds were significantly less porous ($p < 0.05$) in comparison to the IMW and LMW scaffolds, even though the latter appeared to have a more fused surface. This difference is believed to be related to the increase in the internal porosity of the LMW scaffolds, due to a slower solidification rate of

the polymer in the lysozyme-loaded microspheres [202]. The LMW polymer is more soluble in the organic solvent and, hence, remains in solution longer, as opposed to the IMW or HMW polymers, which solidify more readily and precipitate out to form microspheres [202]. This slower rate of solidification would result in a more porous internal structure due to the longer time available for the formation of channels [202].

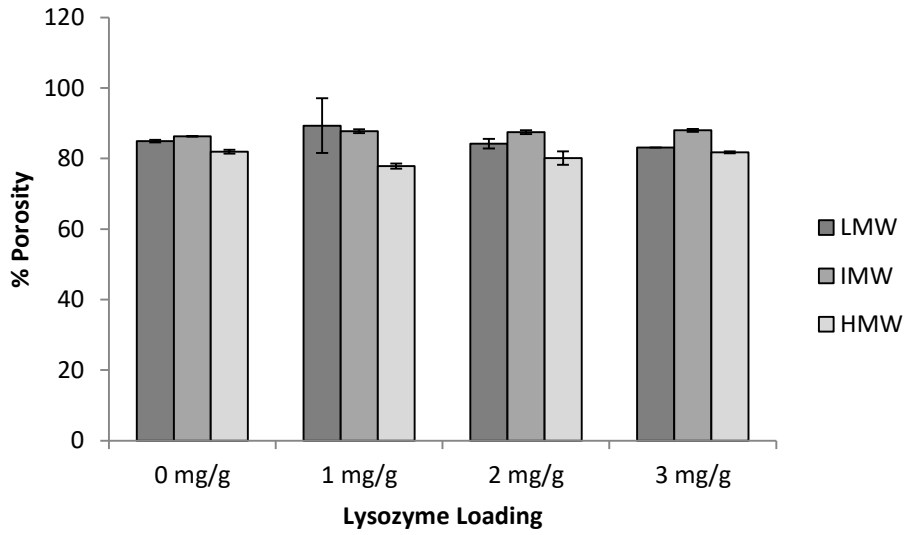


Figure 3.5: Percentage porosity of porous PLGA scaffolds loaded with various lysozyme concentrations.

3.3.3 Compressive strength of scaffolds

The compressive strength of a material is a measure of its resistance to an applied stress. **Figure 3.6** shows the average compressive strengths of the scaffolds with different lysozyme loadings (0, 1, 2 and 3 mg of lysozyme/g of scaffold). Both the control and lysozyme-loaded scaffolds exhibited a reduction in the mechanical strength with the higher polymer molecular weight. There was no statistically significant difference (as determined via an ANOVA analysis) in the compressive strengths of the lysozyme-incorporated LMW and IMW scaffolds ($p > 0.05$). However, there was a reduction in the compressive strength of the HMW scaffolds following the incorporation of lysozyme ($p < 0.05$) when compared with

either the LMW or IMW. This may be attributed to the lysozyme obstructing the weak interactions between the HMW microspheres, resulting in a generally weaker microstructure.

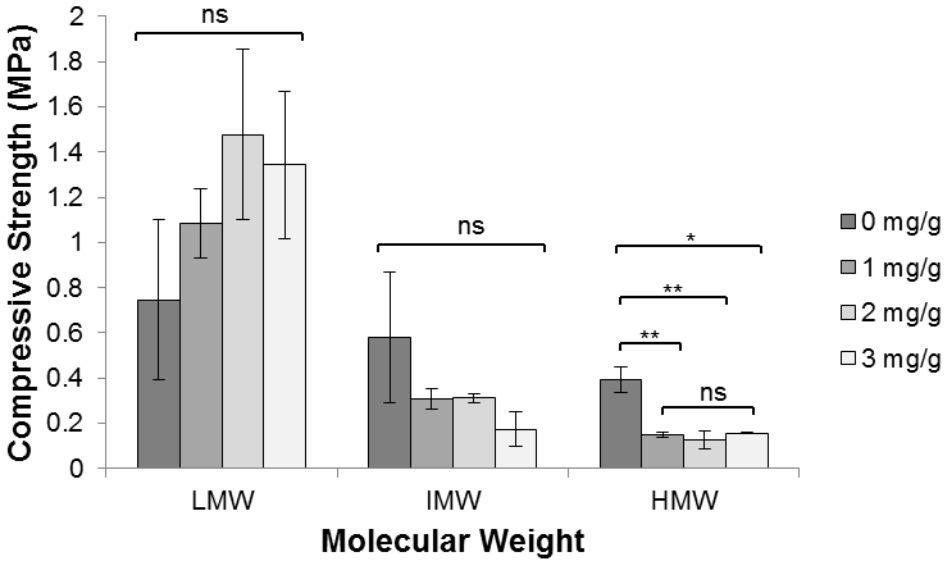


Figure 3.6: Compressive strengths of scaffolds with various lysozyme loadings (ns = statistically not significant, *p < 0.05 and **p < 0.01) [197]

The compressive strength data appear to be in concert with the SEM images of the scaffolds, in which a fused surface appearance was observed on the LMW scaffold. The fused appearance is presumably a measure of the degree of sintering within the scaffolds, and is a result of the reduction in T_g, as explained in section 3.3.2.

A previous study reported the ultimate compressive strength of cancellous bone to be in the range of 0.22 to 10.44 MPa, depending on the area of the body [203]. The compressive strengths of the LMW and IMW scaffolds fabricated in the present study fall within the range of that required for cancellous bone.

3.3.4 Distribution of lysozyme on and within the scaffolds

The distribution of lysozyme on the surface of the three types of scaffolds as a function of the lysozyme loading was assessed using ToF-SIMS. Several secondary ions of

molecular fragments originating from the surface of the scaffolds following their bombardment with primary ions (Bi^+) were obtained. CN^- and CNO^- ions were indicative of lysozyme and appear red on the surface of the scaffolds, whilst $C_3H_3O_2^-$, $C_3H_5O_2^-$ and $C_2H_3O_3^-$ were indicative of the presence of PLGA and appear green. Where PLGA and lysozyme are detected at coincident positions, the resulting colour appears orange. Overlay secondary ion images of lysozyme and PLGA from the surface scans for a control sample and the three types of scaffolds at various lysozyme loadings are shown in **Figure 3.7.**

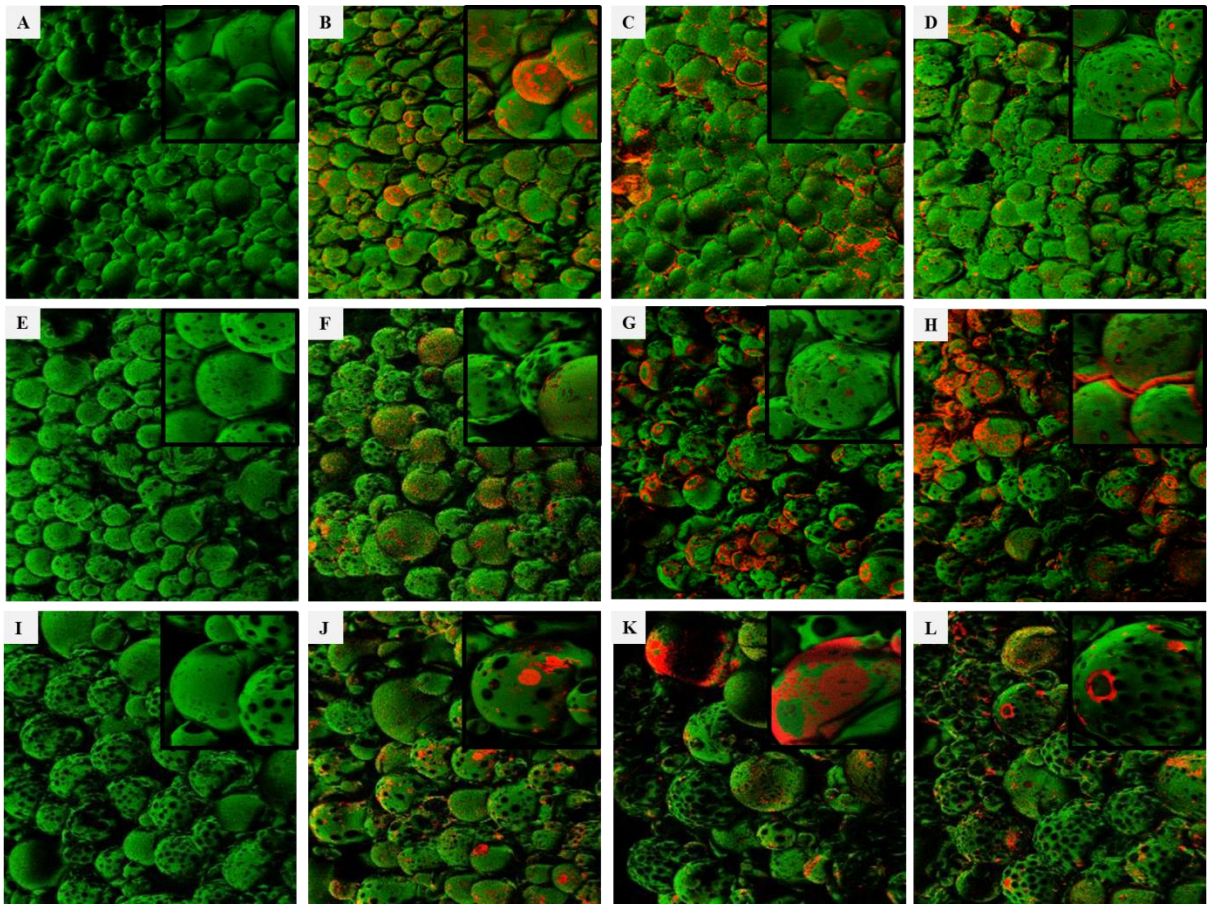


Figure 3.7: Overlay images of ToF-SIMS scans from scaffold surfaces with various lysozyme loadings (A-D = LMW, E-H = IMW and I-L = HMW, 0, 1, 2 and 3 mg/g of lysozyme from left to right respectively). PLGA/green= $C_3H_3O_2^-$, $C_3H_5O_2^-$, $C_2H_3O_3^-$; red/lysozyme = CN^- and CNO^- [197]

The ToF-SIMS data for the control samples showed negligible ion intensities for the CN^- and CNO^- ions, which are indicative of lysozyme. However, significant ion intensities were observed for the CN^- and CNO^- ions (when compared to the blank samples) on the surface of the scaffolds loaded with 1 to 3 mg of lysozyme/g of scaffold. Lysozyme, in some cases, is evident within the gaps between the microspheres, on the surface of microspheres or in the crevices of the pores. The presence of lysozyme in between the microspheres could be attributed to the sintering process, which may lead to the premature leaching of lysozyme near the microsphere surface after its solubilization in PBS. This is confirmed by the presence of Cl^- secondary ions, which can be attributed to the PBS, at the same locations as the lysozyme secondary ions. This would allow the leaching of lysozyme from the microspheres through crevices within the scaffold in order to emerge at the surface. Furthermore, PBS promotes the first hydration stage during the PLGA breakdown process [128, 129], which favours the leaching of the lysozyme from the scaffold framework. Previous work carried out by Rafati et al. [196] concluded that the lysozyme was located within depressed areas on the surface of the microspheres. They suggest that one of the reasons behind the presence of the protein at these locations is due to the incomplete incorporation of the protein-rich droplets at the time of microsphere formation [196]. They found that lysozyme was present within pores of various sizes created via the evaporation of water from the aqueous internal phase [196]. This incomplete incorporation could partly explain the presence of lysozyme within surface pores, along with lysozyme collecting within pores as a result of the sintering process in the present study.

In order to evaluate this process, the scaffolds were cross-sectioned using a microtome and subjected to further ToF-SIMS analyses (**Figure 3.8**).

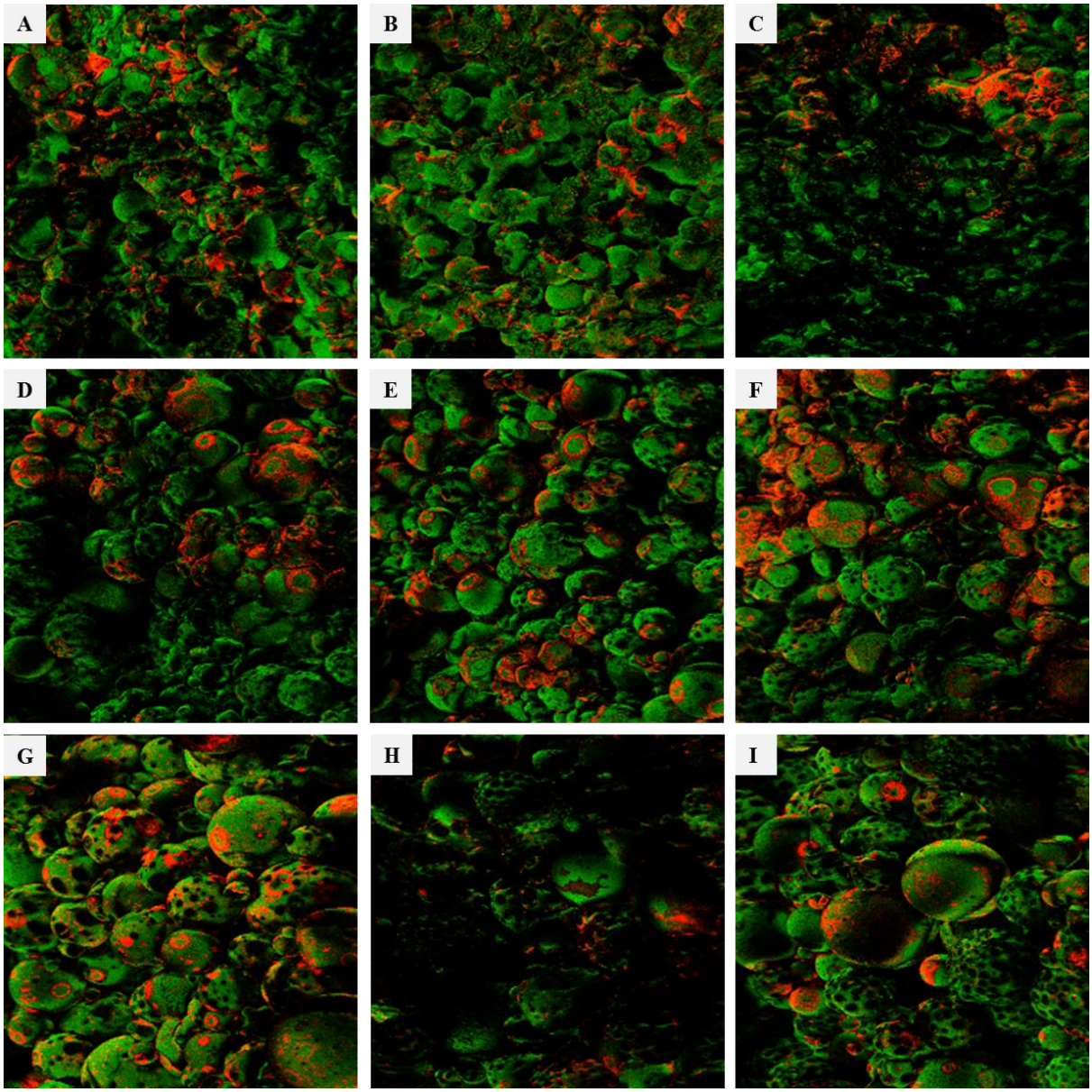


Figure 3.8: Overlay images of ToF-SIMS scans from scaffold cross-sections with various lysozyme loadings (PLGA/green= $C_3H_3O_2^-$, $C_3H_5O_2^-$, $C_2H_3O_3^-$; red/lysozyme = CN^- and CNO^-) [197]

In the cross-sectioned samples shown in **Figure 3.8**, lysozyme is observed throughout the microstructure of the scaffolds at each lysozyme loading. There appears to be a similar distribution of lysozyme across the various loadings, and the images indicate that lysozyme is not only confined to the surface, but is also present within the scaffolds. This apparent scheme of protein distribution within the scaffolds seems favourable for tissue

growth because accessibility to the former is not limited to the surface only, but the entire microstructure of the scaffolds.

3.3.5 Release of lysozyme from non-porous microspheres and scaffolds

In the present study, lysozyme was used as a model protein for BMP-2 [35]. BMP-2 has, in recent years, been shown to be the gold-standard growth factor for bone regeneration [138]. The release of lysozyme from microspheres formulated using LMW, IMW and HMW PLGA is shown in **Figure 3.9**.

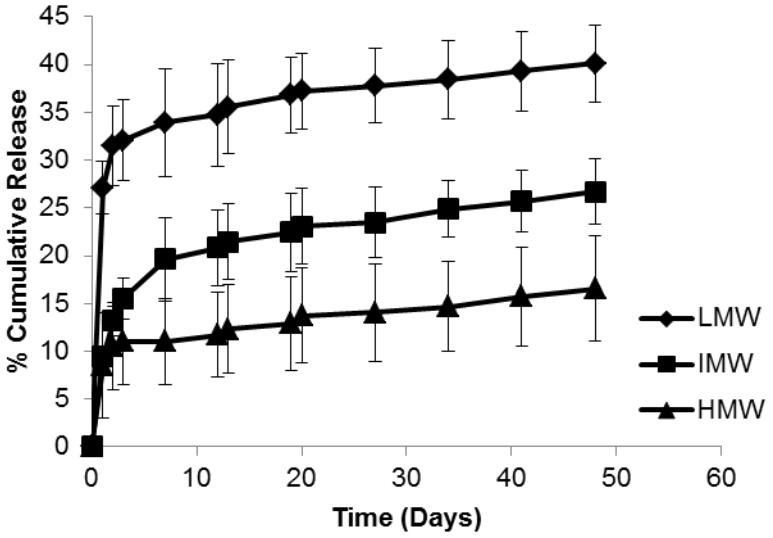


Figure 3.9: *In vitro* lysozyme release from microspheres as a function of PLGA molecular weight (LMW, IMW and HMW) [197]

All three types of microspheres showed an initial burst release of lysozyme within 24 hours, followed by a more sustained and linear release. The burst release after day 1 was significantly higher from the LMW microspheres at 27.1 ± 2.7%, in comparison to the IMW and HMW microspheres, which had similar burst releases of 9.4 ± 1.1% and 8.6 ± 5.5%, respectively ($p < 0.05$). A high standard deviation is indicative of a more erratic release from the microspheres. The maximum amount of lysozyme released from the three types of

microspheres at day 48 was 40.1 ± 4.0%, 26.7 ± 3.5%, and 16.7 ± 5.5% for the LMW, IMW and HMW microspheres, respectively, indicating that a significant amount of lysozyme was retained within the microspheres even after 48 days. This is advantageous as it has been shown that when the release kinetics of recombinant BMP-2 follows the pattern of an initial burst followed by a sustained release, a significant improvement in healing and regeneration of bone in rat femurs was observed [35].

The burst release phenomenon has been shown to be due to the release of any surface-residing protein [196]. However, previous studies on PLGA microspheres have suggested that the protein was mainly distributed within the matrix of the microsphere. The burst release in those cases was attributed to the rapid release of lysozyme through internal pores within the matrix [202, 204]. As mentioned in section 3.3.2, the LMW polymer accounted for a reduced rate of polymer solidification because it is more soluble in the organic solvent and, hence, remains in solution longer. This is as opposed to the IMW or HMW PLGA, which solidify more readily and precipitate out to form microspheres [202]. This slower rate of solidification would result in a more porous internal structure, which would promote the free release of lysozyme into the dissolution media [202]. Furthermore, the LMW microspheres exhibited a larger surface area-to-volume ratio due to their smaller average size (**Figure 3.2**), which means that the total surface area available to the dissolution medium was higher [202].

The release of protein from the scaffolds is crucial in initiating and maintaining the cascade of reactions necessary for tissue regeneration [35, 167]. The percentage release profiles of lysozyme from the scaffolds prepared using LMW, IMW and HMW PLGA microspheres at different lysozyme loadings are shown in **Figure 3.10.**

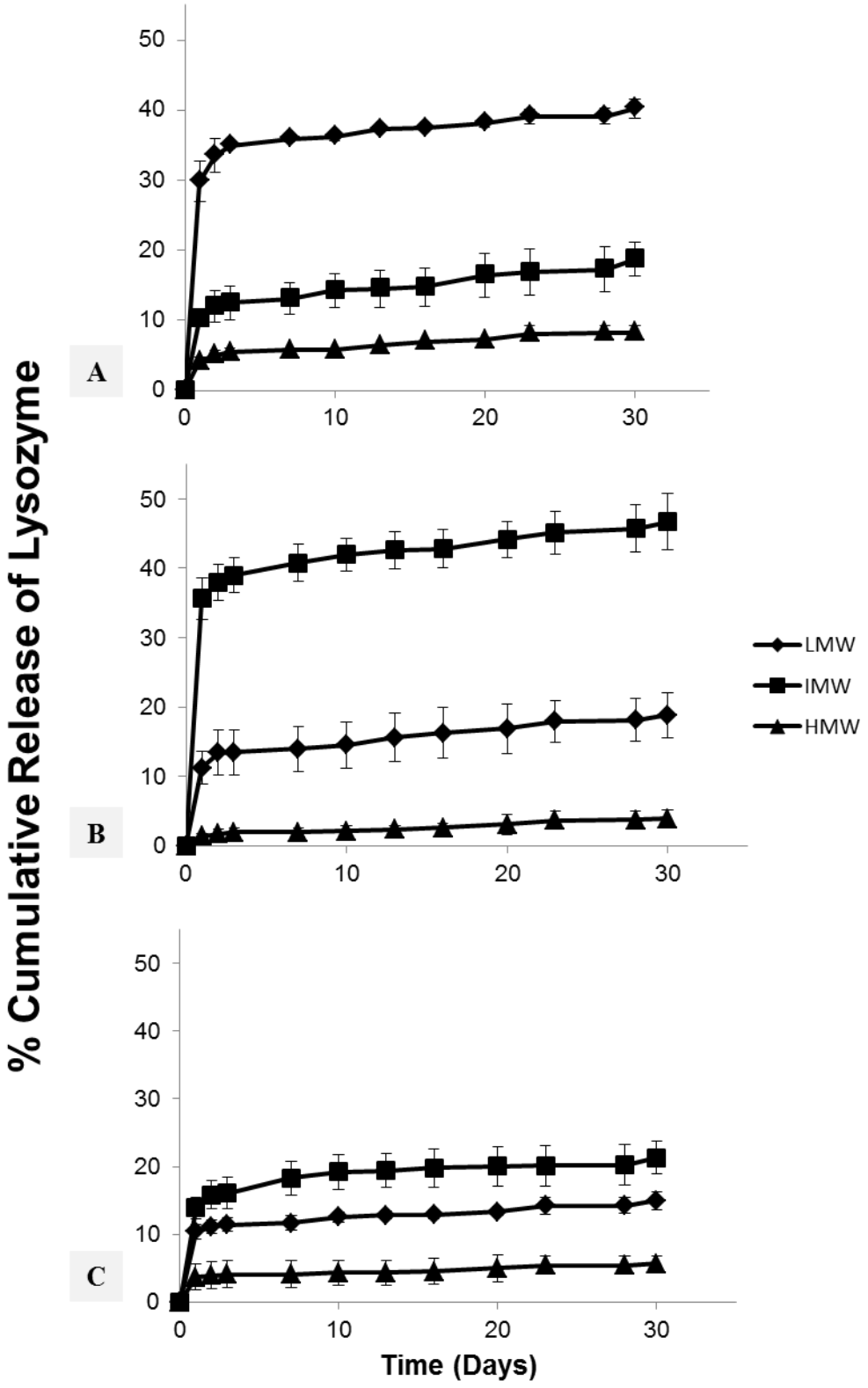


Figure 3.10: ***In vitro*** **lysozyme release from sintered scaffolds as a function of the PLGA molecular weight (A= 1 mg, B = 2 mg and C = 3 mg of lysozyme per gram of scaffold) [197]**

At all the lysozyme loadings and polymer molecular weights, the scaffolds showed a burst release on day 1, followed by a much slower release for the remaining 29 days. A significantly lower burst release ($p < 0.05$) was observed from the HMW scaffolds at the three lysozyme loadings. The HMW scaffolds with 1 mg lysozyme/g of scaffold showed a higher % burst release (4.2 ± 0.7%) in comparison to 2 and 3 mg of lysozyme/g of scaffold (1.37 ± 0.3 and 3.67 ± 1.9%, respectively). The overall percentage release from the HMW scaffolds was also significantly lower ($p < 0.05$) over all the lysozyme loadings. This slower percentage release of lysozyme from the HMW polymer scaffolds is believed to be due to the longer degradation time of the HMW PLGA in contrast with the IMW and LMW scaffolds [124]. Consequently, the rate of lysozyme release from the HMW scaffolds was slower, since the protein must diffuse from deep pockets within the microspheres, which is dependent on the surrounding polymer matrix first degrading in order to create conduits for the protein to escape. The overall percentage release profiles of lysozyme from the scaffolds at the 1 mg/g loading resemble those from the microspheres in respect of the molecular weight (LMW > IMW > HMW). This trend, as explained earlier, can be attributed to the rate of the degradation of the polymer, which is highest for the LMW PLGA. On the other hand, for the 2 and 3 mg of lysozyme/g scaffolds, the order for the cumulative percentage lysozyme release was IMW > LMW > HMW. It appears, therefore, that at higher lysozyme loading (2 and 3 mg/g), the rate of degradation of the IMW scaffolds was higher than that of the LMW scaffolds, which prompted a faster rate of lysozyme release from the IMW scaffolds.

The absolute cumulative release of lysozyme (µg/mg of scaffold) from the scaffolds (**Figure 3.11**), as opposed to the percentage cumulative release described earlier, indicates that all three lysozyme loadings for the LMW and HMW scaffolds demonstrate a very similar lysozyme release profile (LMW, $F_{2.6} = 4.72$, $p = 0.06$; HMW, $F_{2,3} = 1.40$, $p = 0.32$) .

However, for the IMW scaffolds, the 1 mg/g scaffolds exhibited a significantly lower release profile than the 2 and 3 mg/g IMW scaffolds ($p < 0.05$).

The similar release profiles from the LMW and HMW scaffolds lead to the loadings exhibiting an inverse profile when plotted as percentages (Figure 3.10), i.e. the 3 mg/g loading would exhibit a lower percentage release due to the total amount of protein present being higher in comparison to that of the 2 or 1 mg/g scaffolds. There is a strong possibility that during the first 30 days, the release of lysozyme was originating from specific areas near the surface of the scaffolds in which the non-porous microspheres had preferentially collected during the sintering process. However, this seems not to be the case for the IMW scaffolds, with the protein-loaded microspheres being more evenly distributed within the scaffold structure. **Table 3.3** shows the amount of lysozyme released after the initial bust release of 24 hours until the end of the study at day 30. The highest subsequent release of lysozyme was from the IMW 3 and 2 mg/g scaffolds. Further release after the initial burst is necessary for a sustained release of protein, which as stated previously, is required for BMP-2 delivery.

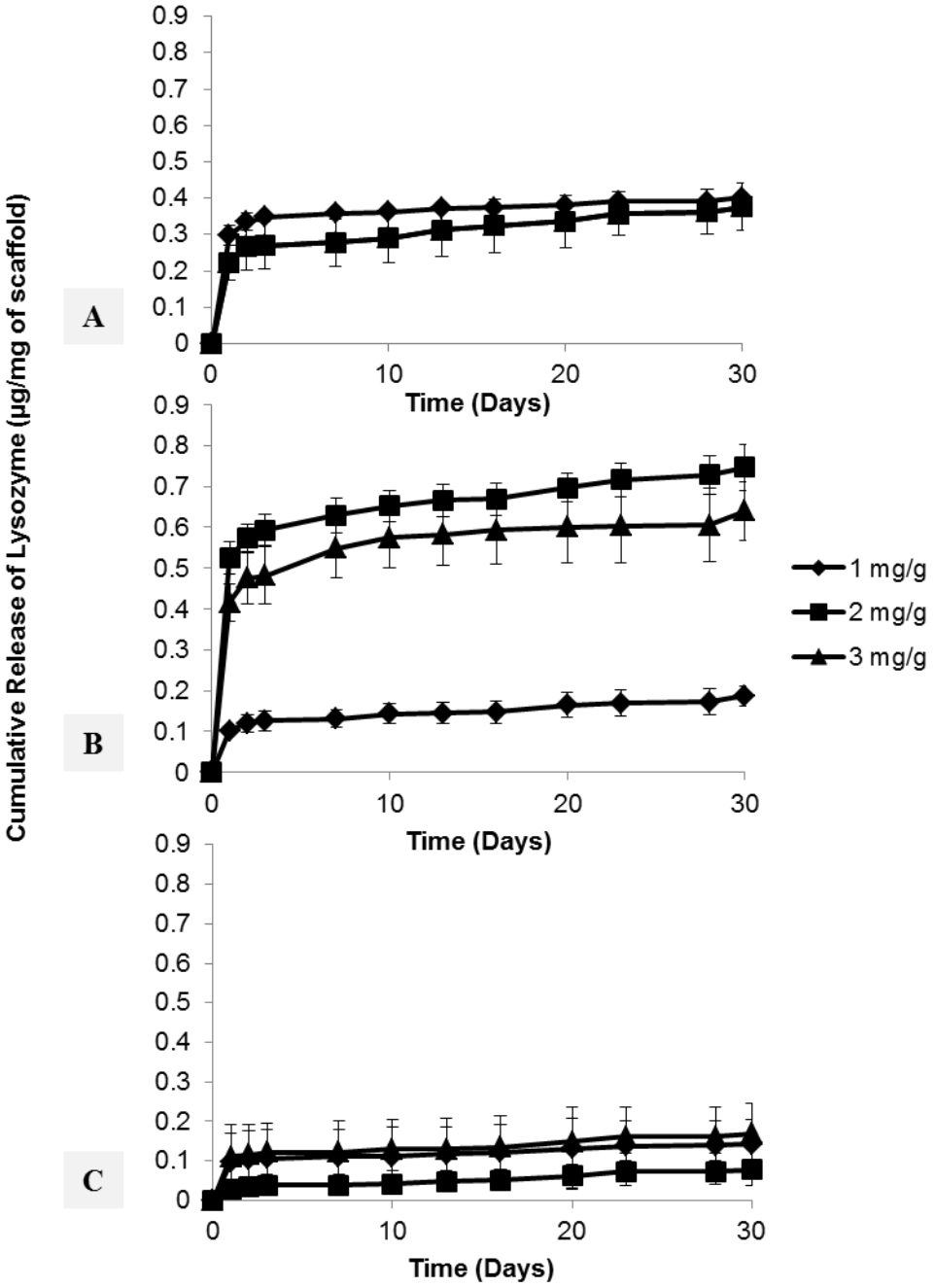


Figure 3.11. ***In vitro*** **lysozyme release from scaffolds over 30 days. (A) LMW, (B) IMW and (C) HMW PLGA scaffolds.**

Table 3.3: Subsequent lysozyme release after the initial burst release at day 1.

	Release of lysozyme after the initial burst release to the end of the study (µg/mg of scaffold)
LMW	
1 mg/g	0.10 ± 0.015
2 mg/g	0.15 ± 0.023
3 mg/g	0.14 ± 0.039
IMW	
1 mg/g	0.085 ± 0.018
2 mg/g	0.22 ± 0.036
3 mg/g	0.22 ± 0.032
HMW	
1 mg/g	0.045 ± 0.014
2 mg/g	0.050 ± 0.024
3 mg/g	0.059 ± 0.024

3.4 Conclusions

In this chapter lysozyme-loaded microspheres were successfully combined with porous microspheres in order to form scaffolds that sinter at 37°C. The LMW and IMW scaffolds elicited sufficient compressive strength comparable to that of cancellous bone, and the lysozyme release from the scaffolds and microspheres was polymer molecular weight-dependent, and remained sustained for at least 30 days. Lysozyme located near the surfaces of the microspheres would have solubilized in PBS during the sintering process and then diffused onto the surfaces of the microspheres. This surface-residing lysozyme accounts for the burst release.

The IMW scaffold formulation had sufficient compressive strength that did not significantly differ across all the loadings ($F_{3,8} = 3.86$, $p = 0.06$); therefore, it was selected to undergo further development in order to address the burst release. Furthermore, the 3 mg/g loading was selected for use in all further work after balancing the higher amount of

lysozyme released at the post-burst release stage (0.22 μg/mg, **Table 3.3**) and lower burst release when compared with the 2 mg/g-loaded IMW scaffold.

Chapter 4: Control of the burst release of protein from PLGA microspheres

4.1 Introduction

The release profile of a model protein is a key consideration when developing scaffold systems. As shown in Chapter 3, PLGA microspheres were prone to a large initial burst release, which was attributed to surface-associated protein [196]. In clinical applications, it is challenging to maintain therapeutic BMP-2 levels, mostly due to its short half-life [138]. Systems eliciting a large burst release of BMP-2, therefore, necessitate some intervention for the maintenance of therapeutic levels for a sufficiently long period e.g. concentrations higher than the therapeutic level. Various approaches can be used to address the burst release of protein from microspheres. As shown in Chapter 3, the molecular weight of PLGA modulates the release of the model protein in an inverse relationship. It has also been reported that freeze-drying microspheres can reduce their initial burst release, possibly through the suppression of convection-induced drug migration [205].

The inclusion of other polymers within the microspheres is another strategy used to reduce the burst-release phenomenon. For example, a PLGA-PEG-PLGA triblock co-polymer, was found to reduce the lag phase between the initial burst release and subsequent release of protein thereafter. Using this formulation they were able to sustain the release of a combination of BMP-2 and human serum albumin (HSA) over a 13-day period [138].

There are various polymers with favourable properties that can be exploited for tailoring the burst release. These include Pluronic F127, poly-$_L$-ornithine (PLO), heparin, pectin, κ-carrageenan and chitosan, to name a few. Pluronic F127 is a non-ionic surfactant, whilst heparin, pectin, κ-carrageenan and chitosan are all naturally derived polysaccharides, which makes them attractive natural choices for tissue engineering applications. Furthermore, the utilisation of PLO was mainly for its electrolyte properties. The choice of the polymer should mirror the intended use of the scaffold system and must be compatible with the other

components used in the preparation process. A review of each of these polymers is discussed below.

The block co-polymer, Pluronic F127 is a non-ionic surfactant that is a member of the poloxamer family. It consists of segments of poly (ethylene oxide) (PEO) with poly (propylene oxide) (PPO) positioned in between [206, 207]. Poloxamers, along with PEG derivatives and poloxamines, have been used to overcome the rapid uptake of intravenously injected particles by cells in the reticuloendothelial system, and also to prevent steric aggregation [208] . Pluronic F127 has also been used previously in combination with PLGA. It was used as an extractable porogen during the preparation of porous pore-closing microspheres for the sustained delivery of human growth hormone [176], and as a hydrogel embedded with PLGA microspheres in order to prolong hirudin delivery [209].

Surfaces that fall to extremes of hydrophilicity or hydrophobicity have been found to be less conducive to cell adherence and growth, with a moderate level of hydrophilicity being preferential [210]. An enhanced cell response was evident when the hydrophilicity of the PLGA surface is increased using Pluronic F127. There was also an increase in the mineralization when PLGA was blended with Pluronic F127 in the form of electrospun fibres [211].

PLO is a cationic polypeptide and has previously been utilized in cell microencapsulation in combination with alginates [212]. Heparin is highly negatively charged and a useful biomolecule. It plays a role in anchoring, localizing and modulating the bioactivity of a number of endogenous growth factors, including BMPs [213].

Pectin and κ-carrageenan are natural polysaccharides. Pectin can be combined with other polysaccharides and proteins in order to form chemically stable and physically strong plant skeletal tissue [214]. Furthermore, the structure of pectin allows it to support bioactive

substances, and it bears a close resemblance to polysaccharides found in the mammalian ECM [214]. κ-Carrageenan is derived from red seaweed and is water soluble. It has been used previously in tissue engineering and has been found to promote cell viability and attachment [215].

Another possible material that may be used to address the burst release of protein from microspheres is chitosan, a natural polysaccharide derived from chitin. It is popular in tissue engineering applications for a variety of reasons, which include its biocompatibility and ability to promote cell adhesion [215, 216]. Chitosan microspheres show promise for use in the encapsulation of proteins and have previously been shown to maintain the activity of a neural growth factor [218]. Moreover, chitosan-based materials are able to sustain the release of growth factors because of their cationic and degradation properties [217]. It has been used in combination with PLGA in various forms such as chitosan scaffolds embedded with PLGA microspheres [219–222]. PLGA/chitosan microspheres have been prepared using a variety of methods. These include the use of supercritical carbon dioxide for controlled drug delivery [223], a modified double emulsion method [224, 225], solvent evaporation [195], an electro-dropping layer by layer approach [226], conjugation and adsorption [227]. Porous microspheres have also been treated with chitosan [228], whilst others have encapsulated protein-loaded chitosan microspheres into large porous PLGA microspheres [229].

In this chapter we aimed to address the burst release of protein from the PLGA microspheres via the application of appropriate polymer coatings. Formulations including the above materials were developed and extensively characterized in terms of their physical properties and release profiles.

4.2 Materials & Methods

4.2.1 Materials

Pluronic F127, PLO 0.01% aqueous solution, heparin sodium salt, κ-carrageenan, chitosan (low molecular weight, ≥ 75% deacetylation) and sodium tripolyphosphate (TPP) were purchased from Sigma-Aldrich. Low methoxy pectin was purchased from CP Kelko (USA). Bovine serum albumin (BSA) was purchased from Nacalai Tesque (Japan).

4.2.2 Preparation of lysozyme-loaded Pluronic F127-coated microspheres

Lysozyme-loaded PLGA microspheres were prepared as described in Chapter 3 (section 3.2.2) and then coated with 0.26, 0.13 or 0.065% Pluronic F127 solution in PBS, using the method reported by Santander-Ortega et al [208] with slight modifications. This involved gently swirling 200 mg of the PLGA microspheres in 50 ml of solutions of varying concentrations of Pluronic F127 at 60 rpm for 20 hours. The suspensions were centrifuged at 4500 rpm for 15 minutes, washed with distilled water and then freeze-dried for 24 hours.

4.2.3 Preparation of lysozyme-loaded PLO/heparin-coated microspheres

Lysozyme-loaded PLGA microspheres were prepared as described in Chapter 3 (section 3.2.2). Microspheres were coated with either PLO or PLO/heparin. For the coating procedure, 50 mg of lysozyme-loaded PLGA microspheres were suspended in 1.5 ml of 0.01% PLO solution and gently swirled at 60 rpm for 30 minutes. A smaller mass of microspheres were used in comparison with the Pluronic coating procedure due to the high cost implications associated with the PLO solution and heparin. They were then centrifuged at 4500 rpm for 2 minutes and washed with distilled water. The supernatant was removed and the microspheres were either frozen and freeze-dried for 24 hours, or suspended in 1 ml of 0.5 mg/ml heparin solution for 15 minutes. The suspensions were then centrifuged at 4500 rpm for 2 minutes and washed with distilled water before freezing and freeze-drying for 24 hours.

4.2.4 Preparation of lysozyme-loaded PLGA/pectin and PLGA/κ-carrageenan microspheres

Lysozyme-loaded PLGA/pectin and PLGA/ κ-carrageenan microspheres were prepared using the double emulsion solvent evaporation method as described in Chapter 3 (section 3.2.2) with one alteration; varying concentrations of pectin or κ-carrageenan were added to the PVA external aqueous phase. All other aspects of the procedure were maintained as per the method described in Chapter 3 (section 3.2.2).

4.2.5 Preparation of protein-loaded PLGA/chitosan microspheres

PLGA/chitosan microspheres were prepared similarly to the normal PLGA microspheres, with a few modifications. Lysozyme was substituted with BSA at the same concentration; 150 ml of 0.4% w/v PVA solution containing 0.05 g of TPP was used as the external aqueous phase, instead of 200 ml of 0.3% w/v PVA solution. For the primary emulsion, in addition to the PVA solution, 50 ml of either a 0.25 or 1.00% w/v chitosan solution in 2% v/v acetic acid was added to the external aqueous phase simultaneously, and homogenized at 2000 rpm as detailed in Chapter 3 (section 3.2.2). All other aspects of the method were maintained as described in Chapter 3 (section 3.2.2).

4.2.6 Characterization of coated microspheres

The morphology of the coated microspheres was determined using SEM. DSC thermal profiles were obtained for the microspheres and their constituents, and the encapsulation efficiency of lysozyme was determined. Detailed methodology relating to these characterization techniques can be found in Chapter 2 and 3 (sections 2.2.7.1 and 3.2.4) for the SEM and DSC, respectively.

X-ray photoelectron spectroscopy (XPS) was performed to study the surface chemistry of the Pluronic F127-coated microspheres. A Kratos Axis Ultra DLD instrument

was utilized with a monochromated X-ray source of aluminium (Al Kα) with the emission set at 1486.6 eV. The data were analysed using the CasaXPS software.

A ToF-SIMS analysis (as described in Chapter 3, section 3.2.7) was carried out in order to complement the XPS analysis of the Pluronic F127-coated microsphere surfaces. Microspheres were loaded onto double-sided adhesive tape and attached to aluminium blocks, which were then secured onto the ToF-SIMS stage. Negative and positive polarity data for 4 × 4 mm areas were analysed using the SurfaceLab 6 software (IONTOF). PLGA was identified in the negative spectra data by $C_3H_3O_2^-$ (*m/z* = 71), $C_3H_5O_2^-$ (*m/z* = 73), $C_3H_3O_3^-$ (*m/z = 87*) and $C_3H_5O_3^-$ (*m/z = 89*) secondary ions [196]. A diagnostic ion peak for Pluronic F127 was identified as $C_7H_7O^+$ from the positive polarity data, as previously reported by Mahoney et al. [230]. Lysozyme was identified by CN^- (*m/z* = 26) and CNO^- secondary ions in the negative spectra data. For a semi-quantitative analysis, the ion intensity data for regions of interest (ROIs) were exported and normalized to the total ion intensity.

4.2.7 Release studies

Release studies were carried out by submerging 10 or 50 mg of freeze-dried microspheres in 1.5 ml of PBS (pH 7.4). The media was replaced at set time points and the amount of lysozyme present was determined in 150 µl aliquots using the BCA assay as described in Chapter 3 (section 3.2.8).

4.3 Results and Discussion

4.3.1 Pluronic F127-coated PLGA microspheres

Pluronic F127 was utilized in this study due to its ability to adsorb onto PLGA microspheres. This adsorption ability is due to the fact that above the critical micelle concentration (CMC), the poly (propylene oxide) (PPO) groups of Pluronic F127, which are more hydrophobic in comparison to the poly (ethylene oxide) (PEO) groups, preferentially

associate together to form micelle-like structures [231]. It has been reported that the CMC of Pluronic F127 is approximately 0.26% w/v [8, 9]. At concentrations below the CMC, the PPO group is able to adhere onto hydrophobic surfaces in order to form a coating [206, 232]. In the present study, a coating of Pluronic F127 was formed on the lysozyme-loaded PLGA microspheres post-production using solutions below its CMC [234]. SEM images of the coated microspheres are shown in **Figure 4.1**. It can be observed that the microspheres appear smooth; furthermore, the Pluronic coating does not appear to have affected the morphology of the microspheres.

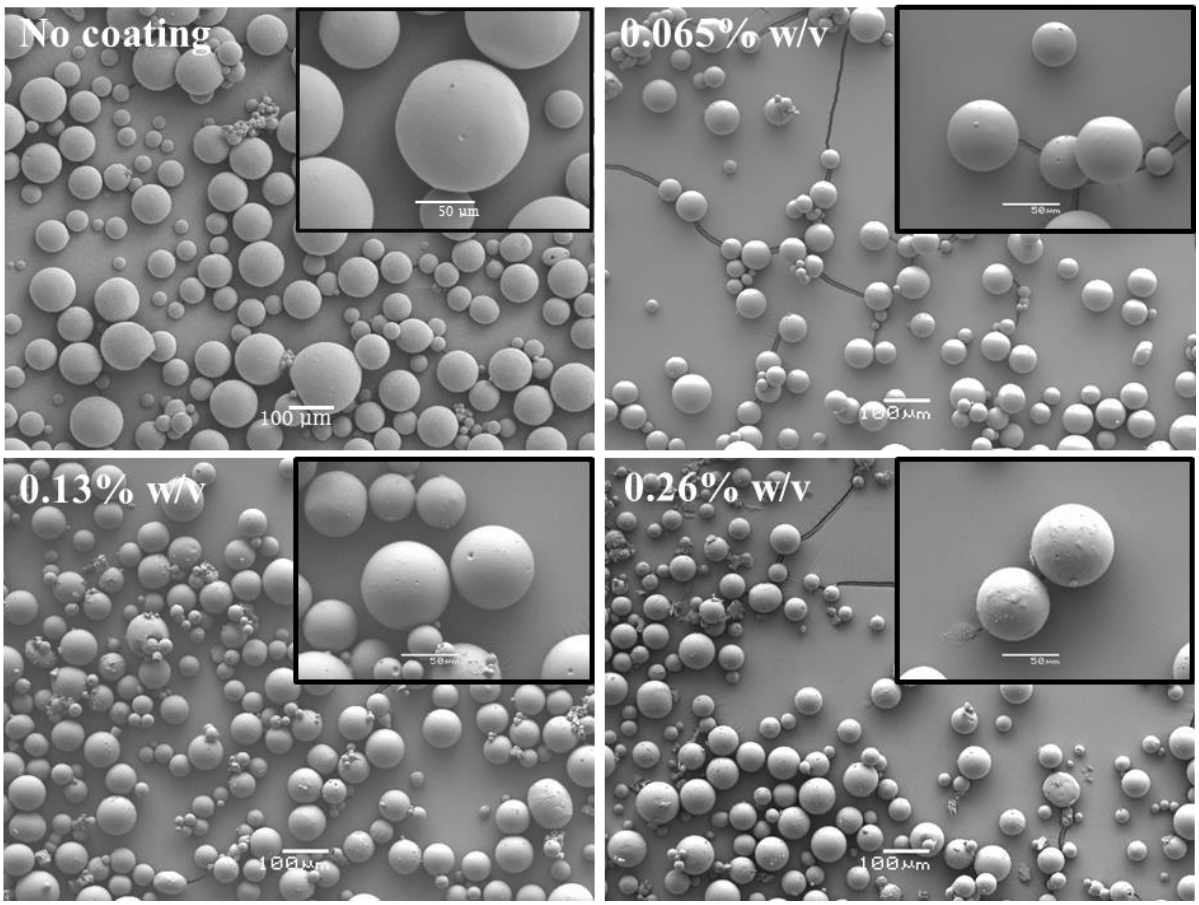


Figure 4.1: SEM images of lysozyme-loaded PLGA microspheres coated with varying concentrations of Pluronic F127 solution.

Figure 4.2 presents the DSC analysis of the lysozyme-loaded microspheres, where a sharp endothermic peak at 56°C on the Pluronic F127 profile corresponds to its melting endotherm [235]. The T_g of PLGA is visible in the non-coated microspheres as a change in the baseline at approximately 50°C. The thermal profile of the 0.065% w/v Pluronic F127-coated microspheres displays a melting endotherm at 55.2°C. Similarly there is a peak at 49.1°C, which accompanies the T_g of PLGA in the thermal profile of the 0.13%-coated microspheres; this is most likely attributable to the Pluronic F127. In the profile of the 0.26% w/v coated-microspheres, the Pluronic F127 peak is present at 46.9°C. Overall, the DSC data provide evidence of the presence of Pluronic F127 in the formulations.

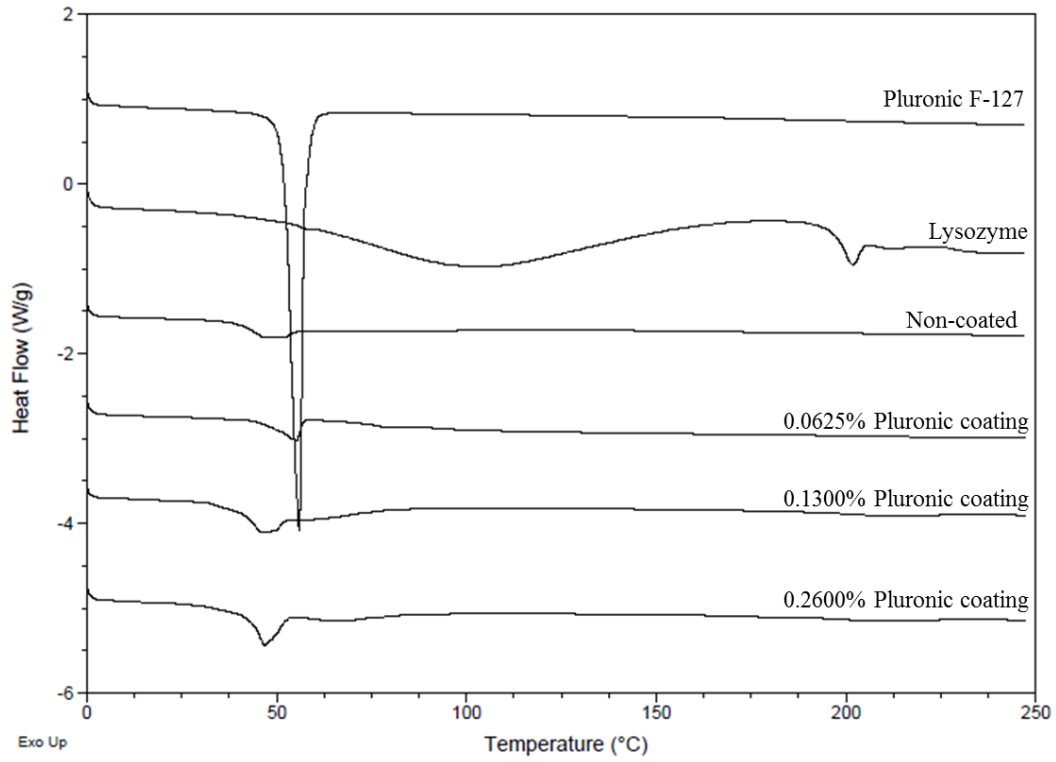


Figure 4.2: DSC thermal profiles of lysozyme-loaded PLGA microspheres coated with Pluronic F127.

XPS was utilized in order to determine the surface chemistry of the microspheres coated with the highest Pluronic F127 concentration, 0.26% w/v. The C-1s spectra of the samples are presented in **Table 4.1**. Four characteristic peaks were observed; C-C, O=C-O,

C-C-O and C-O at 284.9, 286.8, 289.2 and 286.2 eV, respectively. The C-O peak at 286.2 eV has previously been reported to be indicative of the presence of Pluronic; however, it is absent in the PLGA samples [236]. Therefore, the C-O peak was used as the diagnostic peak for Pluronic. The monomer ratio (MnR) and mass ratio (%MsR) were calculated using Equations 3 and 4:

$$MnR = \frac{0.5 \times \%C{-}O}{0.5 \times \%C{-}O + \%O{=}C{-}O} \qquad \textbf{Equation 3}$$

$$\%MsR = \frac{0.5 \times \%C{-}O \times 47.42}{0.5 \times \%C{-}O \times 47.42 + \%O{=}C{-}O \times 69.9} \qquad \textbf{Equation 4}$$

where 47.42 is the monomer molecular weight of Pluronic F127, and 69.9 is the monomer molecular weight of PLGA 85:15 [236]. The degree of accumulation of Pluronic on the surface was determined as the ratio of %MsR to the bulk concentration (65%). The results showed that the coating process resulted in a small amount of Pluronic F127 being adsorbed onto the microsphere surface, despite the fact that a high bulk concentration of Pluronic was utilized.

Table 4.1: Atomic concentrations of components of the C-1s peak derived from XPS spectra data

Microsphere Sample	**Concentration in atomic percentage of C-1s species**						
	C-C (1)	**O=C-O (2)**	**C-C-O (3)**	**C-O (4)**	**MnR**	**%MsR**	**A_s**
	284.9 eV	**286.8 eV**	**289.2 eV**	**286.2 eV**			
PLGA	38.15	41.17	20.67	-			
PLGA/F127	41.68	19.72	17.16	21.44	0.36	29.06	0.45

Abbreviations: MnR, monomer ratio; %MsR, mass ratio; A_s, degree of accumulation and F127, Pluronic F127.

A ToF-SIMS analysis was used to further elucidate the surface chemistry of the microspheres in conjunction with the XPS analysis. The general structure of Pluronic is shown in **Figure 4.3**. The peak at an *m/z* of 59 was chosen to represent Pluronic F127. This

peak corresponds to both the PPO subunit with the addition of H^+, and the PEO subunit with the addition of CH_3^+ ($C_3H_7O^+$).

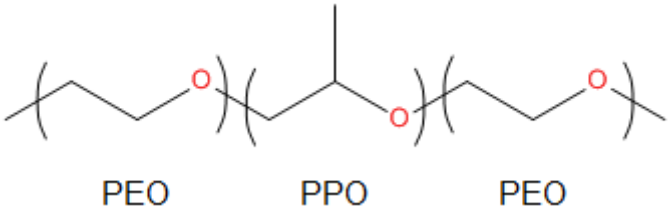


Figure 4.3: Chemical structure of Pluronic.

Secondary ion markers for PLGA were chosen as reported by Rafati et al. [196], as described in Chapter 3 (section 3.2.7). The secondary ion peak areas are shown in **Figure 4.4A**. As expected, peak *m/z* = 59 ($C_3H_7O^+$) in the pure Pluronic sample was the largest in area; whereas, the non-coated microspheres had a much smaller peak area. When the concentration of the Pluronic F127 coating solution was increased from 0.065 to 0.13% w/v, the peak area also increased. However, at 0.26% w/v there was a slight decrease in the diagnostic Pluronic peak area. A possible explanation for the lower area of peak *m/*z = 59 of the microspheres coated with 0.26% Pluronic F127 solution could be that at this concentration, the Pluronic is more inclined to form micelles, rather than adsorb on the microspheres. This is especially the case considering that the CMC of Pluronic has been reported to be approximately 0.26% w/v. An inverse pattern is evident for the PLGA (*m/z* = 71, 73, 83 and 89) and lysozyme (*m/z* = 26 and 42) diagnostic peaks, where the non-coated microspheres demonstrated higher relative areas of PLGA and lysozyme in comparison with the coated microspheres. This is confirmation that peak *m/z* = 59 is a suitable marker for Pluronic. Furthermore, it is consistent with Pluronic being deposited on the surface, as the decreased presence of PLGA and lysozyme would be necessary in order compensate for the increased presence of Pluronic.

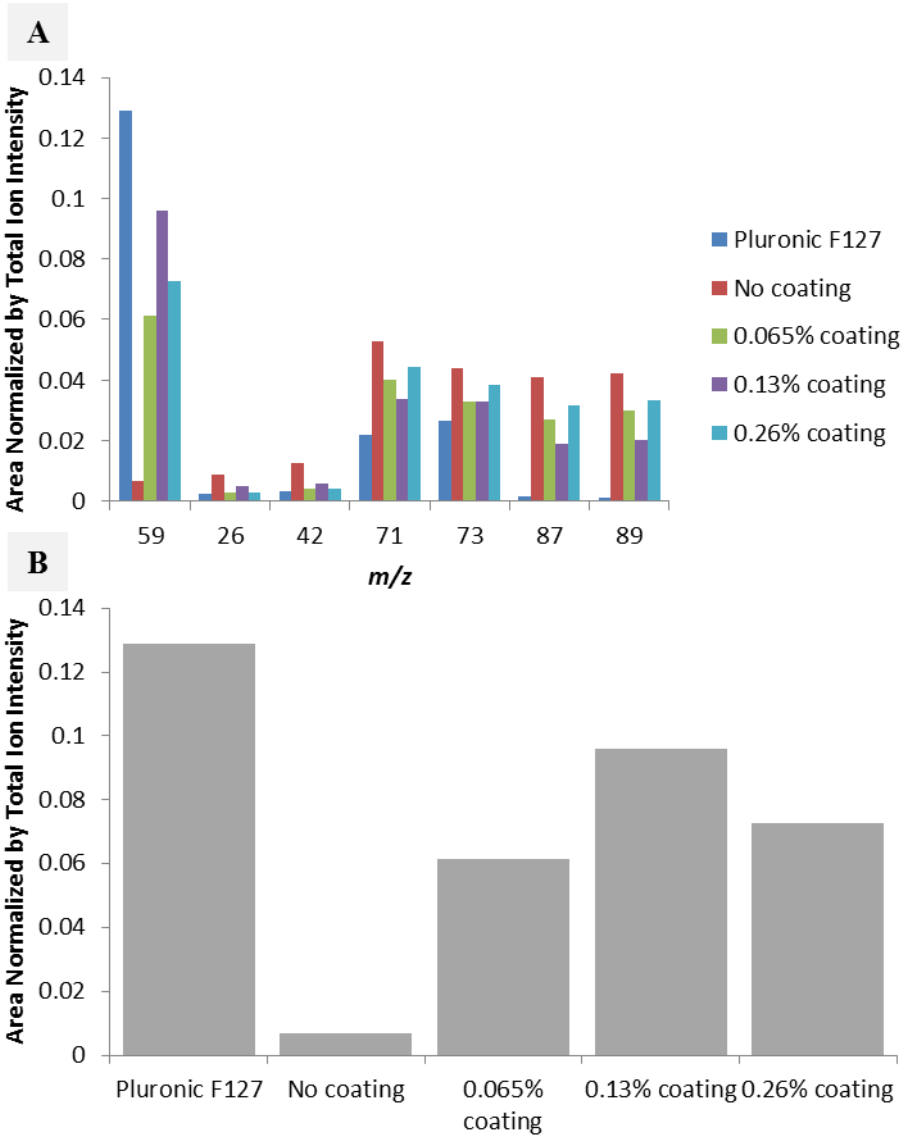


Figure 4.4: Areas of diagnostic peaks identified by TofSIMS in lysozyme-loaded PLGA microspheres. (A) Diagnostic peaks indicative of Pluronic F127 (*m/z* = 59), lysozyme (*m/z* = 26 and 42) and PLGA (*m/z* = 71, 73, 87 and 89). (B) Pluronic F127 diagnostic peak (*m/z* = 59).

Overall, the combined DSC, XPS and ToFSIMS analyses confirmed that the coating process yielded a successful deposition of Pluronic F127 on the surface of the microspheres. After establishing this, it was necessary to determine how the coating process affected the amount of lysozyme present within the microspheres. **Table 4.2** shows the reduction in the lysozyme content post-coating with different concentrations of Pluronic F127 solution. The

mean reduction in the lysozyme content ranged from 30 to 38% in all three formulations. An ANOVA analysis showed that the difference between the three was not statistically significant ($F_{2,6}$ = 2.08, p = 0.21). **Figure 4.5** shows the release of lysozyme from the microspheres as a function of the Pluronic coating. The lowest release of lysozyme was with the 0.065% Pluronic coating. **Figure 4.4** shows that the highest Pluronic adsorption onto the microspheres was observed at 0.13% and then 0.26%, with the least at 0.065%. This pattern of coating was the exact opposite in relation to the cumulative release of lysozyme. Therefore, it seems that the Pluronic coating augmented the release of lysozyme. The higher release of lysozyme from the microspheres coated with 0.13% Pluronic F127 could be attributed to the more hydrophilic surface provided by the Pluronic coating, which favours ingress of the aqueous medium and entices the protein out (as proteins are hydrophilic). However, the lysozyme released after day 1 and 50 was not significantly different between the non-coated and Pluronic F127-coated microspheres, as shown in **Figure 4.5** (day 1, $F_{3,8}$ = 1.42, p = 0.31; day 50, $F_{3,8}$ = 0.70, p = 0.58). Therefore, the large reduction in the lysozyme content as a result of the coating process, and the lack of a significant reduction in the lysozyme release signifies the unsuitability of the Pluronic F127 coating to this application. In practical clinical settings, this significant loss in protein is not conducive, especially for expensive proteins like BMP-2. Therefore, under the present settings, the use of Pluronic for coating the microspheres for the purpose of addressing the burst release is not suitable.

Table 4.2: Effect of the Pluronic F127 coating on the lysozyme content of PLGA microspheres.

Pluronic F-127 coating (%)	Mean % reduction in lysozyme content post coating	Standard deviation
0.065	33.99	6.73
0.130	30.58	1.89
0.260	37.45	1.41

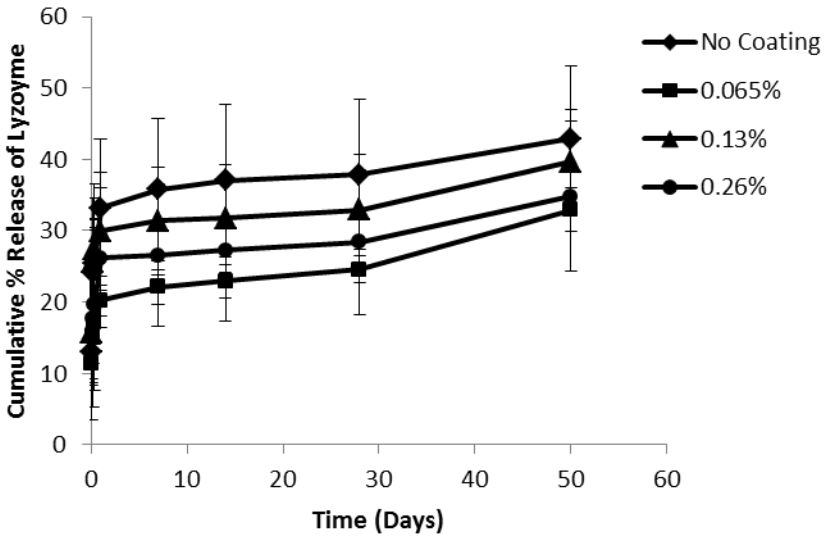


Figure 4.5: Cumulative % release of lysozyme from Pluronic F127-coated microspheres.

4.3.2 PLO/heparin-coated PLGA microspheres

Due to the unsuitability of the Pluronic F127 coating, other strategies were investigated in order to address the burst release of lysozyme from the PLGA microspheres. One of these strategies involved the usage of a polyelectrolyte complex composed of PLO, a cationic polypeptide, and heparin, a highly negatively charged natural polysaccharide. PLO coatings have previously been used with PLGA for the promotion of cell adhesion [237]. It has also been used in conjunction with heparin as a polyelectrolyte complex on alginate microbeads for the purposes of delivering BMP-2 [213]. **Figure 4.6** shows the microspheres coated with the polyelectrolyte complex and PLO alone; where no apparent difference may be drawn from the morphologies of the two.

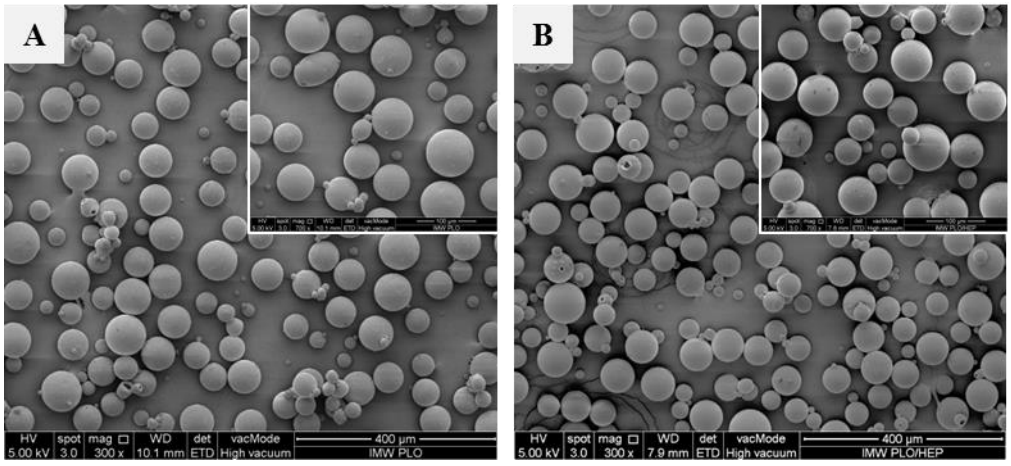


Figure 4.6: SEM images of lysozyme-loaded PLGA microspheres coated with (A) poly-$_L$-ornithine and (B) a poly-$_L$-ornithine/heparin complex.

Thermal profiles of the microspheres obtained via DSC are shown in **Figure 4.7**. A prominent exothermic peak is present on the heparin profile at 248°C, which represents its thermal degradation [238]. This peak is not present in the thermal profile of the PLO/heparin-coated microspheres, which may be as a result of heparin reacting with PLO, resulting in a change in its structure and thermal properties. The T_g ranges of the microspheres appear to be unaffected by the coating procedure.

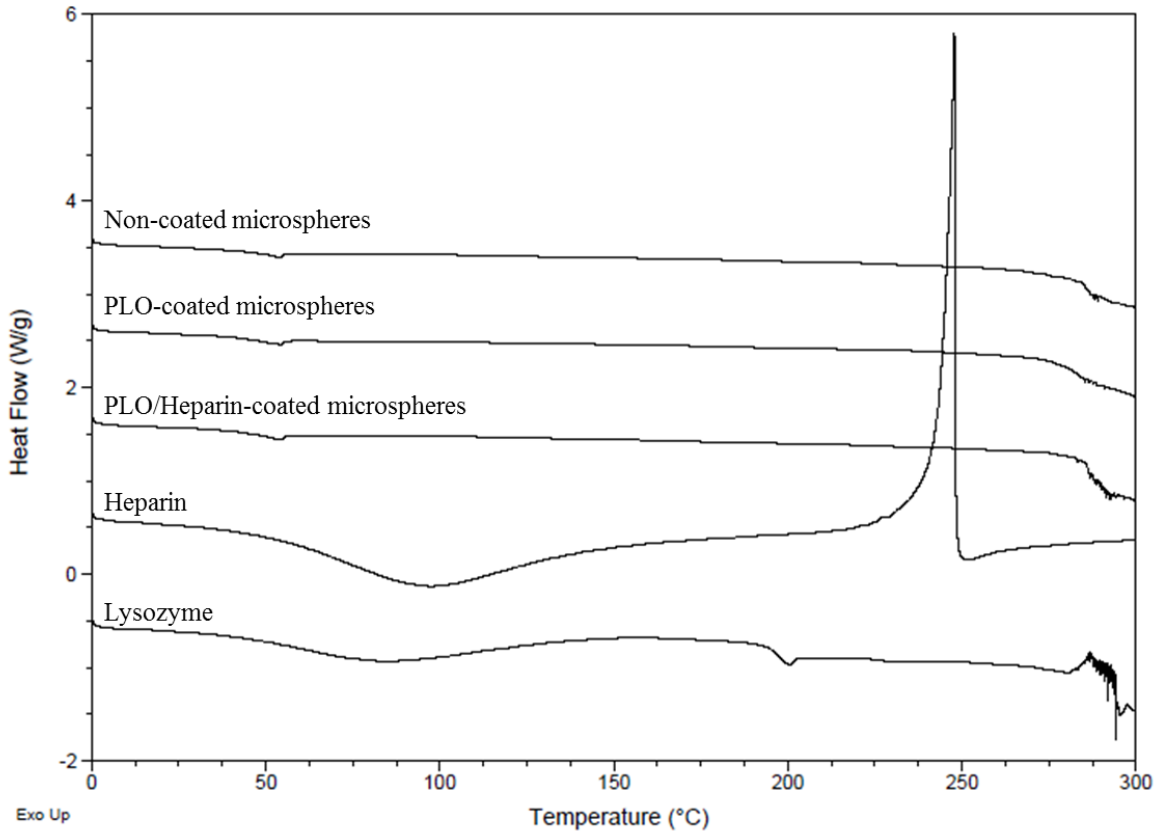


Figure 4.7: DSC thermal profiles of lysozyme-loaded PLGA microspheres coated with poly-$_L$-ornithine or a poly-$_L$-ornithine/heparin polyelectrolyte complex.

Similarly to the Pluronic F127-coated microspheres, the PLO and PLO/heparin coating process resulted in a reduction in the lysozyme content of the microspheres (**Table 4.3**). However, there was no significant difference between the PLO and PLO/heparin-coated microspheres in terms of this reduction ($p > 0.05$). **Figure 4.8** shows the cumulative % release of lysozyme from the microspheres. The burst release at day 1 was significantly reduced by the PLO and PLO/heparin coating ($F_{2,6} = 20.96$, $p = 0.002$). This is most likely due to the polyelectrolyte complex layer formed around the microspheres, which effectively retards the release of the protein. This reduction in the initial burst release is favorable in terms of eliciting a sustained release of protein from the microspheres. However, the large reduction in the lysozyme content as a result of the coating procedure is still a pitfall of this approach.

Table 4.3: Effect of poly-$_L$-ornithine and poly-$_L$-ornithine/heparin polyelectrolyte complex on the lysozyme content of the PLGA microspheres.

Coating	Mean % reduction in lysozyme content post coating	Standard deviation
Poly-$_L$-ornithine	20.91	5.04
Poly-$_L$-ornithine/heparin	16.94	7.15

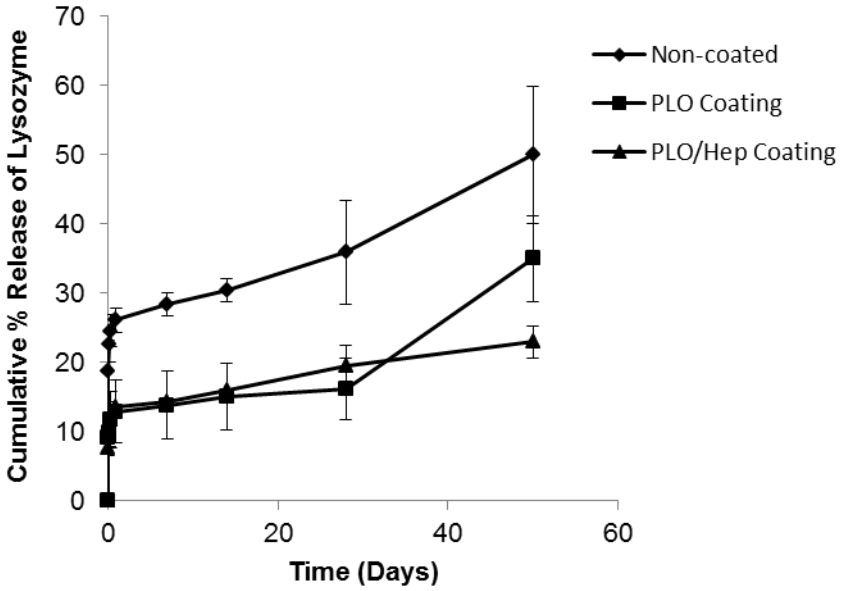


Figure 4.8: Cumulative % lysozyme release from poly-$_L$-ornithine- and poly-$_L$-ornithine/heparin-coated PLGA microspheres

4.3.3 Pectin/κ-carrageenan coated- PLGA microspheres

The use of pectin or κ-carrageenan in combination with PLGA was investigated for the purposes of reducing the burst release of lysozyme from the microspheres. It was hypothesized that the incorporation of a water-soluble polysaccharide into the external aqueous phase would create a hydrophilic coating on the surface on the microsphere, which would help to retard the initial burst release of the surface-associated protein [178]. A

preliminary study was carried out to investigate this. The encapsulation efficiencies of the microspheres were 93.3 ± 3.5, 86.2 ± 1.1 and 91.6 ± 4.0% for the PLGA, PLGA/pectin and PLGA/carrageenan microspheres, respectively. An ANOVA analysis revealed that there was no significant difference between these values ($F_{2,6}$ = 4.24, p = 0.07). The release of lysozyme from the microspheres prepared with 0.1% w/v of either pectin or carrageenan was determined over 24 hours (**Figure 4.9**). As shown in the figure, with the addition of 0.1% pectin or carrageenan, there was a significant increase in the burst release of lysozyme from the microspheres ($p < 0.05$), contrary to our hypothesis. This is most likely due to the increased capability of the aqueous media to penetrate the microspheres [202]. There was a higher burst release from the 0.1% carrageenan formulation when compared with the 0.1% pectin formulation. This may be due to the increased gel formation on the part of κ-carrageenan, as a result of the presence of potassium ions originating from the PBS medium [239]. This gel structure favours the diffusion of more lysozyme out of the microspheres, due to its hydrophilic nature, and results in its subsequent release. Conversely, pectin only forms gels in the presence of divalent cations, which were not present in this study [240].

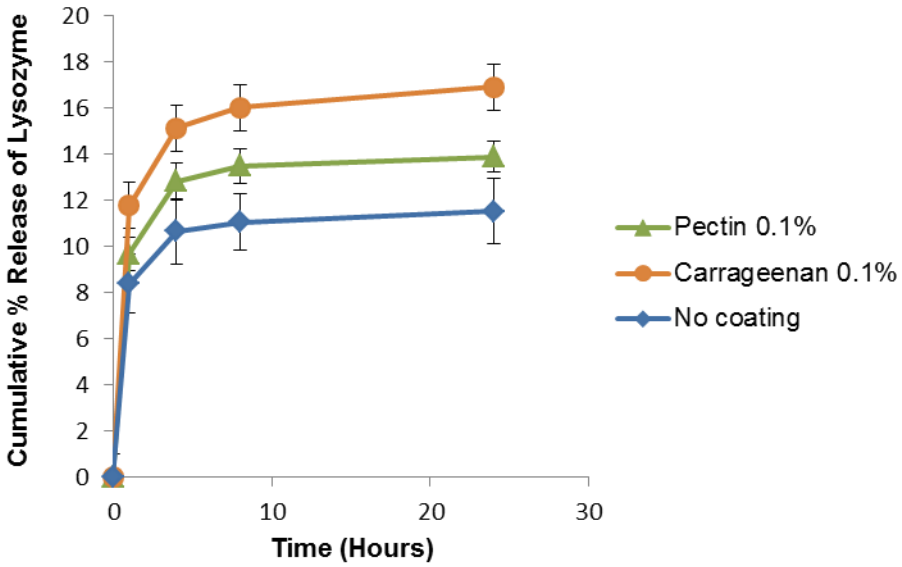


Figure 4.9: Cumulative % lysozyme release from pectin and carrageenan composite microspheres.

In order to see if this was also the case at higher concentrations of pectin and carrageenan, microspheres were formulated with 0.2 and 0.4% w/v of the polysaccharides. The resultant release profiles are shown in **Figure 4.10**. At the highest concentration of carrageenan, 0.4% w/v, the release of lysozyme was significantly higher than that from the PLGA microspheres ($p < 0.05$). The 0.4% w/v pectin/PLGA microspheres also appeared to release more lysozyme; however, this increase in the release was not statistically significant ($p > 0.05$). For both polysaccharides, the 0.2% w/v concentrations did not elicit a significant difference in the release when compared with the PLGA microspheres ($p > 0.05$). Therefore, as this incorporation of the polysaccharides did not elicit the required reduction in the burst release, this coating approach was not taken further.

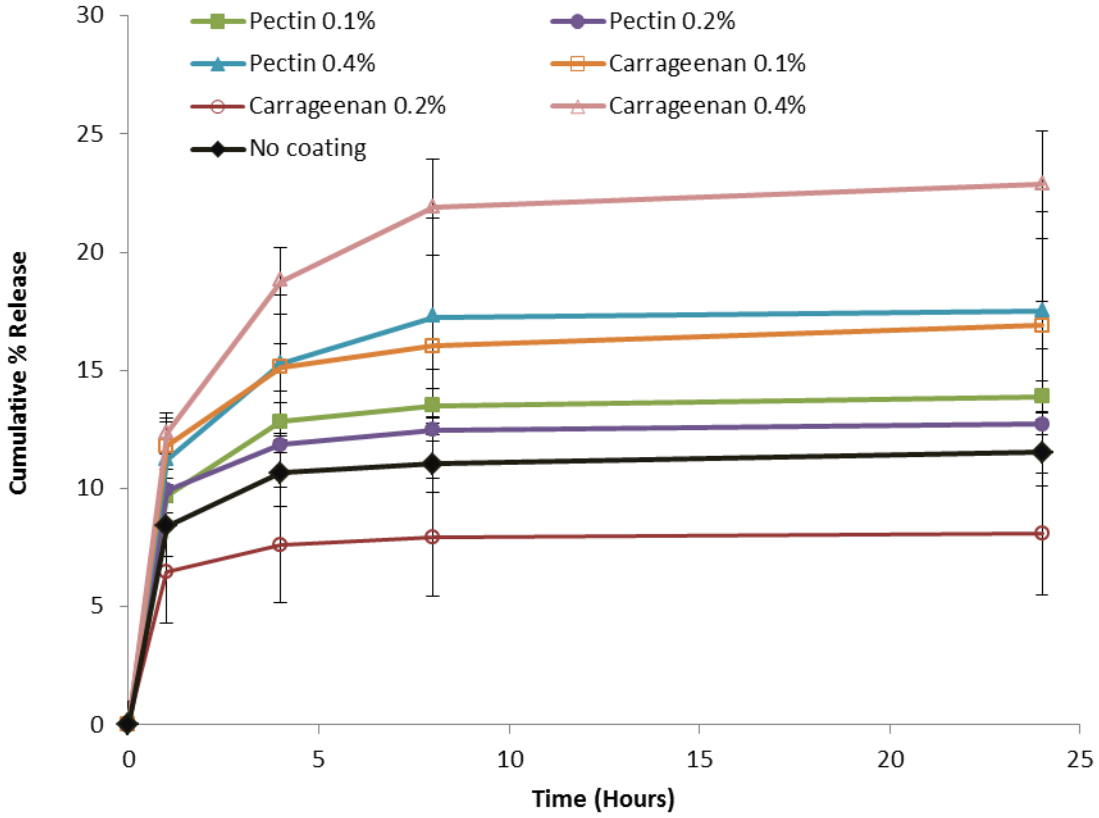


Figure 4.10: Cumulative % lysozyme release from PLGA microspheres prepared with a variety of concentrations of carrageenan and pectin.

4.3.4 Protein-loaded PLGA/chitosan microspheres

Protein-loaded PLGA/chitosan microspheres were prepared using an adapted double emulsion solvent evaporation method, as described in section 4.2.5, with either a low or high concentration of chitosan. SEM images of the resultant microspheres are shown in **Figure 4.11**. Both the PLGA and PLGA/chitosan microspheres demonstrated a smooth, non-porous surface. The size analysis revealed the average diameters of the PLGA, PLGA/low chitosan and PLGA/high chitosan microspheres to be 69.75 ± 21.47, 66.85 ± 22.68 and 66.4 ± 28.39 µm, respectively. The addition of chitosan cross-linked with TPP did not appear to alter the superficial appearance of the microspheres. However, **Figure 4.11C** shows a large amount of debris surrounding the PLGA/high chitosan microspheres, which is not visible in the SEM

images of the PLGA/low chitosan microspheres. Furthermore, **Figure 4.11D** reveals an irregularly shaped size distribution for the PLGA/high chitosan microspheres, which confirms the presence of the debris. This debris is most likely excess chitosan that was not cross-linked by TPP due to the concentrated nature of the 1% w/v chitosan solution.

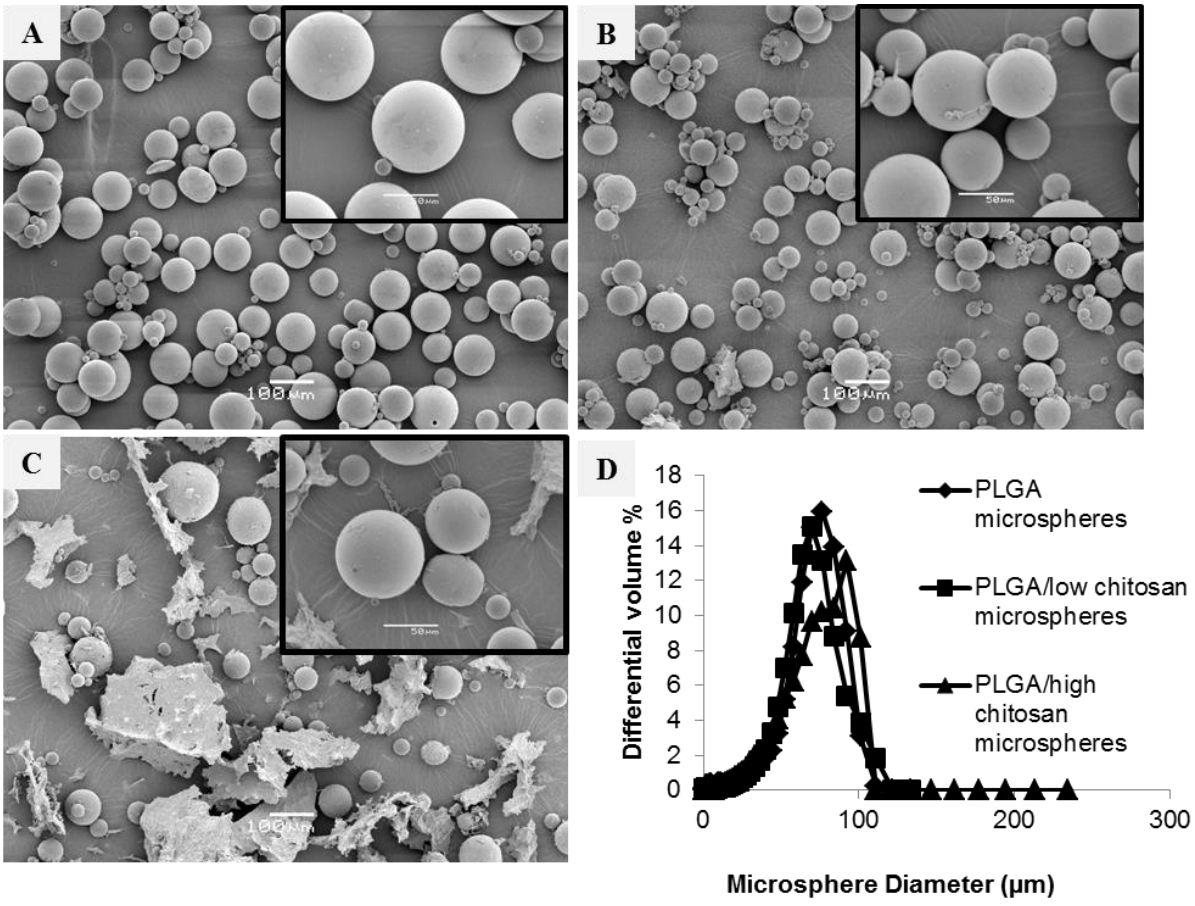


Figure 4.11: Protein-loaded PLGA/chitosan microspheres. SEM images of (A) PLGA microspheres, (B) PLGA/low chitosan microspheres and (C) PLGA/high chitosan microspheres. (C) Size analysis of the microspheres.

For all the previous formulations, lysozyme was used as a model protein. However, in this case lysozyme was found to be unsuitable as a model drug when in combination with chitosan. This is due to the possible enzymatic degradation of chitosan by lysozyme via the hydrolysis of its acetylated residues [217]. For this reason, BSA was selected as an alternative model protein and has previously been used as a substitute for growth factors [46, 58, 220].

The encapsulation efficiencies of BSA in the PLGA, PLGA/low chitosan and PLGA/high chitosan microspheres were 80.58 ± 17.06, 81.57 ± 3.06 and 64.66 ± 1.08%, respectively. There was no significant difference between the PLGA and PLGA/low chitosan encapsulation efficiencies; however, the encapsulation efficiency of the PLGA/high chitosan microspheres was significantly lower than that of the PLGA/low chitosan microspheres.

DSC scans of both the constituent materials and microspheres were carried out from 0 to 250°C and the resulting thermal profiles are shown in **Figure 4.12**. A characteristic T_g of approximately 50°C is evident from the PLGA profile. The thermal profile of TPP shows an endothermic event at 117°C, which emerges due to dehydration. Chitosan showed a broad endothermic peak starting from 50°C and ending at 165°C, which corresponds to its dehydration as a result of the liberation of moisture from the backbone structure [241]. Furthermore, no T_g range is exhibited by chitosan due to the presence of inter- and intra-hydrogen bonding in the backbone. Thermal profiles of the PLGA and PLGA/low chitosan microspheres only show the PLGA T_g. However, the thermal profile of the PLGA/high chitosan microspheres contains a broad peak starting at approximately 58°C and ending at approximately 125°C. This is most likely attributable to chitosan, which further confirms the presence of the debris chitosan within this formulation.

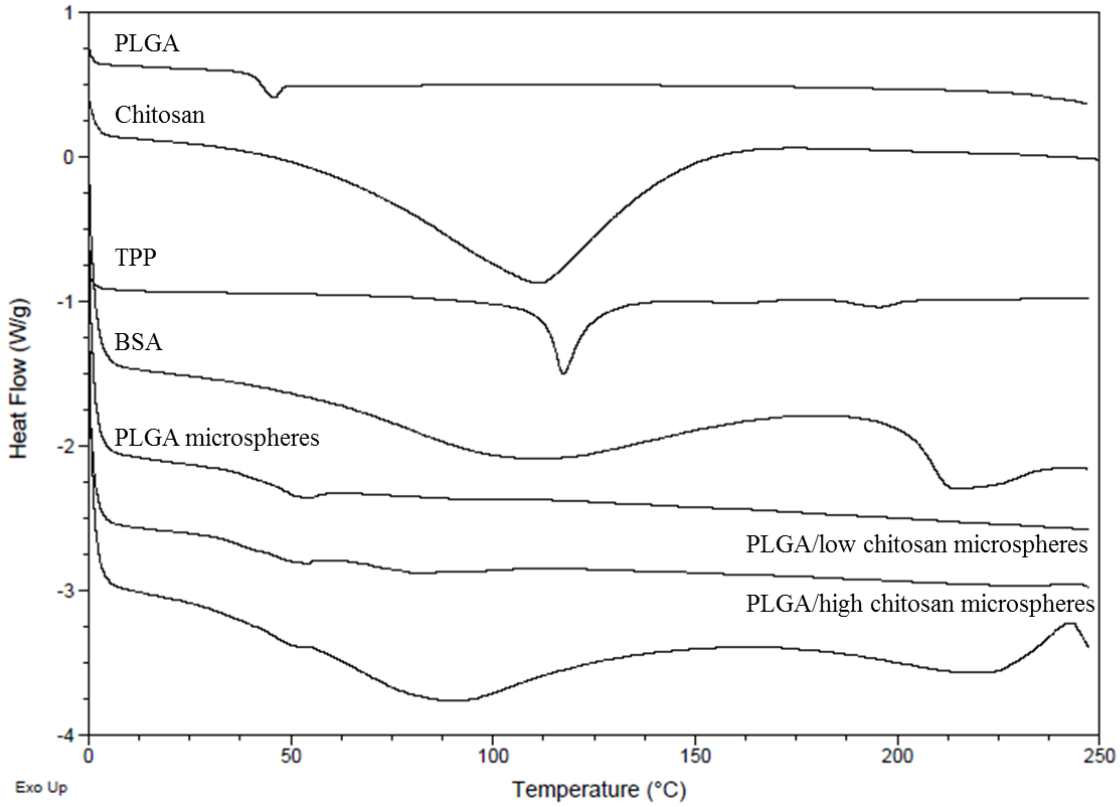


Figure 4.12: DSC thermal profiles of microspheres and their constituents.

Figure 4.13 shows the T_g ranges of the PLGA, PLGA/low chitosan and PLGA/high chitosan microspheres. The microspheres containing chitosan have a lower T_g when compared with the PLGA microspheres. This indicates that the addition of chitosan had a plasticizing effect on the PLGA microspheres. This may be due to the chitosan creating a more hydrophilic environment that is conducive to the retention of water.

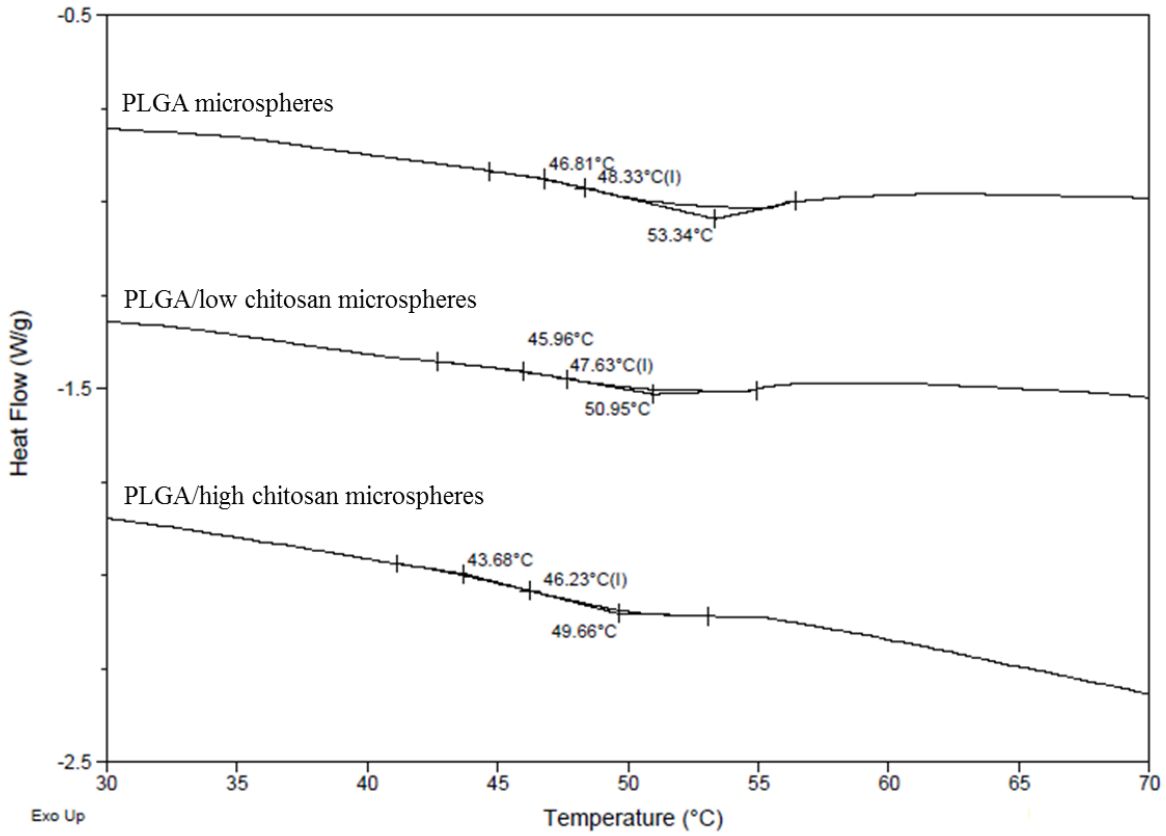


Figure 4.13: DSC thermal profiles indicating the T_g of microspheres.

The release profiles of BSA from the microspheres were mapped over 28 days, as shown in **Figure 4.14**. The initial burst release (24 hours) from PLGA, PLGA/low chitosan and PLGA/high chitosan microspheres was 12.01 ± 0.71, 5.67 ± 0.31 and 10.71 ± 0.51%, respectively. The burst release was significantly lower from the PLGA/low chitosan microspheres when compared with both the PLGA and PLGA/high chitosan microspheres ($p < 0.05$). There was no significant difference between the PLGA and PLGA/high chitosan microspheres ($p > 0.05$).

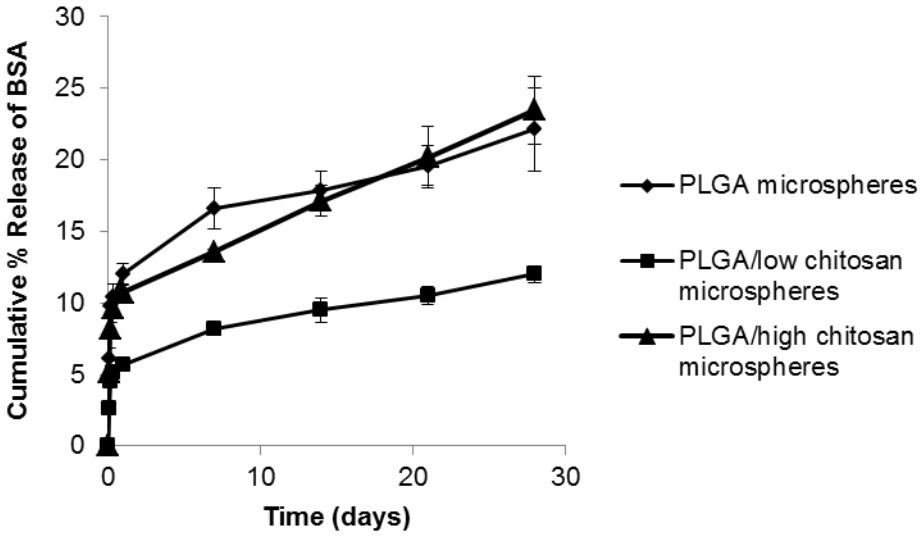


Figure 4.14: Cumulative % BSA release from the PLGA/chitosan microspheres.

The attenuation of the initial burst release exhibited by the PLGA/low chitosan formulation may be attributed to chitosan complexing with BSA (isoelectric point, approximately 5). This is supported by a previous study that confirmed the ability of chitosan, a natural polyelectrolyte, to non-covalently bind to negatively charged proteins [242] . Additionally, the burst release of proteins from PLGA microspheres is usually due to protein adsorbed near or on the surface [243]. The electrostatic interaction between chitosan and TPP helps to form a barrier layer, which in turn retards the release of the protein, hence, contributing to the attenuation in the initial burst release. This effect has been demonstrated in PLGA/chitosan microspheres encapsulated with a non-protein drug, rifampicin, in which the addition of chitosan was able to reduce the burst release [244]. Another reason for the reduction in the burst release is due to the creation of a more hydrophilic environment near the surface, which encourages the retention of BSA in this favourable environment. A similar effect was shown previously with a PLA-PEG copolymer, in which an observed reduction in burst release was attributed to the relative increase in the environment's hydrophilicity as a result of the inclusion of PEG [245].

The lack of significant effects of the PLGA/high chitosan coating on the initial burst release may be attributed to the chitosan debris. In this regard, the reduction in the burst release may be offset by the much greater hydrophilicity that results from the chitosan debris surrounding the microspheres. This may encourage an increased influx of aqueous medium in the areas adjacent to individual microspheres; hence, encouraging the release of BSA. Therefore, the effect of the debris may cancel out the beneficial effect that chitosan has on reducing the initial burst release, resulting in a release similar to that of BSA from PLGA microspheres alone.

4.4 Conclusions

In this chapter, various coatings were investigated for their effect on the initial burst release of protein from the PLGA microspheres. A post-microsphere-production coating of Pluronic F127 resulted in a significant loss of protein from the microspheres as a result of the coating procedure, which was not accompanied with a reduction in the burst release. Therefore, this coating was deemed undesirable. Although we managed to reduce the burst release using a PLO/heparin coating, the coating procedure resulted in a reduced amount of protein loading within the microspheres; therefore, it is not suitable for the current application. When pectin and carrageenan were incorporated into the microspheres, an increase in the burst release was observed at some polysaccharide concentrations; whereas, no difference was observed with others. Finally, PLGA microspheres prepared with a low chitosan coating were found to elicit a reduction in the burst release, whilst maintaining the encapsulation efficiency of the uncoated PLGA microspheres. For this reason, the PLGA/low chitosan formulation was chosen for further investigation in order to characterize it in more detail, and to elucidate its ability to support cell growth and proliferation.

Chapter 5: Further characterisation and *in vitro* testing of PLGA/chitosan composite microspheres and scaffolds

5.1 Introduction

In Chapter 4, we addressed the issue of the initial burst release of protein from the microspheres via the incorporation of chitosan into the protein-loaded microspheres. In this chapter, we report the characterisation of these microspheres and scaffolds further in order to relate the incorporation of chitosan with the physical properties of the microspheres and scaffolds. Specifically, we aimed to characterise these microspheres and scaffolds in order to determine the location of chitosan within them. It was also important to determine the protein release profiles of the microspheres in combination with the porous microspheres, as this presents the potential form of the prototype. Furthermore, the biocompatibility of the scaffolds was ascertained through the application of appropriate cell lines. Different cell lines have been used in bone tissue engineering research, one example is the NIH-3T3 fibroblast cell line that is derived from a Swiss mouse embryo [142]. The ease of obtaining large numbers of these cells in a reproducible manner, in addition to their ability to deposit ECM are some of the reasons for the wide use of NIH-3T3 cells [246]. The MG-63 osteosarcoma cell line is another common choice for evaluating a biomaterial's compatibility for use in bone tissue engineering [247–250]. These cells proliferate more rapidly than other human-derived bone cells that are non-cancerous; therefore, they are an economical cell-line for use in biocompatibility tests [251]. They also possess osteoblastic traits and are considered to be immature osteoblasts [251]. For these reasons, MG-63 cells were selected for the preliminary screening of the PLGA/chitosan composite scaffold biocompatibility studies.

MSCs are adult stem cells that are widely-accepted as a clinically relevant choice of cell type in bone tissue engineering due to their role in the natural process for the development of bone [17]. Furthermore, MSCs have great osteogenic potential and have previously been used for the *in vitro* testing of scaffolds [46, 252]. For this reason, we chose to use primary human MSCs (hMSCs) for further biocompatibility and osteogenic screening,

following the use of MG-63 cells. Primary cells are derived directly from the human tissue of a specific person; therefore, they increase the clinical relevance in comparison with the use of immortalized cells, which may have slight differences to their primary counterparts. They are one step closer to *in vivo* testing conditions than an immortalized cell line would be; therefore, we opted to use them in this phase of the work. The use of the primary cells in this study did not require a Human Tissue Authority (HTA) licence as all the original cells had divided prior to purchase; therefore, they were not classified as "relevant material" by the HTA and did not require ethical approval under the Human Tissue Act [253].

5.2 Materials & Methods

5.2.1 Materials

For MG-63 cell culture, Eagle's minimum essential medium (EMEM) was purchased from ATCC (USA). Foetal bovine serum (FBS), trypsin EDTA, antibiotic-antimycotic solution (×100) and Presto Blue cell viability reagent were purchased from Gibco, Life Technologies (USA). Dulbecco's phosphate-buffered saline (modified 10×) liquid was purchased from Sigma-Aldrich. A live/dead cell double staining kit (04511-1KT-F) was purchased from Sigma-Aldrich.

For stem cell culture, hMSCs, an MSCGM hMSC SingleQuot kit, an hMSC Osteogenic BulletKit, trypsin/EDTA for MSC and HEPES-buffered saline were purchased from Lonza (Switzerland). For immunostaining, anti-osteocalcin polyclonal antibody was purchased from Merck Millipore (USA) and Alexa Flour 488 goat anti-rabbit IgG was purchased from Invitrogen (USA). Triton X-100, goat serum, Hoechst 33258, sodium thiosulphate solution, silver nitrate solution, formalin 10% v/v and paraformaldehyde 10% v/v solutions were all purchased from Sigma-Aldrich. Glacial acetic acid was purchased from R&M Chemicals (UK).

5.2.2 Preparation of non-porous and porous microspheres

BSA-loaded and blank PLGA/chitosan and PLGA microspheres, in addition to porous microspheres, were prepared as detailed in the previous chapters (section 2.2.3, 3.2.2 and 4.2.5). In order to determine the effect of the molarity of the sodium hydroxide used for the pH of adjustment of chitosan on the morphology, size and biocompatibility of PLGA/chitosan microspheres, 0.5 M, 1 M and 2 M sodium hydroxide solutions were utilised.

5.2.3 Fourier transform infrared (FTIR) spectroscopy analysis of PLGA/chitosan non-porous microspheres

FTIR spectra of PLGA, chitosan, TPP, BSA, PLGA microspheres and PLGA/chitosan composite microspheres were obtained using a Spectrum RX 1 FTIR spectrophotometer (Perkin Elmer, USA). The samples were mixed with potassium bromide (KBr) and compressed with a 5-tonne force into disks and 256 scans were acquired from 400 to 4000 cm^{-1}.

5.2.4 Preparation of 3D scaffolds

3D scaffolds were prepared by forming a paste, as described in Chapter 3 (section 3.2.6).

5.2.5 Encapsulation efficiency of the scaffolds

The encapsulation efficiencies of BSA within the scaffolds were determined by gently submerging 1 scaffold in 13 ml of DMSO for 1 hour. This was then followed by the addition of 37.27 ml of 0.02% (w/v) SDS in 0.2 M NaOH. The solution was left standing at room temperature (25°C) for 1 hour. Standard concentrations of BSA were calibrated with a BCA reagent so that sample absorbance could be matched with standard concentrations on an

Infinite 200 plate reader (Tecan, Switzerland) at 562 nm. The encapsulation efficiency (%EE) of BSA within the scaffolds was then calculated using Equation 5.

$$\%\mathbf{EE} = \frac{\textbf{Actual mass of BSA in 1 scaffold}}{\textbf{Theoretical mass of BSA used for 1 scaffold}} \times \mathbf{100} \qquad \textbf{Equation 5}$$

5.2.6 ToF-SIMS analysis

The level of chitosan coating on the scaffold surfaces was assessed using ToF-SIMS as detailed in Chapter 3 (section 3.2.7). Negative and positive polarity data for 500 × 500 µm areas were analysed using the SurfaceLab 6® software (IONTOF). BSA-loaded and blank PLGA/chitosan scaffolds were analysed in order to determine the marker secondary ion peaks for chitosan and BSA; however, as shown in **Figure 5.1,** there was an overlap in the peaks, which made it difficult to differentiate between the two. Due to this difficulty, blank PLGA and PLGA/chitosan scaffolds were analysed and examples of these spectra are shown in **Figure 5.2.** PLGA was identified by the presence of $C_3H_3O_2^-$ (*m/z* = 71) and $C_3H_5O_2^-$ (*m/z* = 73) [196]. Diagnostic secondary ion peaks for chitosan were identified as CN^- (*m/z* = 26) from the negative polarity data, in addition to CH_4N^+ (*m/z* = 30) and $C_4H_5N_2^+$ (*m/z* = 81) from the positive polarity data. For a semi-quantitative analysis, each area was split into four regions of interest, and the ion intensity data for these peaks of interest were exported and normalized to the total ion intensity.

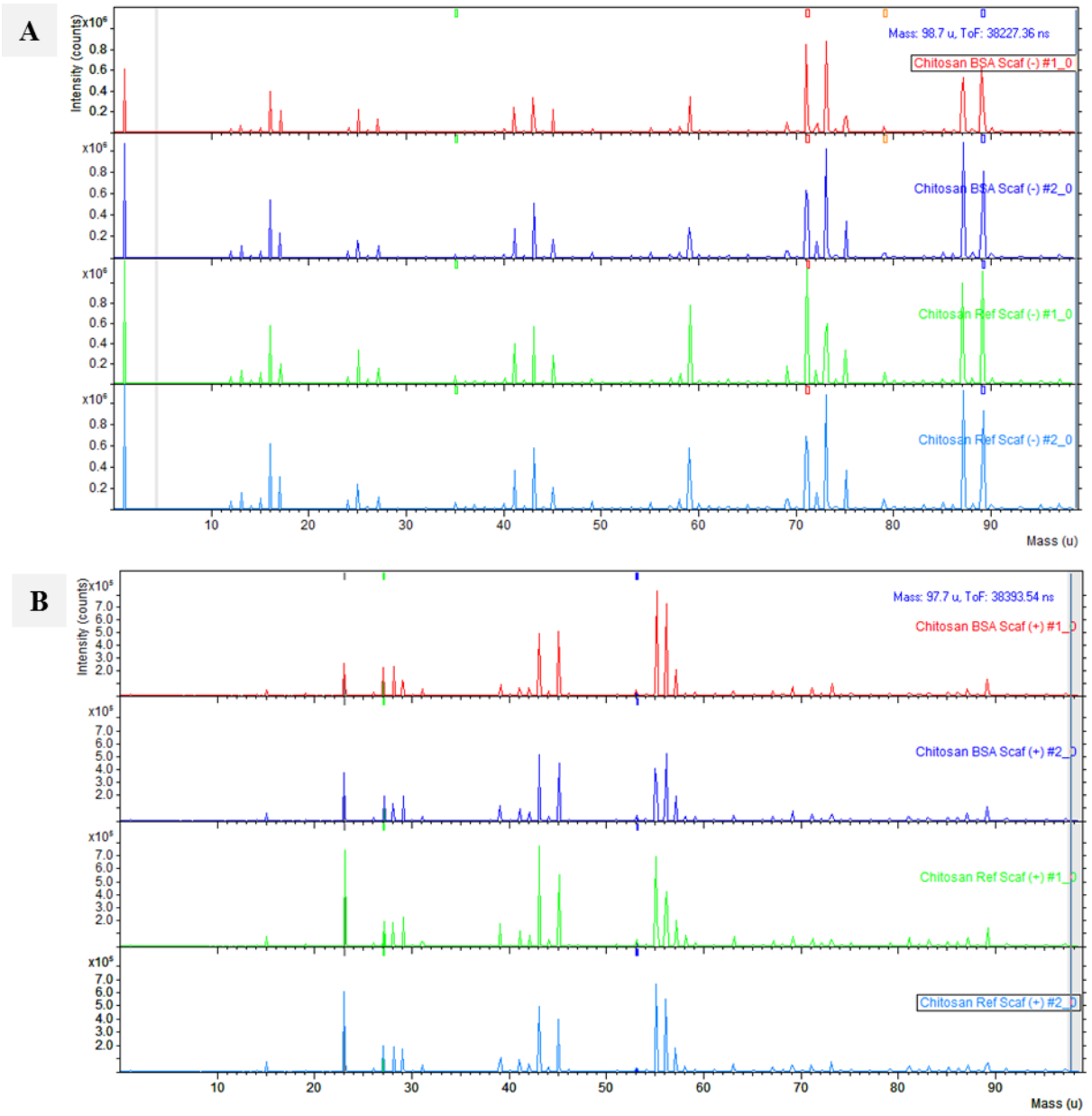


Figure 5.1: ToF-SIMS (A) negative and (B) positive spectra of BSA-loaded and blank PLGA/chitosan scaffolds.

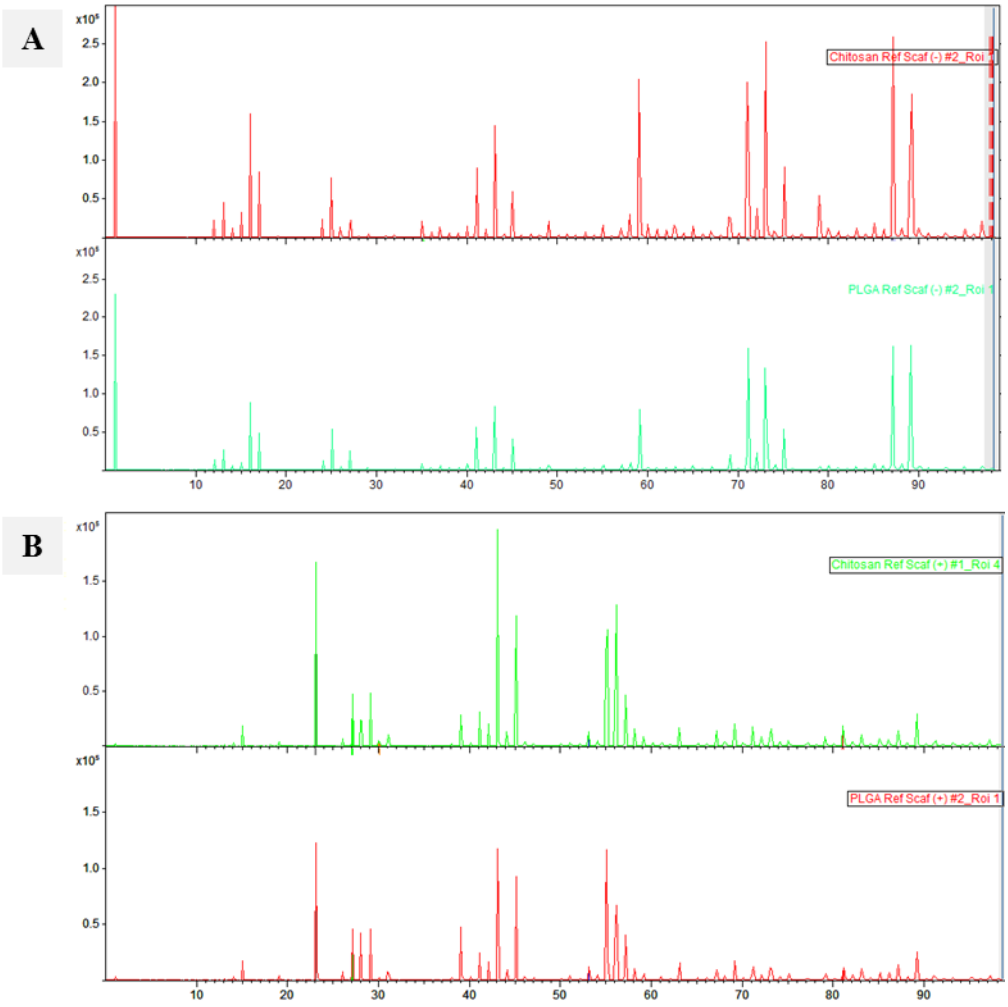


Figure 5.2: ToF-SIMS (A) negative and (B) positive spectra of PLGA and PLGA/chitosan scaffolds.

5.2.7 Release of BSA from the scaffolds

Release studies of BSA from the PLGA and PLGA/chitosan composite scaffolds were carried out as detailed in Chapter 3 (section 3.2.8).

5.2.8 Preparation of 3D scaffolds after injection through a needle

Microsphere mixtures were prepared at a 1:1 ratio of porous to non-porous microspheres and an approximate BSA loading of 3 mg of BSA/g of mixture. The mixture was suspended in PBS at a concentration of 50 mg of microspheres/ml, vortex-mixed briefly

and then drawn into a 1 ml syringe (BD Fine) fitted with a 19-G needle (1.1 × 50 mm, BD fine). Finally, the contents of the syringe were injected into the PTFE scaffold mould.

5.2.9 Compressive strength of scaffolds

The compressive strength of the scaffolds was assessed as detailed in Chapter 3 (section 3.2.7) using a TA.HD+ texture analyser (Stable Microsystems, UK) equipped with a 50-kg load cell at a speed of 0.04 mm/second over a contact area of approximately 28.75 mm^2. BSA-loaded PLGA and BSA-loaded PLGA/chitosan scaffolds prepared using the paste and post-injection methods were subjected to a compressive force and the stress at the maximum strain was determined.

5.2.10 Cell culture and seeding onto scaffolds

MG-63 osteosarcoma cells were cultured in EMEM supplemented with 10% FBS and 1% antibiotic-antimycotic solution. Primary hMSCs were cultured in hMSC basal media supplemented with the contents of an MSCGM hMSC SingleQuot kit. Both cell-types were maintained in a humidified tissue-culture incubator at 37°C and 5% CO_2.

The biocompatibility test was carried out on BSA-free scaffolds in order to investigate cell behaviour (i.e. growth and differentiation) on the scaffold material. Scaffolds were prepared directly into a 24-well plate. A 1:1 porous to non-porous microsphere mixture was UV-sterilised for 80 minutes [252] and then transferred to the well. Basal growth media was then added at a ratio of 0.25:1 of media to microspheres, respectively. After 17 hours of sintering, each scaffold was seeded with either 2×10^5 MG-63 cells or 1×10^5 hMSCs and incubated for 2 hours, followed by the addition of 1 ml of media to each scaffold/well. The cell-seeded scaffolds were maintained at 37°C and 5% CO_2. For all the cell experiments, either one independent experiment of 3–5 replicates was carried out or two independent experiments, each comprising at least 3 replicates.

5.2.11 Cell viability assay

Each scaffold was submerged in 1 ml of media and 111 µl of Presto Blue reagent and the cell viability was determined at day 1, 3, 6 and 8 post-seeding using the Presto Blue cell viability reagent. The well plate was protected from light and incubated at 37°C for 25 minutes. Aliquots of 100 µl were withdrawn from each well in triplicate and the absorbance was read on a Varioskan Flash plate reader (Thermo Scientific) or an Infinite 200 plate reader (Tecan, Switzerland) at excitation and emission wavelengths of 560 and 590 nm, respectively, for the MG-63-seeded and hMSC-seeded scaffolds. In the case of the hMSC-seeded scaffolds, the Presto Blue reagent was replaced with fresh media and the scaffolds were returned to the incubator. In the case of the MG-63-seeded scaffolds, three new scaffolds were studied at each separate time point. After measuring the cell viability on day 8, the scaffolds seeded with hMSCs were washed with PBS and the cells were fixed with 10% v/v formalin solution for 20 minutes and then underwent SEM.

5.2.12 Assessment of mineralization

The mineralisation on the hMSC seeded-scaffolds was studied using the von Kossa assay. Briefly, cells were seeded onto the scaffolds as described in section 5.2.10 and incubated in basal or osteogenic media for 21 days. On day 21, cells were fixed with 10% v/v formalin for 20 minutes and thoroughly washed with PBS. A 450-µl aliquot of 1% w/v silver nitrate solution was added to each scaffold and incubated under a UV light source for 1 hour. The solution was then removed and the scaffolds were washed three times with deionized water. This was followed by treatment with sodium thiosulphate solution for 5 minutes in order to remove any excess silver nitrate solution. The scaffolds were washed with PBS prior to imaging under a dissection microscope (Leica, Germany).

5.2.13 Osteocalcin immunostaining

For the osteocalcin immunostaining, cells were seeded onto the scaffolds, as described in section 5.2.10. The scaffolds were incubated in basal or osteogenic growth media for 21 days, after which they were fixed using 10% v/v paraformaldehyde for 20 minutes and then thoroughly washed with PBS. The cells were permeabilised with 500 µl of 0.1% v/v Triton X-100 solution for 40 minutes; the solution was aspirated and the cells were washed with PBS. Blocking of unspecific binding sites as a result of epitomes on the cell layers was carried out via the addition of 500 µl of 3% v/v goat serum in 1% w/v BSA in PBS for 40 minutes. The blocking solution was removed and 500 µl of anti-OCN primary antibody solution (1:200 dilution in 1% w/v BSA in PBS) was added. The scaffolds were incubated at 4°C overnight, and then washed with PBS and incubated at room temperature for 2 hours in 500 µl of a 1:200 solution of Alexa Flour 488 goat anti-rabbit secondary IgG, in 1% w/v BSA in PBS. After incubation, the secondary antibody solution was removed and the scaffolds were washed with PBS. In order to stain the DNA of the cells, the scaffolds were incubated for a further 15 minutes in 1 µg/ml Hoechst dye dissolved in 1% w/v BSA in PBS at room temperature. After this incubation, the Hoechst dye was removed and the scaffolds were thoroughly washed with PBS and then viewed under a dissection microscope. Four images of each scaffold were taken and the PLGA and composite scaffolds were processed and compared using the ImageJ software (Version 1.48, National Institute of Health, USA).

5.3 Results and Discussion

The PLGA/chitosan composite microspheres were further characterised and studied in order to determine their suitability for bone tissue engineering applications. Their compatibility with two different cell lines was also studied, as this is a key indicator that influences the regenerative potential of a biomaterial. The various aspects of the studies are presented and discussed in detail in the following sections.

5.3.1 FTIR

The FTIR spectra of the excipients and microspheres are presented in **Figure 5.3**. The chitosan spectrum shows a high-intensity peak at 3400 cm^{-1}, which corresponds to stretching vibrations of the O-H and N-H bonds, in addition to hydrogen bonding in the backbone [254]. The characteristic peak at 1647 cm^{-1} is a result of the amide functionality and may be present as a consequence of the axial deformation of the C=O bond [254] and strong N-H bending [241]. Peaks present at 1019 and 1086 cm^{-1} (corresponding to C-O stretch vibrations), and 1152 cm^{-1} (asymmetric stretch of the C-O-C bond) are also indicative of moieties within chitosan [254]. The TPP spectrum, similarly, shows a peak of significant intensity at 3390 cm^{-1}, corresponding to the stretching vibrations of the O-H bond. Peaks around the 1095 cm^{-1} region indicate the presence of a P=O phosphate group. The PLGA spectrum presents a peak at 3473 cm^{-1}, which is indicative of the vibration of the terminal O-H groups. Other peaks that indicate PLGA are present at 743 cm^{-1} (C-H bend), 1086 and 1180 cm^{-1} (C-O stretch), 1381 cm^{-1} (C-H bend), 1771 cm^{-1} (the carbonyl C=O) and 2876 cm^{-1} (CH_2 bend) [241]. The spectra of both PLGA and PLGA/chitosan composite BSA-loaded microspheres show peaks at identical wavelengths, which suggests that the microspheres are predominantly composed of PLGA. Moreover, the spectra of PLGA and PLGA/chitosan composite microspheres show peaks at 1621 cm^{-1} and 1639 cm^{-1}, respectively, which are attributed to the C=O bond of the amide groups that are found both in BSA and chitosan. However, there appears to be a slightly more pronounced peak at 1639 cm^{-1} on the spectrum of the PLGA/chitosan composite microspheres, which corresponds to the amide C=O bond suggesting the presence of chitosan in the formulation.

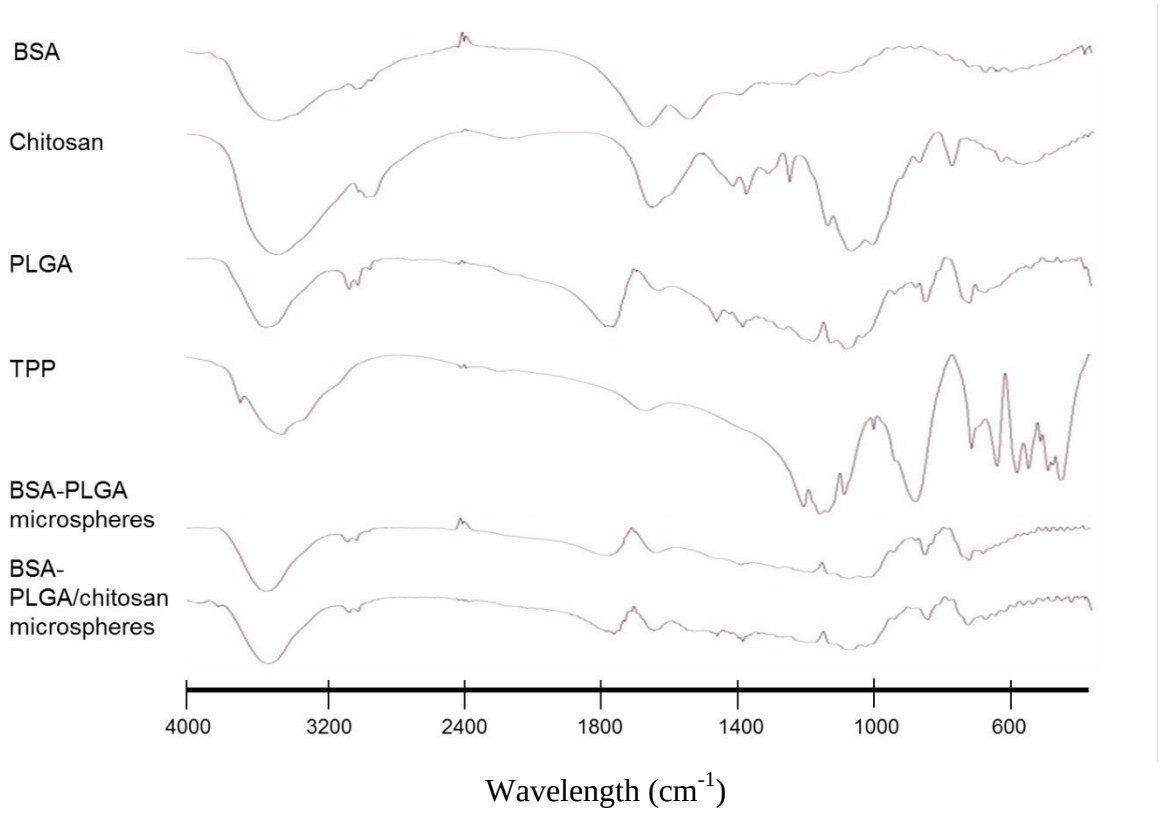


Figure 5.3: FTIR spectroscopy of PLGA and PLGA/chitosan microspheres and their constituents.

5.3.2 Encapsulation Efficiency

The incorporation of chitosan did not elicit a significant change in the encapsulation efficiency of BSA in the microspheres, with 80.58 ± 17.06 and 81.57 ± 3.06% of the protein being encapsulated into the PLGA and composite microspheres, respectively (section 4.3.4, Chapter 4). Moreover, there was no statistical difference (as determined by an ANOVA analysis and t tests) between the encapsulation efficiencies of the PLGA and composite scaffolds (2.81 and 2.52 mg/g for the PLGA and PLGA/chitosan composite scaffolds, respectively). The initial phase during the primary emulsion formation was identical for both formulations. At this point, the protein solution is emulsified in the PLGA solution. Therefore, the data suggest that the addition of chitosan did not affect this procedure.

Furthermore, these observations point to the formation of a surface coating of chitosan (discussed in detail in 5.3.3).

5.3.3 ToF-SIMS analyses of the scaffold surfaces

The ToF-SIMS analyses were carried out in order to ascertain the presence of chitosan on the scaffold surfaces. The intensities of the nitrogen-containing positive secondary ion peaks CH_4N^+ (*m/z* = 30) and $C_4H_5N_2^+$ (*m/*z = 81), as well as the negative ion peak CN^- (*m/z* = 26) were all significantly higher in the composite PLGA/chitosan scaffolds when compared with the chitosan-free scaffolds, as shown in **Figure 5.4A**. However, there was no significant difference between the profiles of the diagnostic PLGA ion peaks of the PLGA and composite scaffolds (**Figure 5.4B**). Representative ion intensity maps are shown in **Figure 5.5**, and confirm the higher intensity of the secondary ion peaks at *m/z* of 26, 30 and 81. The ToF-SIMS analysis, therefore, confirms that chitosan is also present on the surface of the scaffolds.

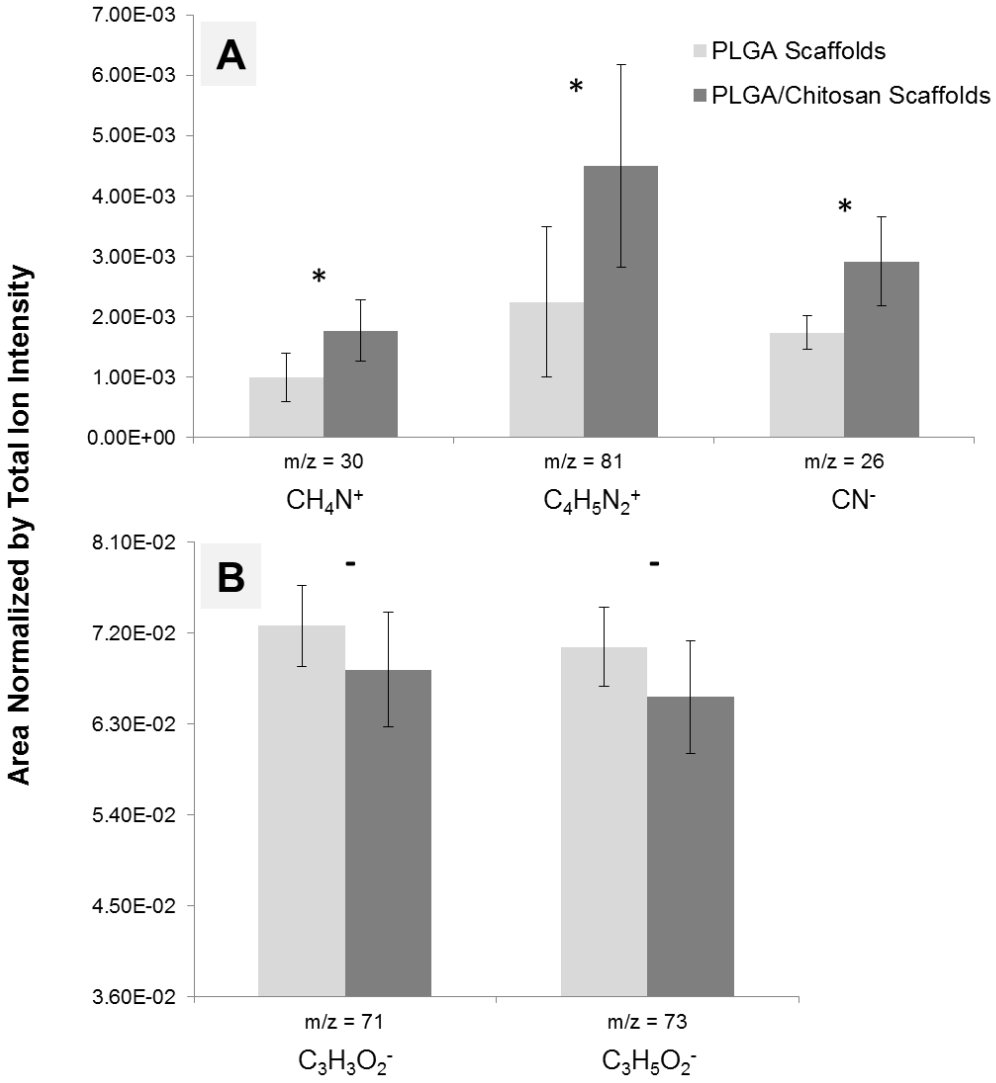


Figure 5.4: ToF-SIMS analysis of PLGA and PLGA/chitosan scaffolds. Areas of diagnostic ion peaks for (A) chitosan and (B) PLGA. Data points represent the mean ± standard deviation; * $p < 0.05$, - $p > 0.05$.

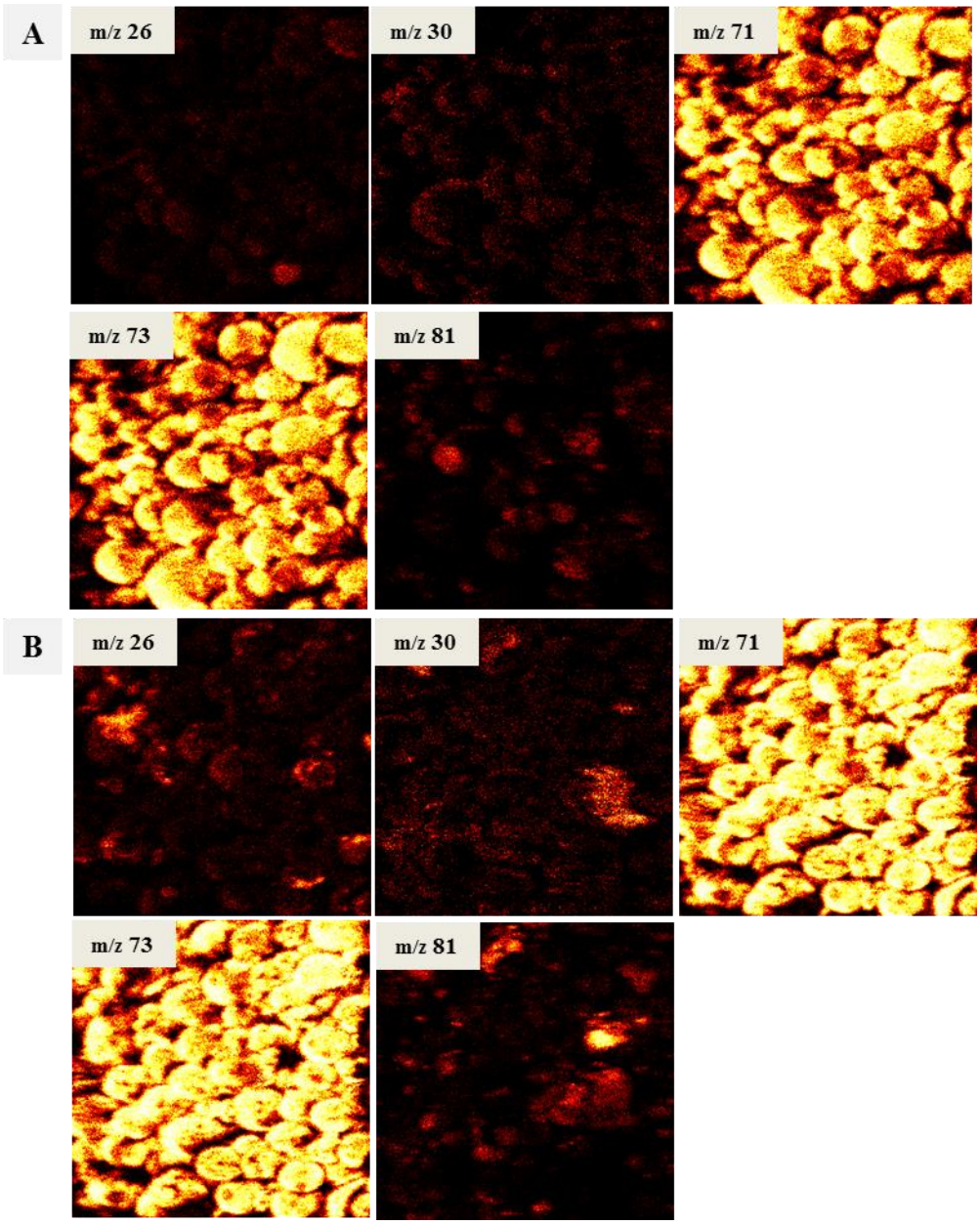


Figure 5.5: Secondary ion intensity maps of (A) PLGA and (B) PLGA/chitosan scaffolds.

5.3.4 Release of BSA from scaffolds

There was a significant retardation of the initial burst release (after 24 hours) of BSA from the PLGA/chitosan composite scaffolds (0.10 ± 0.02 µg/mg), in comparison with the PLGA scaffolds (0.16 ± 0.01 µg/mg, $p < 0.05$), as shown in **Figure 5.6B**. **Figure 5.6A** shows that the overall percentage release of BSA from the PLGA/chitosan composite scaffolds was

lower than that from the PLGA scaffolds; however, this was not statistically significant ($p > 0.05$).

This attenuation of the initial burst release, as mentioned in the previous chapter, is most likely attributable to chitosan complexing with BSA and the formation of a matrix layer between chitosan and TPP. These factors in turn slow the release of the protein and, hence, result in an attenuation of the initial burst release.

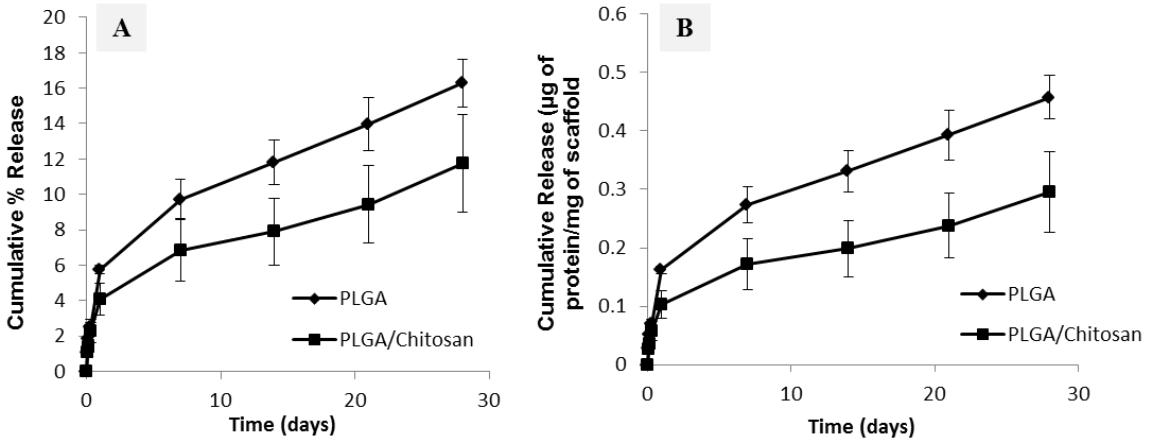


Figure 5.6: Release of BSA from PLGA/chitosan composite and PLGA scaffolds. (A) Cumulative percentage release and (B) cumulative release (µg of protein/mg of scaffold).

5.3.5 Sintering and compressive strength

In order to study the effect of the preparation method of the scaffolds on their subsequent morphology and mechanical strength, the PLGA and PLGA/chitosan composite scaffolds were prepared using two different methods. Firstly, the microspheres were made into a paste, as reported in Chapter 3 (section 3.2.6). In the second method, we aimed to study the ability of the microspheres to sinter post-injection through a 19-G needle into a scaffold mould. This was then followed by a 17-hour incubation period at 37°C. The resulting scaffolds and their compressive strengths are presented in **Figure 5.7**.

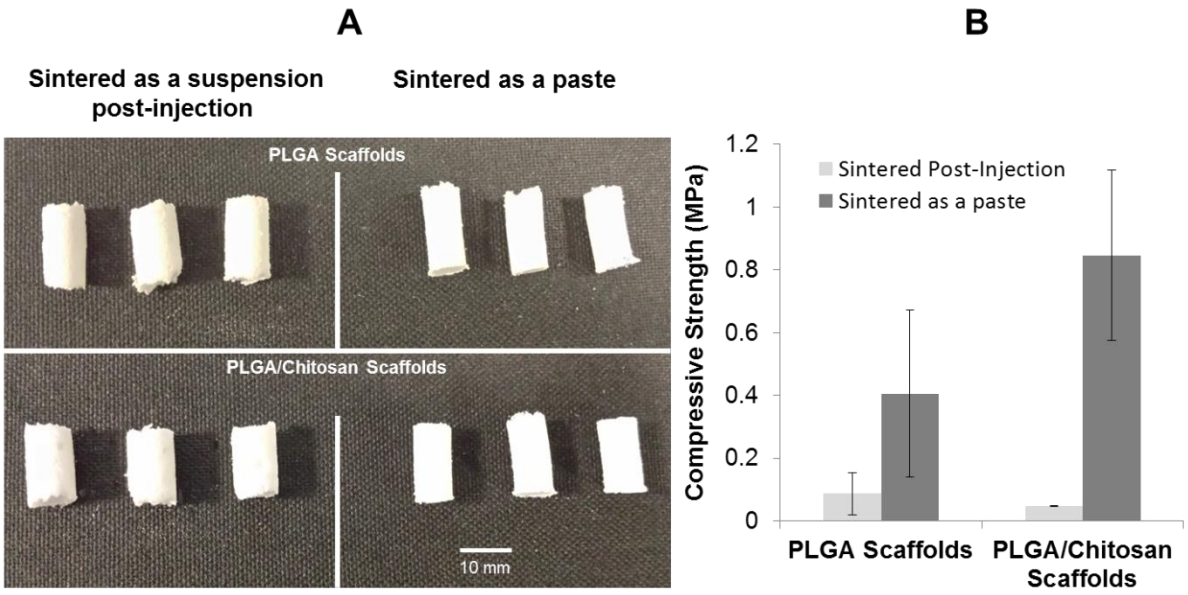


Figure 5.7: Morphology and compressive strength of PLGA and PLGA/chitosan scaffolds. (A) Images of PLGA and PLGA/chitosan scaffolds sintered as a suspension, post-injection through a 19 G needle and as a paste. (B) Compressive strength of scaffolds sintered post-injection through a 19 G needle and as a paste. Data points represent the mean ± standard deviation.

The overall appearances of the PLGA and composite scaffolds were very similar. However, when comparing the scaffolds prepared using the paste method, the PLGA/chitosan composite scaffolds had a significantly higher compressive strength (0.846 ± 0.272 MPa) than the PLGA scaffolds that were prepared using the same method (0.406 ± 0.265 MPa, $p < 0.05$). This increased strength could be due to interactions between the microspheres as a result of the negatively charged PLGA [255] interacting with protonated amine groups in the chitosan structure. Additionally, the reduction in the T_g (shown in section 4.3.4, Chapter 4) of the composite microspheres may favour more effective sintering between the microspheres [197]. It is also important to note that the compressive strength demonstrated by the composite scaffolds falls within an acceptable range of 0.22–10.44 MPa, as reported by Misch et al. [203].

Figure 5.7A shows that it was possible to successfully sinter a microsphere suspension into a scaffold following injection through a needle. This crucially confirms the injectable potential of the microspheres. When scaffolds were sintered as a suspension post-injection, there was no significant difference between the compressive strengths of the PLGA and composite scaffolds, 0.086 ± 0.068 and 0.048 ± 0.00096 MPa, respectively ($p < 0.05$, **Figure 5.7B**). The lower compressive strength of the scaffolds prepared via the injection method may be due to the retention of liquid during the sintering process. This required a longer drying time, which is likely to enhance the strength of the scaffolds.

These results show that the system possesses dual-functionality arising from the formulation's potential of having two application modes (i) a paste that is implanted within degenerated bone tissue, takes the shape of the defect area and then sinters at body temperature (37°C) and (ii) the injection of the microsphere suspension directly into the defect area, which then sinter. The former would be useful in applications requiring a relatively strong scaffold, such as the regeneration of cancellous bone for which the ultimate compressive strength has been reported to range from 0.22 to 10.44 MPa [203]. Whereas, the latter, due to its lower compressive strength, is more suited to applications in which the delivery system may be injected and remain in one location, hence, allowing the controlled delivery of a specific, known dose of protein to the site. To our knowledge, this is the first time that the ability of microspheres to sinter at 37°C, post-injection, has been demonstrated.

5.3.6 Cell proliferation on scaffolds

The ability of cells to attach and grow on the scaffolds is paramount in the development of protein delivery systems in regenerative medicine. The biocompatibility of the scaffolds with a human osteoblast cell-line, MG-63 cells, was determined using the Presto Blue viability reagent on day 1, 3 and 6 (**Figure 5.8**). The cell proliferation increased over time on both scaffold types. On day 1, the cell numbers on PLGA and composite scaffolds

were 4.58×10^4 and 4.37×10^4, respectively. Both types of scaffolds exhibited a very similar cell growth profile with no statistically significant difference found between them ($p > 0.05$) on day 1, 3 and 6. The treatment of samples with calcein-AM allowed for the staining of live cells. Calcein-AM is not itself fluorescent; however, when it is converted to calcein by the esterase enzyme present in living cells, it emits green fluorescence at 490 nm. The images in **Figure 5.8** show a good distribution of the cells on both types of scaffolds by day 3.

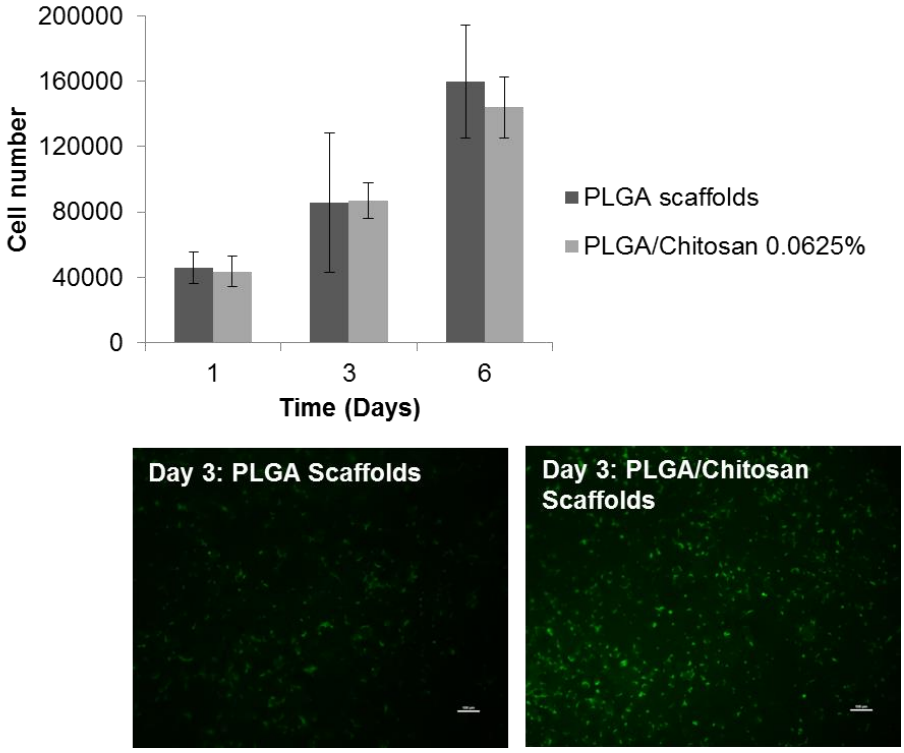


Figure 5.8: Biocompatibility of MG-63 osteosarcoma cells with PLGA and PLGA/chitosan scaffolds. Data points represent the mean ± standard deviation. Live cells were stained with calcein-AM on day 3.

In order to replicate the potential clinical conditions more closely, primary hMSCs were grown on the scaffolds. As with the MG-63 cells, hMSC proliferation increased over time on both scaffold types (**Figure 5.9**). On day 1, the cell numbers on the PLGA and PLGA/chitosan composite scaffolds were 1.06×10^4 and 1.03×10^4, respectively. Both types of scaffolds exhibited a very similar cell growth profile with no statistically significant

difference found between them ($p > 0.05$) on day 1, 3 and 6. However, the cell number on day 8 was significantly higher on the PLGA scaffolds ($p < 0.05$); 6.25×10^4 and 4.45×10^4 for the PLGA and PLGA/chitosan composite scaffolds, respectively. The SEM images of the cell-scaffold constructs on day 8 are shown in **Figure 5.9B and C**, with the spreading of cells visible on both scaffold types.

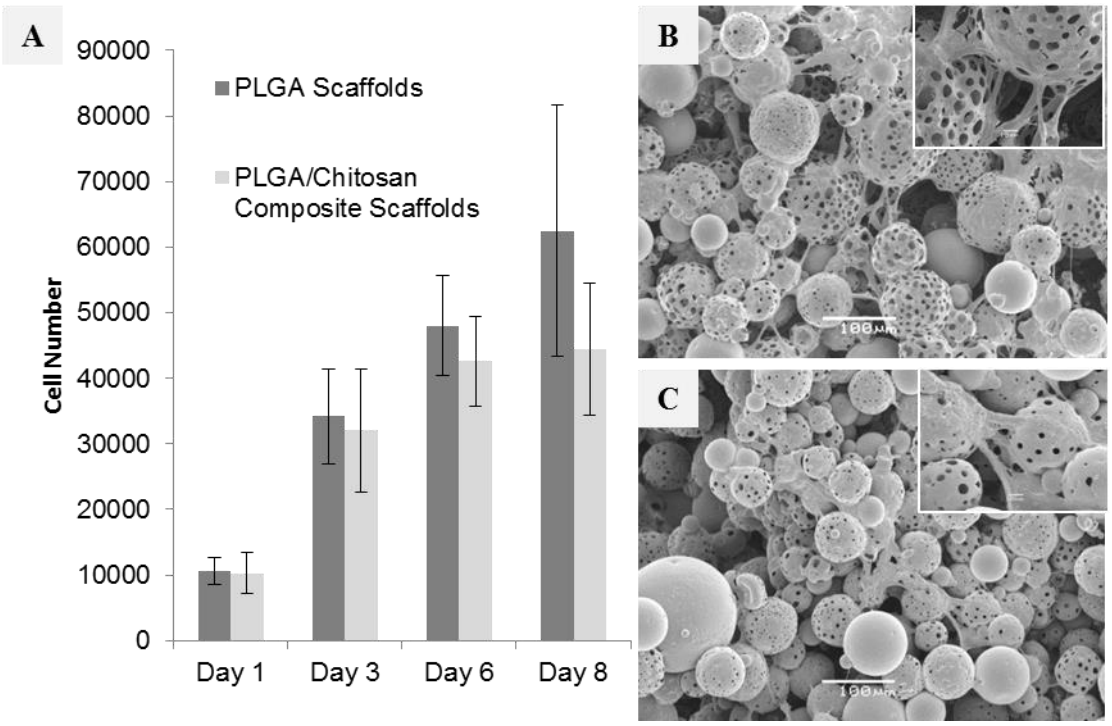


Figure 5.9: Biocompatibility of primary hMSCs with PLGA and PLGA/chitosan composite scaffolds. (A) Cell viability of hMSCs on scaffolds at various time points. Data points represent the mean ± standard deviation. SEM images of hMSCs on (B) PLGA and (C) PLGA/chitosan composite scaffolds on day 8.

The initial cell adhesion to chitosan has been attributed to non-specific electrostatic interactions that occur between the protonated amine groups of chitosan and the proteoglycans on the cell surface that are negatively charged [256]. A previous study reported similar biocompatibility results to those found in this study, with the cell attachment lower on chitosan- and N-succinyl chitosan-treated PLGA scaffolds than on PLGA alone. However, the osteogenic potential of the chitosan-treated scaffolds was greater than that of the PLGA

scaffolds [257]. The degree of deacetylation of chitosan has been found to affect the cell attachment. Chitosan films with a higher degree of deacetylation were found to elicit increased affinity to fibroblasts, chondrocytes and Schwann cells [258]. The chitosan used in the present study was 75 to 85% deacetylated, which may well account for the lower cell number observed on day 8, with the possibility of improving this with the use of a chitosan variety with a higher degree of deacetylation.

5.3.7 Osteogenic differentiation

Mineralization is a key process involved in the regeneration of bone. It can be detected using various stains, which include alizarin red and von Kossa staining. The alizarin red stain was found to be inappropriate for this scaffold system, as chitosan binds to the stain, even in the absence of cells. Therefore, von Kossa staining was used in order to determine the mineralization status. The principle behind this procedure involves the binding of silver ions to phosphate (often associated with calcium) in an acidic environment [259]. The photodegradation of this silver phosphate then leads to the formation of silver, which can be visualized on the sample. The results of the von Kossa assay on the scaffolds after 21 days in the culture media are shown in **Figure 5.10**. Dark brown/black nodules are visible on the scaffolds and represent positive staining for phosphate. A qualitative analysis shows that there was more positive staining on both scaffold types when the cells were grown in the osteogenic media when compared with the basal media, which was expected. However, in the case of the cell-scaffold constructs in the basal media, the PLGA/chitosan composite scaffolds appear darker, which indicates more positive staining.

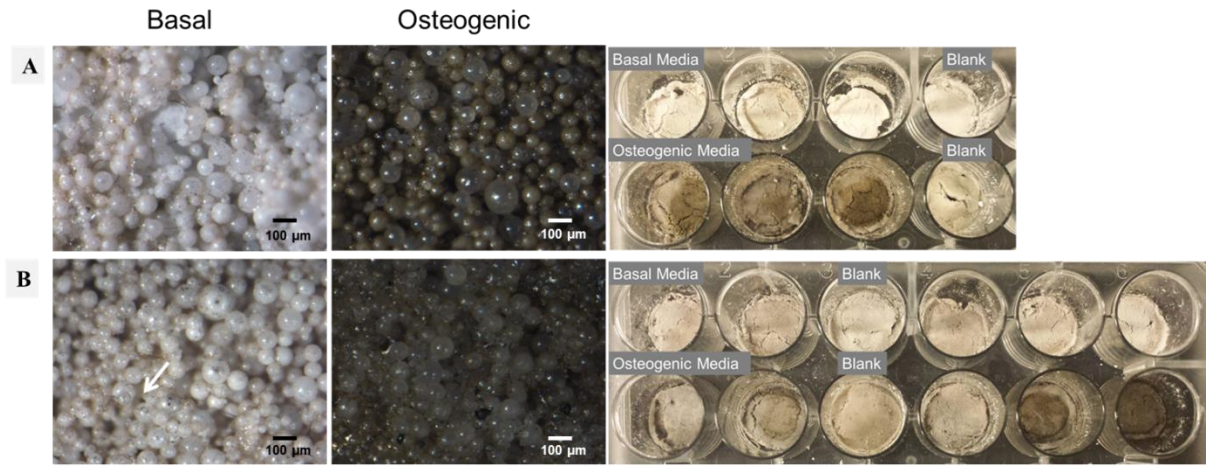


Figure 5.10: Von Kossa staining of (A) PLGA and (B) PLGA/chitosan composite scaffold-cell constructs 21 days after seeding. Arrow indicates the presence of a nodule.

The presence of the bone marker protein, osteocalcin, was detected using the immunostaining technique. Its expression is known to rise with an increase in mineralization [260]; therefore, it is a good indicator of osteogenic differentiation. **Figure 5.11** shows the resultant scaffold images, where there appears to be less green osteocalcin staining on the PLGA scaffolds than on the PLGA/chitosan composite scaffolds in basal media. However, in osteogenic media, there appears to be slightly more green patches on the PLGA scaffolds than on the PLGA/chitosan composite scaffolds.

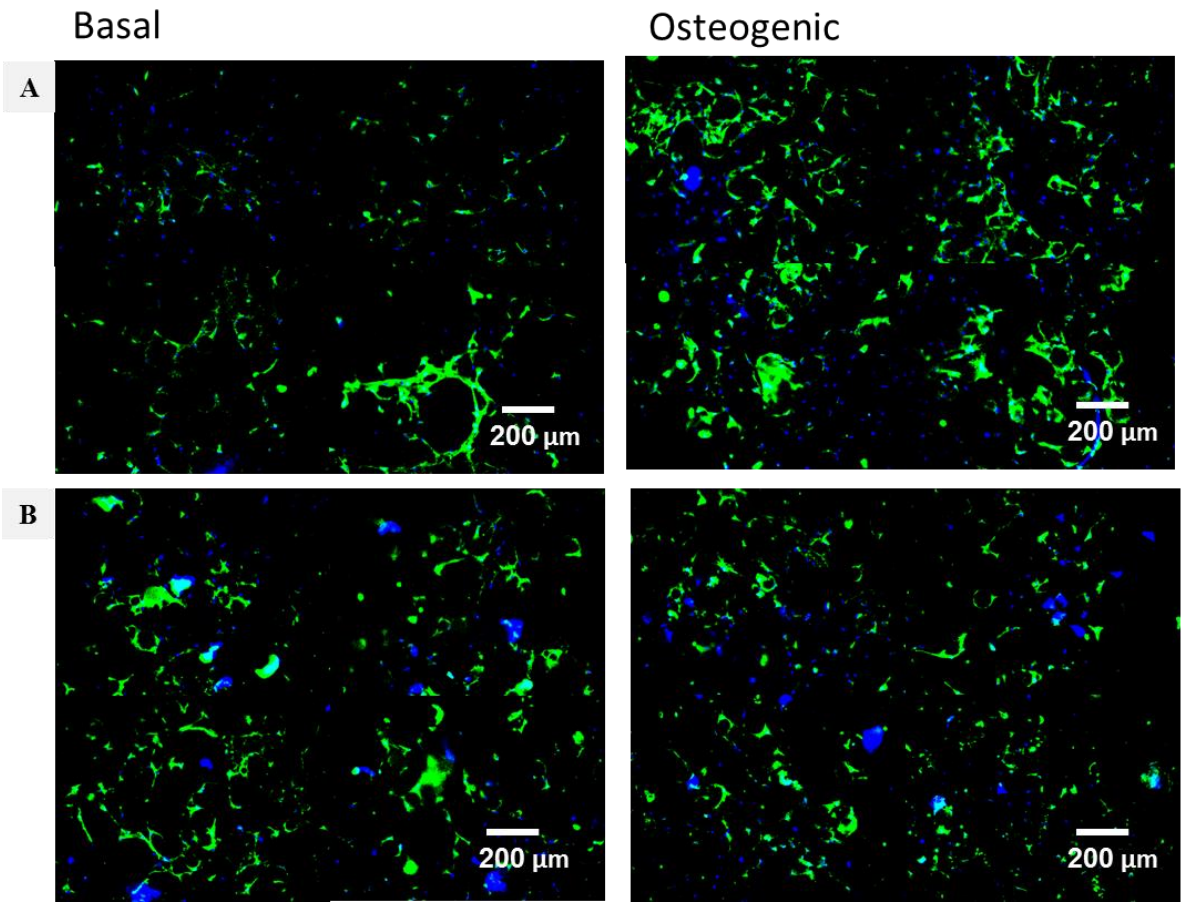


Figure 5.11: Osteocalcin presence on (A) PLGA and (B) PLGA/chitosan composite scaffolds seeded with hMSCs. Green = osteocalcin, blue = Hoechst staining of the cell DNA.

In order to quantify this, the images were processed further using ImageJ as shown in **Figure 5.12**.

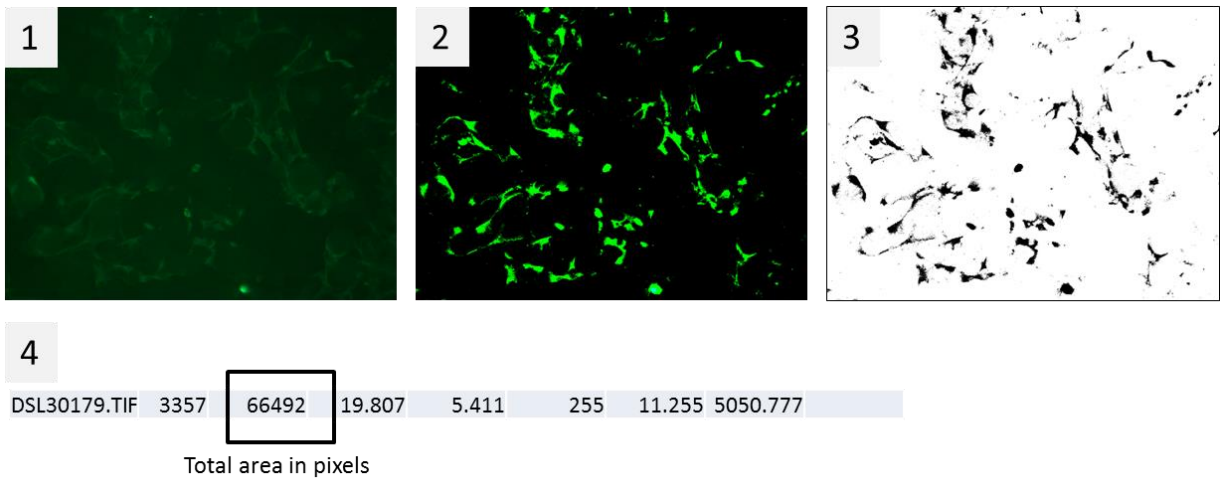


Figure 5.12: ImageJ processing of osteocalcin images. (1) Original image, (2) original image adjusted for brightness and contrast, (3) converted to binary format and (4) total area in pixels exported.

The data of this analysis show that there was increased osteocalcin staining on the composite scaffolds than on the PLGA scaffolds when the cells were grown in the basal media ($p < 0.05$, **Figure 5.13**). However, when the cells were grown in the osteogenic media, the osteocalcin staining on the PLGA/chitosan and PLGA scaffolds was not significantly different ($p > 0.05$).

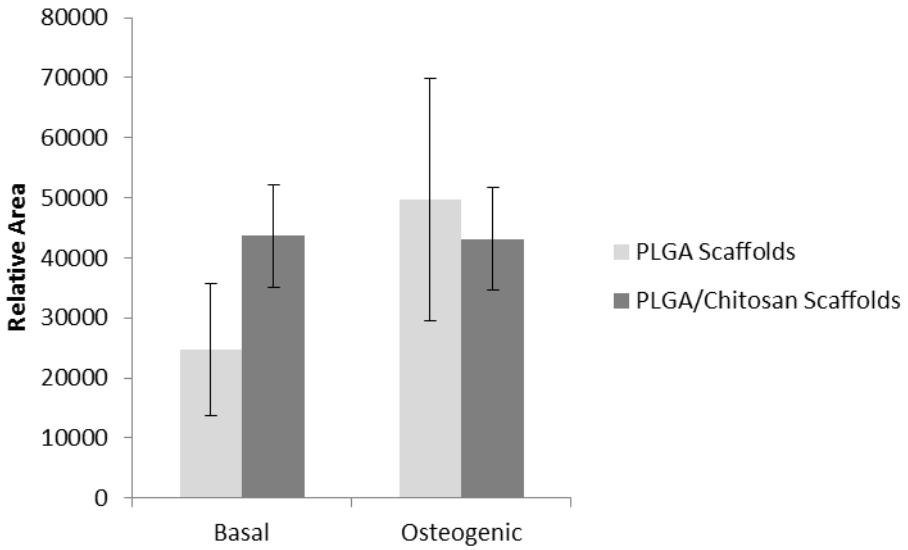


Figure 5.13: Comparison of osteocalcin staining on PLGA and PLGA/chitosan scaffolds in basal and osteogenic media.

Although there was no significant difference between the degree of osteocalcin staining in the osteogenic media, in the basal media, the PLGA/chitosan scaffolds did show more extensive staining. Therefore, considering both the von Kossa and osteocalcin staining results, it can be concluded that the PLGA/chitosan composite scaffolds show superior osteogenic potential compared with the PLGA scaffolds. Previous studies have demonstrated the ability of chitosan-containing scaffolds to induce differentiation in the presence of osteogenic media [155], which we also confirmed. However, there is less evidence demonstrating this in basal growth media.

5.3.8 Effect of chitosan processing on the toxicity of scaffolds

Chitosan is known to be a biocompatible polymer; however, in order to process and incorporate it into PLGA microspheres, it is necessary to dissolve it in dilute acidic media. Adjusting the pH of the chitosan solution to pH 5 is important for ionic gelation between chitosan's NH_3^+ groups and the $P_3O_{10}^{5-}$ of TPP [261]. During the PLGA/chitosan composite microsphere production process, it was observed that the molarity of the sodium hydroxide solution used to adjust the chitosan solution had a significant effect on the properties of the microspheres. Therefore, the effect of the molarity of the sodium hydroxide solution on the microspheres, scaffolds and cell activity was examined in more detail.

SEM images of PLGA/chitosan microspheres prepared with 0.25% w/v chitosan solution adjusted to pH 5 using 0.5, 1 and 2 M sodium hydroxide solutions are shown in **Figure 5.14**. Debris is visible amongst the 0.5 M and 1 M adjusted- microspheres; however, no debris is present with the 2 M-adjusted microspheres.

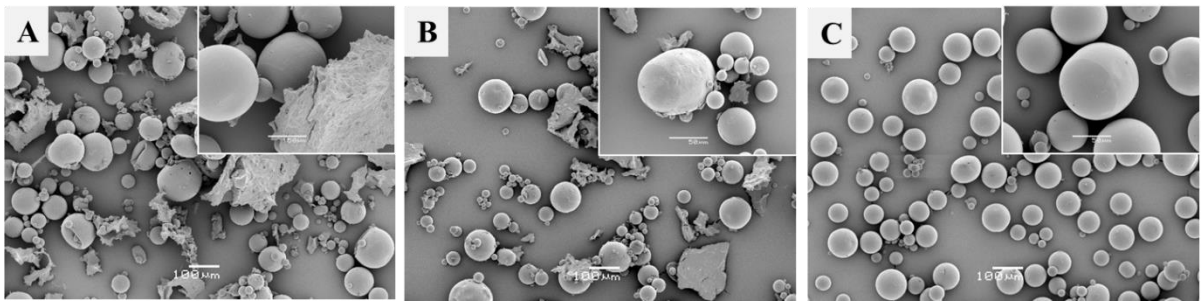


Figure 5.14: SEM images of PLGA/chitosan microspheres prepared with 0.25% w/v chitosan solution in 2% v/v acetic acid adjusted with (A) 0.5 M, (B) 1 M and (C) 2 M sodium hydroxide.

The size distributions of the different formulations were determined and a summary of the results is presented in **Figure 5.15**. The average diameter of the microspheres decreased with the increase in the sodium hydroxide molarity. The mean diameters of the microspheres were 116.9 µm, 108.9 µm and 79.9 µm, when prepared with the 0.5 M-, 1 M- and 2 M-adjusted chitosan solutions, respectively. The microspheres prepared with the 0.5 M- and 1 M-adjusted chitosan solution display large standard deviations, 67.82 µm and 64.89 µm, respectively, with a smaller standard deviation of 34.77 µm for the microspheres prepared with the 2 M-adjusted chitosan solution. This disparity confirms the presence of the debris observed in the SEM images, as irregularly shaped debris would create greater variation in the diameter.

The debris that is present at the lower molarities could be a result of the slightly larger volume of sodium hydroxide that was required for the pH adjustment. Therefore, a more dilute TPP/chitosan external aqueous phase was created, which may have impeded the effective interaction between TPP and chitosan. This would give rise to debris of unreacted chitosan.

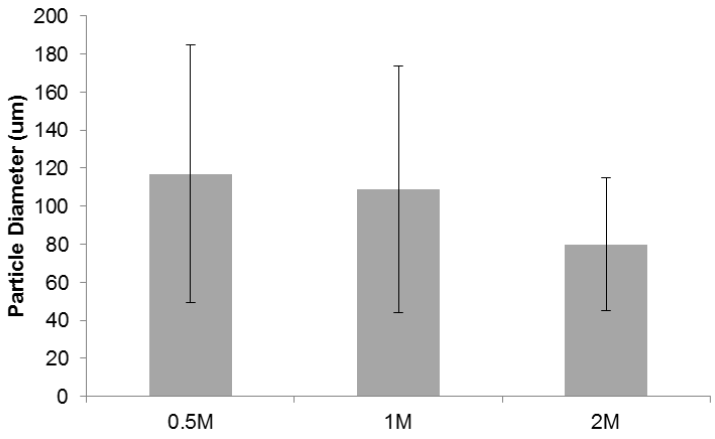


Figure 5.15: Size distribution of PLGA/chitosan microspheres prepared with 0.25% w/v chitosan solution adjusted with different molarities of sodium hydroxide solution.

In order to investigate the effect of the debris on the primary hMSC cell proliferation on the scaffolds, the cells were cultured on the scaffolds, as described in section 5.2.10. **Figure 5.16** shows that the cell numbers increased on the scaffolds prepared with 2 M-adjusted microspheres over an 8-day period, but remained unchanged on the scaffolds prepared with the 1 M-adjusted microspheres over the same period. Furthermore, a change in the colour of the basal media from a red/orange colour to yellow was observed on the 1 M-adjusted scaffolds, which is indicative of an acidic pH. This was not the case for the media on the 2 M-adjusted scaffolds.

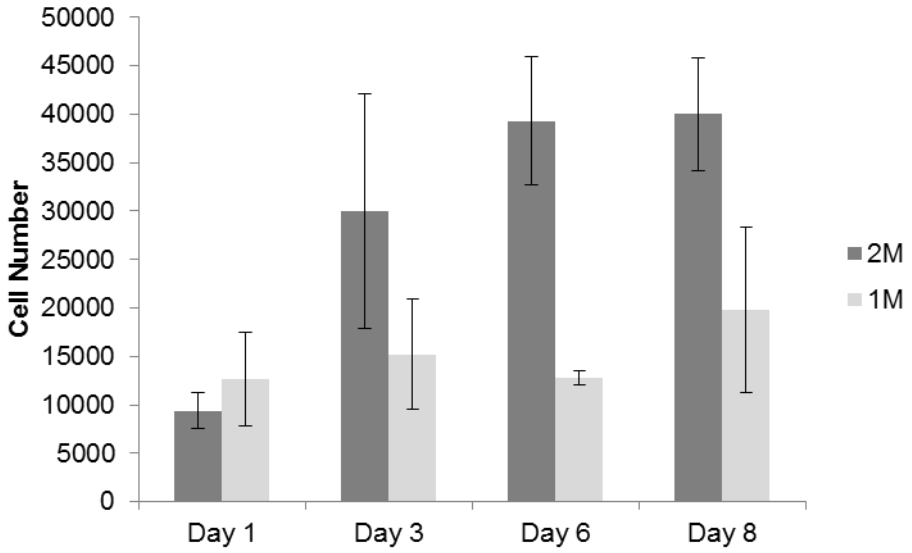


Figure 5.16: Cell proliferation on scaffolds prepared with 2 M and 1 M-adjusted PLGA/chitosan microspheres in combination with porous PLGA microspheres.

SEM images of the cell-scaffold constructs on day 8 confirm hMSC growth on the scaffolds prepared with the 2 M-adjusted microspheres (**Figure 5.17B)**. However, **Figure 5.17A** shows very few visible cells on the scaffolds prepared with the 1 M-adjusted microspheres. Moreover, the presence of debris on the individual microspheres' surfaces can also be clearly observed.

The scaffolds prepared with the 2 M-adjusted microspheres did not contain any debris (as shown in **Figure 5.17**), which indicates that the debris is responsible for the attenuation of the cell growth. This detrimental effect on the scaffolds' biocompatibility may be due to the large amount of chitosan debris remaining in a protonated state, therefore, creating an acidic environment.

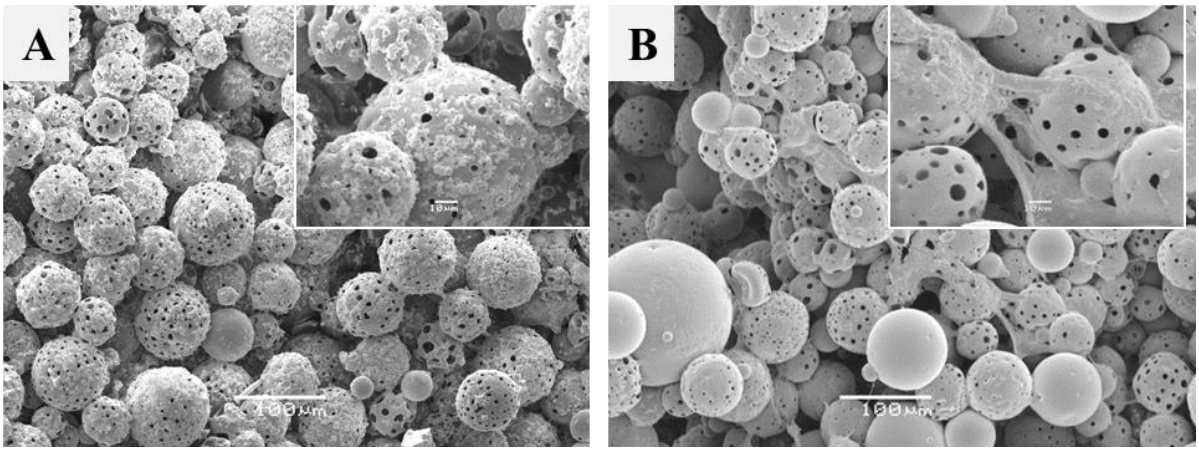


Figure 5.17: SEM images of primary hMSCs on porous PLGA/chitosan composite scaffolds after 8 days in culture prepared with 0.25% w/v chitosan solution in 2% acetic acid adjusted with (A) 1 M and (B) 2 M sodium hydroxide solution.

The ability of hMSCs to undergo osteogenic differentiation on the scaffolds was determined after a 21-day period via immunohistochemistry. **Figure 5.18** shows the presence of osteocalcin, a late protein marker for osteogenic differentiation, on the scaffolds. Osteocalcin staining is visible to a much larger extent on the 2 M-adjusted scaffolds when compared with the 1 M-adjusted scaffolds. The lack of osteocalcin staining on the 1 M-adjusted scaffolds indicates that osteogenic differentiation did not occur, or that it did not reach the late stage. This may be as a consequence of the significantly reduced cell growth exhibited on these scaffolds; in addition to an acidic environment that is unconducive to differentiation.

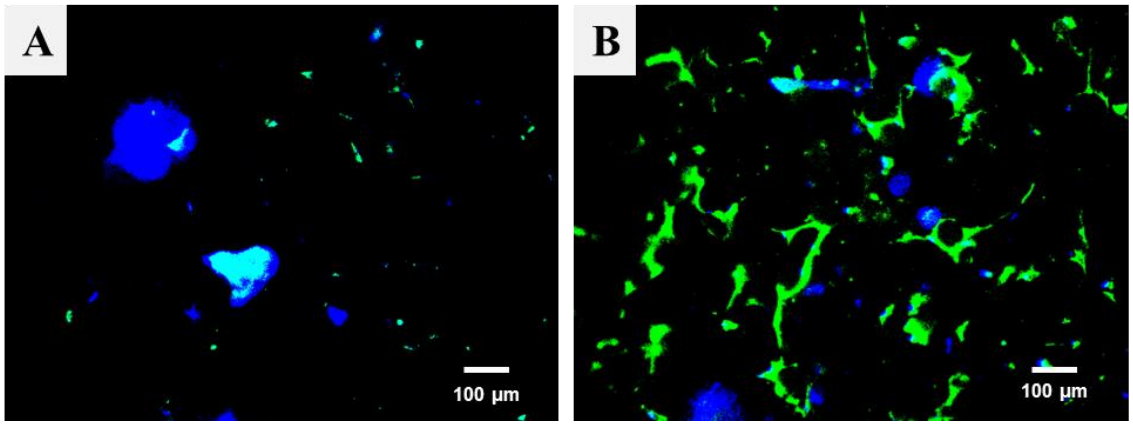


Figure 5.18: Osteocalcin staining on PLGA/chitosan scaffolds prepared with (A) 1 M-adjusted and (B) 2 M-adjusted chitosan solution.

5.4 Conclusions

In this chapter, the novel dual-function nature of the PLGA/chitosan composite microsphere system, with the ability to fuse together as a paste at 37°C, was elucidated. Furthermore, the ability of a suspension of the microspheres to sinter post-injection was also demonstrated. It was shown that the burst release of a model protein for BMP-2, BSA, was attenuated via the inclusion of the composite PLGA/chitosan microspheres; moreover, a slow release of the protein over 28 days was demonstrated. The scaffold's biocompatibility and ability to promote osteogenesis were also demonstrated. This formulation, therefore, shows potential as a scaffold for bone regeneration and is an excellent candidate for further *in vitro* and *in vivo* testing.

The importance of the strength of the sodium hydroxide solution used to adjust the pH of the chitosan solution was also demonstrated. The toxic effects on hMSCs of the PLGA/chitosan microspheres prepared with chitosan solutions adjusted with lower molarity sodium hydroxide were investigated. Microspheres prepared with chitosan adjusted with 2 M sodium hydroxide were able to sustain cell growth over an 8-day period and supported osteogenic differentiation. However, those prepared with a lower molarity sodium hydroxide

did not sustain cell growth or support osteogenic differentiation. The presence of protonated debris chitosan was attributed to the toxic effect, as toxicity was not observed in the absence of the afore-mentioned debris. Very crucially, to our knowledge, this is the first study to discuss this effect and highlight the importance of the chitosan and TPP concentrations on the resultant microspheres.

Chapter 6: Final conclusions and future work

6.1 Final conclusions

The focus of this work was on the formulation and *in vitro* characterisation of an injectable microparticulate system with the ability to deliver a growth factor in a controlled manner. The first phase of work resulted in the production of porous PLGA microspheres through the adjustment of the formulation and processing variables.

We then went on to study the effect of the PLGA molecular weight on the properties of non-porous protein-loaded microspheres. We noted that the molecular weight of the PLGA had a profound effect on the release profiles of a model protein for BMP-2. There was an inverse relationship between the rate of release of the model protein and the PLGA molecular weight. The protein-loaded and porous microspheres were sintered into scaffolds and then physically characterised. The intermediate molecular weight scaffolds were chosen for further investigation based on balancing the need for retaining sufficient compressive strength and a slower protein release.

Subsequently, we focused on addressing the burst release of protein observed from the microspheres and scaffolds. Various coating materials were studied and chitosan was found to confer the most favourable properties. The physicochemical properties of the scaffolds formulated with the chitosan-coated microspheres were then determined and further subjected to biocompatibility testing. The biocompatibility and osteogenic potential of the scaffolds was confirmed; additionally, the injectable potential of the microspheres was also demonstrated. Overall, the PLGA/chitosan composite microspheres in combination with porous PLGA microspheres show great potential for use in bone tissue engineering.

6.2 Future work

Further work is required before this system could be considered for animal studies. Suggestions for the further work are described below.

1. Further *in vitro* tests aimed at helping to understand the injection application method, as described in Chapter 5 (section 5.3.5), in a scenario where the formulation is injected in combination with cells. This would involve combining the microsphere mixtures with primary hMSCs and determining the cell activity post injection through a needle.

2. In this study the lactic acid to glycolic acid ratio of PLGA was fixed at 85:15; however, other ratios could be studied, which would result in a formulation with variable release properties depending on the ratio used i.e. a higher proportion of lactic acid in the polymer results in a slower degradation time (excluding the 50:50 variety, which is an exception to this general rule) [127].

3. The degree of deacetylation of chitosan is also a parameter than can affect cell behaviour. In this study, the chitosan was 75 to 85% deacetylated. It has been shown previously that a higher degree of deacetylation promotes a greater affinity to the ECM glycoprotein, fibronectin [256], and human bone marrow stromal cell attachment was enhanced on fibronectin-coated substrates [262]. Furthermore, chitosan with a higher degree of deacetylation promoted the osteogenesis of stem cells to a greater extent. Therefore, further work to investigate the effect of the degree of deacetylation of the chitosan on the cell behaviour *in vitro* would be another avenue to explore.

4. In this study, model proteins were used in the place of BMP-2 due to the cost implications. Therefore, the next step would involve the substitution of the model proteins with BMP-2 itself and then further characterization and cell-line studies.

It is a well-accepted paradigm in the formulation of tissue engineering scaffolds that after the characterisation and optimisation *in vitro*, the next step is the study of the system in an *in vivo* biological model [263]. These kinds of studies allow the use of complex biochemical and biomechanical environments that are key in the development of bone. Therefore, it is very important to determine the capability of the scaffold to sustain and promote bone growth in such an environment. *In vivo* tests would be undertaken in either dogs, guinea pigs, rats or rabbit models, as these are well-established for the investigation of factors that affect bone healing [264]. At this point, BMP-2 would be used instead of the model protein.

References

[1] W. C. Hall, D. Liotta, and M. E. De Bakey, "Artificial skin," *Am. Soc. Artif. Intern. Organs*, vol. 12, no. 1, pp. 340–343, 1966.

[2] M. Spira, J. Fissette, W. Hall, S. B. Hardy, and F. J. Gerow, "Evaluation of synthetic fabrics as artificial skin grafts to experimental burn wounds," *J. Biomed. Mater. Res.*, vol. 3, no. 2, pp. 213–234, 1969.

[3] R. I. Leininger, J. P. Crowley, R. D. Falb, and G. A. Grode, "Three years experience in vivo and in vitro with surfaces and devices treated by the heparin complex method," *Am. Soc. Artif. Intern. Organs*, vol. 2, no. 1, pp. 312–315, 1972.

[4] F. Bischoff, "Organic Polymer Biocompatibility and Toxicology," *Clin. Chem.*, vol. 18, no. 9, pp. 869–894, 1972.

[5] M. P. Levin, P. J. Tsaknis, and D. E. Cutright, "Healing of the Oral Mucosa with the Use of Collagen Artificial Skin," *J. Periodontol.*, vol. 50, no. 5, pp. 250–253, 1979.

[6] J. F. Burke, I. V Yannas, D. Ph, W. C. Quinby, and C. C. Bondoc, "Successful Use of a Physiologically Acceptable Artificial Skin in the Treatment of Extensive Burn Injury," *Ann. Surg.*, vol. 194, no. 4, pp. 413–427, 1981.

[7] J. P. Vacanti, "Beyond Transplantation: Third Annual Samuel Jason Mixter Lecture," *Arch. Surg.*, vol. 123, no. 5, pp. 545–549, 1988.

[8] U. Meyer, T. Meyer, J. Handschel, and H. P. Wiesmann, *Fundamentals of Tissue Engineering and Regenerative Medicine*. Springer Science & Business Media, 2009.

[9] R. Langer and J. P. Vacanti, "Tissue engineering," *Science.*, vol. 260, no. 5110, pp. 920–926, 1993.

[10] L. J. Bonassar and C. A. Vacanti, "Tissue engineering: the first decade and beyond.," *J. Cell. Biochem. Suppl.*, vol. 30–31, no. September, pp. 297–303, 1998.

[11] M. J. Whitaker, R. A. Quirk, S. M. Howdle, and K. M. Shakesheff, "Growth factor release from tissue engineering scaffolds.," *J. Pharm. Pharmacol.*, vol. 53, no. 11, pp. 1427–37, Nov. 2001.

[12] Y. Wang, X. Shi, L. Ren, Y. Yao, F. Zhang, and D.-A. Wang, "Poly(lactide-co-glycolide)/titania composite microsphere-sintered scaffolds for bone tissue engineering applications," *J. Biomed. Mater. Res. B. Appl. Biomater.*, vol. 93, no. 1, pp. 84–92, Apr. 2010.

[13] E. Bible, D. Y. S. Chau, M. R. Alexander, J. Price, K. M. Shakesheff, and M. Modo, "Attachment of stem cells to scaffold particles for intra-cerebral transplantation.," *Nat. Protoc.*, vol. 4, no. 10, pp. 1440–1453, 2009.

[14] R. Roux, C. Ladavière, A. Montembault, and T. Delair, "Particle assemblies: Toward new tools for regenerative medicine," *Mater. Sci. Eng. C*, vol. 33, no. 3, pp. 997–1007, Apr. 2013.

[15] T. N. Vo, F. K. Kasper, and A. G. Mikos, "Strategies for controlled delivery of growth factors and cells for bone regeneration," *Adv. Drug Deliv. Rev.*, vol. 64, no. 12, pp. 1292–1309, Sep. 2012.

[16] S. Martino, F. D'Angelo, I. Armentano, J. M. Kenny, and A. Orlacchio, "Stem cell-biomaterial interactions for regenerative medicine," *Biotechnol. Adv.*, vol. 30, no. 1,

pp. 338–351, 2012.

[17] A. R. Amini, C. T. Laurencin, and S. P. Nukavarapu, “Bone Tissue Engineering: Recent Advances and Challenges,” *Crit. Rev. Biomed. Eng.*, vol. 40, no. 5, pp. 363–408, 2012.

[18] C. Delloye, O. Cornu, V. Druez, and O. Barbier, “Bone allografts: What they can offer and what they cannot,” *J. Bone Joint Surg. Br.*, vol. 89, no. 5, pp. 574–579, 2007.

[19] R. Bostrom and A. G. Mikos, “Tissue Engineering of Bone,” in *Synthetic Biodegradable Polymer Scaffolds*, 1997, pp. 215–234.

[20] G. M. Calori, E. Mazza, M. Colombo, and C. Ripamonti, “The use of bone-graft substitutes in large bone defects: Any specific needs?,” *Injury*, vol. 42, no. SUPPL. 2, pp. S56–S63, 2011.

[21] K. J. Burg, S. Porter, and J. F. Kellam, “Biomaterial developments for bone tissue engineering,” *Biomaterials*, vol. 21, no. 23, pp. 2347–2359, 2000.

[22] F. M. Chen, M. Zhang, and Z. F. Wu, “Toward delivery of multiple growth factors in tissue engineering,” *Biomaterials*, vol. 31, no. 24, pp. 6279–6308, Aug. 2010.

[23] D. Puppi, F. Chiellini, A. M. Piras, and E. Chiellini, “Polymeric materials for bone and cartilage repair,” *Prog. Polym. Sci.*, vol. 35, no. 4, pp. 403–440, Apr. 2010.

[24] R. Jahagirdar and B. E. Scammell, “Principles of fracture healing and disorders of bone union,” *Surgery*, vol. 27, no. 2, pp. 63–69, 2009.

[25] W. Southard, “Long Bone Orthopedics,” 2010. [Online]. Available: http://bme240.eng.uci.edu/students/10s/wsouthar/index.html.

[26] S. F. Gilbert, “Osteogenesis: The Development of Bones,” in *Developmental Biology*, 6th ed., Sunderland (MA): Sinauer Associates, 2000.

[27] Z. Thompson, T. Miclau, D. Hu, and J. A. Heims, “A model for intramembranous bone healing during fracture repair,” *J. Orthop. Res.*, vol. 20, no. 5, pp. 1091–1098, 2002.

[28] W. A. Horton, “The biology of bone growth,” *Growth Genet. Horm.*, vol. 6, no. 2, pp. 1–3, 1990.

[29] F. Deschaseaux, L. Sensébé, and D. Heymann, “Mechanisms of bone repair and regeneration,” *Trends Mol. Med.*, vol. 15, no. 9, pp. 417–429, 2009.

[30] D. J. Hadjidakis and I. I. Androulakis, “Bone remodeling,” *Ann. N. Y. Acad. Sci.*, vol. 1092, pp. 385–396, 2006.

[31] C. H. Kim, E. Takai, H. Zhou, D. von Stechow, R. Müller, D. W. Dempster, and X. E. Guo, “Trabecular bone response to mechanical and parathyroid hormone stimulation: the role of mechanical microenvironment.,” *J. Bone Miner. Res.*, vol. 18, no. 12, pp. 2116–2125, 2003.

[32] Q. Liu, Q. Wan, R. Yang, H. Zhou, and Z. Li, “Effects of intermittent versus continuous parathyroid hormone administration on condylar chondrocyte proliferation and differentiation,” *Biochem. Biophys. Res. Commun.*, vol. 424, no. 1, pp. 182–188, 2012.

[33] S. Kobsa and W. M. Saltzman, “Bioengineering approaches to controlled protein delivery.,” *Pediatr. Res.*, vol. 63, no. 5, pp. 513–9, 2008.

[34] L. C. Gerstenfeld, D. M. Cullinane, G. L. Barnes, D. T. Graves, and T. A. Einhorn, “Fracture healing as a post-natal developmental process: molecular, spatial, and

temporal aspects of its regulation.," *J. Cell. Biochem.*, vol. 88, no. 5, pp. 873–84, 2003.

[35] L. J. White, G. T. S. Kirby, H. C. Cox, R. Qodratnama, O. Qutachi, F. R. A. J. Rose, and K. M. Shakesheff, "Accelerating protein release from microparticles for regenerative medicine applications," *Mater. Sci. Eng. C. Mater. Biol. Appl.*, vol. 33, no. 5, pp. 2578–2583, 2013.

[36] W. K. Hsu and J. C. Wang, "Contemporary concepts in spine care- the use of bone morphogenetic protein in spine fusion," *Spine J.*, vol. 8, no. 3, pp. 419–425, 2008.

[37] A. Nauth, B. Ristevski, R. Li, and E. H. Schemitsch, "Growth factors and bone regeneration: how much bone can we expect?," *Injury*, vol. 42, no. 6, pp. 574–579, 2011.

[38] H. M. Ryoo, M. H. Lee, and Y. J. Kim, "Critical molecular switches involved in BMP-2-induced osteogenic differentiation of mesenchymal cells," *Gene*, vol. 366, no. 1, pp. 51–57, 2006.

[39] S. Putney and P. Burke, "Improving protein therapeutics with sustained-release formulations," *Nat. Biotechnol.*, vol. 16, pp. 153–157, 1998.

[40] Z. S. Patel, M. Yamamoto, H. Ueda, Y. Tabata, and A. G. Mikos, "Biodegradable gelatin microparticles as delivery systems for the controlled release of bone morphogenetic protein-2," *Acta Biomater.*, vol. 4, no. 5, pp. 1126–1138, 2008.

[41] FDA, "FDA Public Health Notification: Life-threatening Complications Associated with Recombinant Human Bone Morphogenetic Protein in Cervical Spine Fusion," 2008. [Online]. Available: http://www.fda.gov/MedicalDevices/Safety/AlertsandNotices/PublicHealthNotifications/ucm062000.htm. [Accessed: 24-Oct-2016].

[42] Y. Shiozaki, T. Kitajima, T. Mazaki, A. Yoshida, M. Tanaka, A. Umezawa, M. Nakamura, Y. Yoshida, Y. Ito, T. Ozaki, and A. Matsukawa, "Enhanced in vivo osteogenesis by nanocarrier-fused bone morphogenetic protein-4.," *Int. J. Nanomedicine*, vol. 8, pp. 1349–60, 2013.

[43] N. Yamamoto, S. Akiyama, T. Katagiri, M. Namiki, T. Kurokawa, and T. Suda, "Smad1 and Smad5 act downstream of intracellular signalings of BMP-2 that inhibits myogenic differentiation and induces osteoblast differentiation in C2C12 myoblasts.," *Biochem. Biophys. Res. Commun.*, vol. 238, no. 2, pp. 574–580, 1997.

[44] V. Luginbuehl, L. Meinel, H. P. Merkle, and B. Gander, "Localized delivery of growth factors for bone repair," *Eur. J. Pharm. Biopharm.*, vol. 58, no. 2, pp. 197–208, 2004.

[45] C. Li, C. Vepari, H.-J. Jin, H. J. Kim, and D. L. Kaplan, "Electrospun silk-BMP-2 scaffolds for bone tissue engineering.," *Biomaterials*, vol. 27, no. 16, pp. 3115–3124, 2006.

[46] P. Yilgor, K. Tuzlakoglu, R. L. Reis, N. Hasirci, and V. Hasirci, "Incorporation of a sequential BMP-2/BMP-7 delivery system into chitosan-based scaffolds for bone tissue engineering," *Biomaterials*, vol. 30, no. 21, pp. 3551–3559, 2009.

[47] H. Wang, Q. Zou, O. C. Boerman, A. W. G. Nijhuis, J. A. Jansen, Y. Li, and S. C. G. Leeuwenburgh, "Combined delivery of BMP-2 and bFGF from nanostructured colloidal gelatin gels and its effect on bone regeneration in vivo," *J. Control. Release*, vol. 166, no. 2, pp. 172–181, 2013.

[48] S. Kim, Y. Kang, C. A. Krueger, M. Sen, J. B. Holcomb, D. Chen, J. C. Wenke, and Y. Yang, "Sequential delivery of BMP-2 and IGF-1 using a chitosan gel with gelatin

microspheres enhances early osteoblastic differentiation," *Acta Biomater.*, vol. 8, no. 5, pp. 1768–1777, 2012.

[49] G. Bhakta, B. Rai, Z. X. H. Lim, J. H. Hui, G. S. Stein, A. J. van Wijnen, V. Nurcombe, G. D. Prestwich, and S. M. Cool, "Hyaluronic acid-based hydrogels functionalized with heparin that support controlled release of bioactive BMP-2," *Biomaterials*, vol. 33, no. 26, pp. 6113–6122, 2012.

[50] J. L. Holloway, H. Ma, R. Rai, K. D. Hankenson, and J. A. Burdick, "Synergistic Effects of SDF-1α and BMP-2 Delivery from Proteolytically Degradable Hyaluronic Acid Hydrogels for Bone Repair," *Macromol. Biosci.*, vol. 15, no. 9, pp. 1218–1223, 2015.

[51] Medtronic, "INFUSE® Bone Graft: Information for Healthcare Providers," 2016. [Online]. Available: http://www.infusebonegraft.com/healthcare-providers/about-infuse-bonegraft/index.htm. [Accessed: 25-Oct-2016].

[52] L. Moore, M. Gatica, H. Kim, E. Osawa, and D. Ho, "Multi-protein delivery by nanodiamonds promotes bone formation.," *J. Dent. Res.*, vol. 92, no. 11, pp. 976–981, 2013.

[53] L. Li, G. Zhou, Y. Wang, G. Yang, S. Ding, and S. Zhou, "Controlled dual delivery of BMP-2 and dexamethasone by nanoparticle-embedded electrospun nanofibers for the efficient repair of critical-sized rat calvarial defect," *Biomaterials*, vol. 37, pp. 218–229, 2015.

[54] H. Nie, B. W. Soh, Y.-C. Fu, and C.-H. Wang, "Three-dimensional fibrous PLGA/HAp composite scaffold for BMP-2 delivery," *Biotechnol. Bioeng.*, vol. 99, no. 1, pp. 223–234, 2008.

[55] R. C. De Guzman, J. M. Saul, M. D. Ellenburg, M. R. Merrill, H. B. Coan, T. L. Smith, and M. E. Van Dyke, "Bone regeneration with BMP-2 delivered from keratose scaffolds," *Biomaterials*, vol. 34, no. 6, pp. 1644–1656, 2013.

[56] H. S. Yang, W.-G. La, Y.-M. Cho, W. Shin, G.-D. Yeo, and B.-S. Kim, "Comparison between heparin-conjugated fibrin and collagen sponge as bone morphogenetic protein-2 carriers for bone regeneration," *Exp. Mol. Med.*, vol. 44, no. 5, pp. 350–355, 2012.

[57] Stryker, "An Overview of OP-1 Products," 2016. [Online]. Available: http://www.stryker.com/cn/products/Orthobiologicals/Osteoinductive/OP-1/index.htm. [Accessed: 25-Oct-2016].

[58] P. Yilgor, N. Hasirci, and V. Hasirci, "Sequential BMP-2/BMP-7 delivery from polyester nanocapsules," *J. Biomed. Mater. Res. Part A*, vol. 93, no. 2, pp. 528–536, 2010.

[59] D. H. R. Kempen, L. Lu, A. Heijink, T. E. Hefferan, L. B. Creemers, A. Maran, M. J. Yaszemski, and W. J. A. Dhert, "Effect of local sequential VEGF and BMP-2 delivery on ectopic and orthotopic bone regeneration.," *Biomaterials*, vol. 30, no. 14, pp. 2816–25, 2009.

[60] U. Helmrich, N. Di Maggio, S. Güven, E. Groppa, L. Melly, R. D. Largo, M. Heberer, I. Martin, A. Scherberich, and A. Banfi, "Osteogenic graft vascularization and bone resorption by VEGF-expressing human mesenchymal progenitors.," *Biomaterials*, vol. 34, no. 21, pp. 5025–35, 2013.

[61] E. Jabbarzadeh, M. Deng, Q. Lv, T. Jiang, Y. M. Khan, L. S. Nair, and C. T.

Laurencin, “VEGF-incorporated biomimetic poly(lactide-co-glycolide) sintered microsphere scaffolds for bone tissue engineering,” *J. Biomed. Mater. Res. Part B Appl. Biomater.*, vol. 100, no. 8, pp. 2187–2196, 2012.

[62] E. Zelzer, W. McLean, Y.-S. Ng, N. Fukai, A. M. Reginato, S. Lovejoy, P. A. D’Amore, and B. R. Olsen, “Skeletal defects in VEGF (120/120) mice reveal multiple roles for VEGF in skeletogenesis.,” *Development*, vol. 129, no. 8, pp. 1893–1904, 2002.

[63] J. Street, M. Bao, L. DeGuzman, S. Bunting, F. V Peale, N. Ferrara, H. Steinmetz, J. Hoeffel, J. L. Cleland, A. Daugherty, N. van Bruggen, H. P. Redmond, R. A. D. Carano, and E. H. Filvaroff, “Vascular endothelial growth factor stimulates bone repair by promoting angiogenesis and bone turnover.,” *Proc. Natl. Acad. Sci. USA*, vol. 99, no. 15, pp. 9656–9661, 2002.

[64] S. Young, Z. S. Patel, J. D. Kretlow, M. B. Murphy, P. M. Mountziaris, L. S. Baggett, H. Ueda, Y. Tabata, J. A. Jansen, M. Wong, and A. G. Mikos, “Growth factor and bone morphogenetic protein-2 on bone regeneration in a rat critical-size defect model,” *Tissue Eng. Part A*, vol. 15, no. 9, pp. 2347–2362, 2009.

[65] S. Ohba, H. Hojo, and U. Chung, “Bioactive factors for tissue regeneration: state of the art,” *Muscles. Ligaments Tendons J.*, vol. 2, no. 3, pp. 193–203, 2012.

[66] A. R. Shrivats, M. C. McDermott, and J. O. Hollinger, “Bone tissue engineering: State of the union,” *Drug Discov. Today*, vol. 19, no. 6, pp. 781–786, 2014.

[67] M. M. Stevens, “Biomaterials for bone tissue engineering,” *Mater. Today*, vol. 11, no. 5, pp. 18–25, 2008.

[68] T. Kokubo, H. M. Kim, and M. Kawashita, “Novel bioactive materials with different mechanical properties,” *Biomaterials*, vol. 24, no. 13, pp. 2161–2175, 2003.

[69] L.-C. Gerhardt and A. R. Boccaccini, “Bioactive Glass and Glass-Ceramic Scaffolds for Bone Tissue Engineering,” *Materials (Basel).*, vol. 3, no. 7, pp. 3867–3910, 2010.

[70] K. Rezwan, Q. Z. Chen, J. J. Blaker, and A. R. Boccaccini, “Biodegradable and bioactive porous polymer/inorganic composite scaffolds for bone tissue engineering,” *Biomaterials*, vol. 27, no. 18, pp. 3413–3431, 2006.

[71] I. D. Xynos, A. J. Edgar, L. D. K. Buttery, L. L. Hench, and J. M. Polak, “Gene-expression profiling of human osteoblasts following treatment with the ionic products of Bioglass® 45S5 dissolution,” *J. Biomed. Mater. Res.*, vol. 55, no. 2, pp. 151–157, 2001.

[72] L. L. Hench, R. J. Splinter, W. C. Allen, and T. K. Greenlee, “Bonding mechanisms at the interface of ceramic prosthetic materials,” *J. Biomed. Mater. Res.*, vol. 5, no. 6, pp. 117–141, 1971.

[73] L. L. Hench, “The story of Bioglass,” *J. Mater. Sci. Mater. Med.*, vol. 17, no. 11, pp. 967–978, 2006.

[74] H. Yoshikawa and A. Myoui, “Bone tissue engineering with porous hydroxyapatite ceramics,” *J. Artif. Organs*, vol. 8, no. 3, pp. 131–136, 2005.

[75] E. Rumpel, E. Wolf, E. Kauschke, V. Bienengräber, T. Bayerlein, T. Gedrange, and P. Proff, “The biodegradation of hydroxyapatite bone graft substitutes in vivo,” *Folia Morphol. (Warsz).*, vol. 65, no. 1, pp. 43–48, 2006.

[76] A. Sugawara, K. Asaoka, and S.-J. Ding, “Calcium phosphate-based cements: clinical needs and recent progress,” *J. Mater. Chem. B*, vol. 1, no. 8, pp. 1081–1089, 2013.

[77] K. Sariibrahimoglu, J. G. C. Wolke, S. C. G. Leeuwenburgh, L. Yubao, and J. A. Jansen, “Injectable biphasic calcium phosphate cements as a potential bone substitute,” *J. Biomed. Mater. Res. Part B Appl. Biomater.*, vol. 102, no. 3, pp. 415–422, 2014.

[78] S. Bose, M. Roy, and A. Bandyopadhyay, “Recent advances in bone tissue engineering scaffolds,” *Trends Biotechnol.*, vol. 30, no. 10, pp. 546–554, 2012.

[79] Y. F. Zheng, X. N. Gu, and F. Witte, “Biodegradable metals,” *Mater. Sci. Eng. R Reports*, vol. 77, pp. 1–34, 2014.

[80] C. H. Lee, A. Singla, and Y. Lee, “Biomedical applications of collagen,” *Int. J. Pharm.*, vol. 221, no. 1–2, pp. 1–22, 2001.

[81] F. J. O’Brien, B. A. Harley, I. V. Yannas, and L. J. Gibson, “The effect of pore size on cell adhesion in collagen-GAG scaffolds,” *Biomaterials*, vol. 26, no. 4, pp. 433–441, 2005.

[82] H. S. Yu, G. Z. Jin, J. E. Won, I. Wall, and H. W. Kim, “Macrochanneled bioactive ceramic scaffolds in combination with collagen hydrogel: A new tool for bone tissue engineering,” *J. Biomed. Mater. Res. Part A*, vol. 100 A, no. 9, pp. 2431–2440, 2012.

[83] M. M. Villa, L. Wang, J. Huang, D. W. Rowe, and M. Wei, “Bone tissue engineering with a collagen-hydroxyapatite scaffold and culture expanded bone marrow stromal cells,” *J. Biomed. Mater. Res. Part B Appl. Biomater.*, vol. 103, no. 2, pp. 243–253, 2014.

[84] A. A. Al-Munajjed, N. A. Plunkett, J. P. Gleeson, T. Weber, C. Jungreuthmayer, T. Levingstone, J. Hammer, and F. J. O’Brien, “Development of a biomimetic collagen-hydroxyapatite scaffold for bone tissue engineering using a SBF immersion technique,” *J. Biomed. Mater. Res. Part B Appl. Biomater.*, vol. 90, no. 2, pp. 584–591, 2009.

[85] C. Liu and J. T. Czernuszka, “Engineered collagen-hydroxyapatite scaffolds for bone tissue engineering,” *Eur. Cells Mater.*, vol. 16, no. Suppl. 3, p. 74, 2008.

[86] N. Epstein E, “Pros, cons, and costs of INFUSE in spinal surgery,” *Surg. Neurol. Int.*, vol. 2, no. 10, 2011.

[87] P. Angele, J. Abke, R. Kujat, H. Faltermeier, D. Schumann, M. Nerlich, B. Kinner, C. Englert, Z. Ruszczak, R. Mehrl, and R. Mueller, “Influence of different collagen species on physico-chemical properties of crosslinked collagen matrices,” *Biomaterials*, vol. 25, no. 14, pp. 2831–2841, 2004.

[88] H. Lu, N. Kawazoe, T. Kitajima, Y. Myoken, M. Tomita, A. Umezawa, G. Chen, and Y. Ito, “Spatial immobilization of bone morphogenetic protein-4 in a collagen-PLGA hybrid scaffold for enhanced osteoinductivity.,” *Biomaterials*, vol. 33, no. 26, pp. 6140–6146, Sep. 2012.

[89] W. Dai, N. Kawazoe, X. Lin, J. Dong, and G. Chen, “The influence of structural design of PLGA/collagen hybrid scaffolds in cartilage tissue engineering.,” *Biomaterials*, vol. 31, no. 8, pp. 2141–2152, Mar. 2010.

[90] K. H. Stenzel, T. Miyata, and A. L. Rubin, “Collagen as a biomaterial.,” *Annu. Rev. Biophys. Bioeng.*, vol. 3, no. 0, pp. 231–253, 1974.

[91] S. Mathews, P. K. Gupta, R. Bhonde, and S. Totey, “Chitosan enhances mineralization during osteoblast differentiation of human bone marrow-derived mesenchymal stem cells, by upregulating the associated genes.,” *Cell Prolif.*, vol. 44, no. 6, pp. 537–549, 2011.

[92] R. Raftery, F. J. O'Brien, and S.-A. Cryan, "Chitosan for gene delivery and orthopedic tissue engineering applications.," *Molecules*, vol. 18, no. 5, pp. 5611–5647, 2013.

[93] C. Heinemann, S. Heinemann, A. Bernhardt, H. Worch, and T. Hanke, "Novel textile chitosan scaffolds promote spreading, proliferation, and differentiation of osteoblasts.," *Biomacromolecules*, vol. 9, no. 10, pp. 2913–2920, 2008.

[94] G. E. Park, M. A. Pattison, K. Park, and T. J. Webster, "Accelerated chondrocyte functions on NaOH-treated PLGA scaffolds.," *Biomaterials*, vol. 26, no. 16, pp. 3075–3082, Jun. 2005.

[95] C. H. Zheng, J. Q. Gao, Y. P. Zhang, and W. Q. Liang, "A protein delivery system: Biodegradable alginate-chitosan-poly(lactic-co- glycolic acid) composite microspheres," *Biochem. Biophys. Res. Commun.*, vol. 323, no. 4, pp. 1321–1327, 2004.

[96] E. Wenk, A. J. Meinel, S. Wildy, H. P. Merkle, and L. Meinel, "Microporous silk fibroin scaffolds embedding PLGA microparticles for controlled growth factor delivery in tissue engineering.," *Biomaterials*, vol. 30, no. 13, pp. 2571–2581, 2009.

[97] P. Coimbra, P. Ferreira, H. C. de Sousa, P. Batista, M. A. Rodrigues, I. J. Correia, and M. H. Gil, "Preparation and chemical and biological characterization of a pectin/chitosan polyelectrolyte complex scaffold for possible bone tissue engineering applications," *Int. J. Biol. Macromol.*, vol. 48, no. 1, pp. 112–118, 2011.

[98] L. Liu, M. L. Fishman, and K. B. Hicks, "Pectin in controlled drug delivery – a review," *Cellulose*, vol. 14, pp. 15–24, 2006.

[99] T. H. Kim, Y. H. Park, K. J. Kim, and C. S. Cho, "Release of albumin from chitosan-coated pectin beads in vitro," *Int. J. Pharm.*, vol. 250, no. 2, pp. 371–383, 2003.

[100] M. G. Sankalia, R. C. Mashru, J. M. Sankalia, and V. B. Sutariya, "Stability improvement of alpha-amylase entrapped in kappa-carrageenan beads: Physicochemical characterization and optimization using composite index," *Int. J. Pharm.*, vol. 312, no. 1–2, pp. 1–14, 2006.

[101] C. Li, S. Hein, and K. Wang, "Chitosan-Carrageenan Polyelectrolyte Complex for the Delivery of Protein Drugs," *ISRN Biomater.*, vol. 2013, pp. 1–6, 2013.

[102] A. Grenha, M. E. Gomes, M. Rodrigues, V. E. Santo, J. F. Mano, N. M. Neves, and R. L. Reis, "Development of new chitosan/carrageenan nanoparticles for drug delivery applications," *J. Biomed. Mater. Res. Part A*, vol. 92, no. 4, pp. 1265–1272, 2010.

[103] V. E. Santo, A. M. Frias, M. Carida, R. Cancedda, M. E. Gomes, J. F. Mano, and R. L. Reis, "Carrageenan-based hydrogels for the controlled delivery of PDGF-BB in bone tissue engineering applications," *Biomacromolecules*, vol. 10, no. 6, pp. 1392–1401, 2009.

[104] O. Jeon, S. J. Song, S. W. Kang, A. J. Putnam, and B. S. Kim, "Enhancement of ectopic bone formation by bone morphogenetic protein-2 released from a heparin-conjugated poly(l-lactic-co-glycolic acid) scaffold," *Biomaterials*, vol. 28, no. 17, pp. 2763–2771, 2007.

[105] H. Lin, Y. Zhao, W. Sun, B. Chen, J. Zhang, W. Zhao, Z. Xiao, and J. Dai, "The effect of crosslinking heparin to demineralized bone matrix on mechanical strength and specific binding to human bone morphogenetic protein-2," *Biomaterials*, vol. 29, no. 9, pp. 1189–1197, 2008.

[106] A. Luciani, V. Coccoli, S. Orsi, L. Ambrosio, and P. A. Netti, "PCL microspheres

based functional scaffolds by bottom-up approach with predefined microstructural properties and release profiles," *Biomaterials*, vol. 29, no. 36, pp. 4800–4807, 2008.

[107] H. Sun, L. Mei, C. Song, X. Cui, and P. Wang, "The in vivo degradation, absorption and excretion of PCL-based implant," *Biomaterials*, vol. 27, no. 9, pp. 1735–1740, 2006.

[108] J. Reignier and M. A. Huneault, "Preparation of interconnected poly(ε-caprolactone) porous scaffolds by a combination of polymer and salt particulate leaching," *Polymer (Guildf).*, vol. 47, no. 13, pp. 4703–4717, Jun. 2006.

[109] R. M. Allaf, I. V Rivero, N. Abidi, and I. N. Ivanov, "Porous poly(ε-caprolactone) scaffolds for load-bearing tissue regeneration: solventless fabrication and characterization," *J Biomed Mater Res Part B*, vol. 101, no. 6, pp. 1050–1060, 2013.

[110] G. Q. Chen and Q. Wu, "The application of polyhydroxyalkanoates as tissue engineering materials," *Biomaterials*, vol. 26, no. 33, pp. 6565–6578, 2005.

[111] F. Kok and V. Hasirci, "Polyhydroxybutyrate and its copolymers: applications in the medical field," in *Tissue engineering And Novel Delivery Systems*, 2004, pp. 543–562.

[112] C. Guo, X. Guo, N. Cai, and Y. Dong, "Novel fabrication method of porous poly(lactic acid) scaffold with hydroxyapatite coating," *Mater. Lett.*, vol. 74, pp. 197–199, 2012.

[113] X. Niu, Y. Luo, Y. Li, C. Fu, J. Chen, and Y. Wang, "Design of bioinspired polymeric materials based on poly(D,L-lactic acid) modifications towards improving its cytocompatibility.," *J. Biomed. Mater. Res. A*, vol. 84, no. 4, pp. 908–9016, 2008.

[114] G. Sui, X. Yang, F. Mei, X. Hu, G. Chen, X. Deng, and S. Ryu, "Poly- L -lactic acid / hydroxyapatite hybrid membrane for bone tissue regeneration," *J. Biomed. Mater. Res. Part A*, vol. 82, no. 2, pp. 445–454, 2007.

[115] A. K. Jaiswal, S. S. Kadam, V. P. Soni, and J. R. Bellare, "Improved functionalization of electrospun PLLA/gelatin scaffold by alternate soaking method for bone tissue engineering," *Appl. Surf. Sci.*, vol. 268, pp. 477–488, 2013.

[116] L. Klouda and A. G. Mikos, "Thermoresponsive hydrogels in biomedical applications A seven-year update," *Eur. J. Pharm. Biopharm.*, vol. 97, pp. 338–349, 2015.

[117] C. V Rahman, G. Kuhn, L. J. White, G. T. S. Kirby, O. P. Varghese, J. S. McLaren, H. C. Cox, F. R. A. J. Rose, R. Müller, J. Hilborn, and K. M. Shakesheff, "PLGA/PEG-hydrogel composite scaffolds with controllable mechanical properties," *J. Biomed. Mater. Res. B. Appl. Biomater.*, vol. 101, no. 4, pp. 648–655, 2013.

[118] R. Vasita, G. Mani, C. M. Agrawal, and D. S. Katti, "Surface hydrophilization of electrospun PLGA micro-/nano-fibers by blending with Pluronic® F-108," *Polymer (Guildf).*, vol. 51, no. 16, pp. 3706–3714, 2010.

[119] W. Schloegl, V. Marschall, M. Y. Witting, E. Volkmer, I. Drosse, U. Leicht, M. Schieker, M. Wiggenhorn, F. Schaubhut, S. Zahler, and W. Friess, "Porosity and mechanically optimized PLGA based in situ hardening systems.," *Eur. J. Pharm. Biopharm.*, vol. 82, no. 3, pp. 554–562, 2012.

[120] Y. Wang, X. Shi, L. Ren, C. Wang, and D.-A. Wang, "Porous poly (lactic-co-glycolide) microsphere sintered scaffolds for tissue repair applications," *Mater. Sci. Eng. C*, vol. 29, no. 8, pp. 2502–2507, 2009.

[121] V. T. Tran, J. P. Benoît, and M. C. Venier Julienne, "Why and how to prepare biodegradable, monodispersed, polymeric microparticles in the field of pharmacy?," *Int. J. Pharm.*, vol. 407, no. 1–2, pp. 1–11, 2011.

[122] E. A. El-Hefian, M. M. Nasef, and A. H. Yahaya, “Preparation and Characterization of Chitosan/Poly(Vinyl Alcohol) Blended Films: Mechanical, Thermal and Surface Investigations,” *E-Journal Chem.*, vol. 8, no. 1, pp. 91–96, 2011.

[123] Z. Pan and J. Ding, “Poly(lactide-co-glycolide) porous scaffolds for tissue engineering and regenerative medicine,” *Interface Focus*, vol. 2, no. 3, pp. 366–377, 2012.

[124] H. K. Makadia and S. J. Siegel, “Poly lactic-co-glycolic acid (PLGA) as biodegradable controlled drug delivery carrier,” *Polymers (Basel).*, vol. 3, no. 3, pp. 1377–1397, 2011.

[125] S. Zhou, X. Deng, X. Li, W. Jia, and L. Liu, “Synthesis and characterization of biodegradable low molecular weight aliphatic polyesters and their use in protein-delivery systems,” *J. Appl. Polym. Sci.*, vol. 91, no. 3, pp. 1848–1856, 2004.

[126] Z. Y. Wang, Y. M. Zhao, F. Wang, and J. Wang, “Syntheses of poly(lactic acid-co-glycolic acid) serial biodegradable polymer materials via direct melt polycondensation and their characterization,” *J. Appl. Polym. Sci.*, vol. 99, no. 1, pp. 244–252, 2006.

[127] P. Gentile, V. Chiono, I. Carmagnola, and P. V. Hatton, “An overview of poly(lactic-co-glycolic) acid (PLGA)-based biomaterials for bone tissue engineering,” *Int. J. Mol. Sci.*, vol. 15, no. 3, pp. 3640–3659, 2014.

[128] X. S. Wu and N. Wang, “Synthesis, characterization, biodegradation, and drug delivery application of biodegradable lactic/glycolic acid polymers: Part III. Drug delivery application,” *J. Biomater. Sci. Polym. Ed.*, vol. 12, no. 1, pp. 21–34, 2001.

[129] N. Wang, X. S. Wu, C. Li, and M. F. Feng, “Synthesis, characterization, biodegradation, and drug delivery application of biodegradable lactic/glycolic acid polymers: I. Synthesis and characterization,” *J. Biomater. Sci. Polym. Ed.*, vol. 11, no. 3, pp. 301–318, 2000.

[130] W. B. Liechty, D. R. Kryscio, B. V Slaughter, and N. A. Peppas, “Polymers for drug delivery systems.,” *Annu. Rev. Chem. Biomol. Eng.*, vol. 1, pp. 149–73, 2010.

[131] P. I. P. Park and S. Jonnalagadda, “Predictors of glass transition in the biodegradable polylactide and poly-lactide-co-glycolide polymers,” *J. Appl. Polym. Sci.*, vol. 100, no. 3, pp. 1983–1987, 2006.

[132] S. Lyu, C. Huang, H. Yang, and X. Zhang, “Electrospun fibers as a scaffolding platform for bone tissue repair,” *J. Orthop. Res.*, vol. 31, no. 9, pp. 1382–1389, 2013.

[133] P. V. Kolluru, J. Lipner, W. Liu, Y. Xia, S. Thomopoulos, G. M. Genin, and I. Chasiotis, “Strong and tough mineralized PLGA nanofibers for tendon-to-bone scaffolds,” *Acta Biomater.*, vol. 9, no. 12, pp. 9442–9450, 2013.

[134] W. J. Li, C. T. Laurencin, E. J. Caterson, R. S. Tuan, and F. K. Ko, “Electrospun nanofibrous structure: A novel scaffold for tissue engineering,” *J. Biomed. Mater. Res.*, vol. 60, no. 4, pp. 613–621, 2002.

[135] M. H. Ho, P. Y. Kuo, H. J. Hsieh, T. Y. Hsien, L. T. Hou, J. Y. Lai, and D. M. Wang, “Preparation of porous scaffolds by using freeze-extraction and freeze-gelation methods,” *Biomaterials*, vol. 25, no. 1, pp. 129–138, 2004.

[136] L. Lu, S. J. Peter, M. D. Lyman, H. L. Lai, S. M. Leite, J. A. Tamada, S. Uyama, J. P. Vacanti, Robert Langer, and A. G. Mikos, “In vitro and in vivo degradation of porous poly(DL-lactic-co-glycolic acid) foams,” *Biomaterials*, vol. 21, no. 18, pp. 1837–1845, 2000.

[137] J. S. Park, H. N. Yang, S. Y. Jeon, D. G. Woo, K. Na, and K.-H. Park, “Osteogenic

differentiation of human mesenchymal stem cells using RGD-modified BMP-2 coated microspheres.," *Biomaterials*, vol. 31, no. 24, pp. 6239–48, 2010.

[138] G. T. S. Kirby, L. J. White, C. V. Rahman, H. C. Cox, O. Qutachi, F. R. A. J. Rose, D. W. Hutmacher, K. M. Shakesheff, and M. A. Woodruff, "PLGA-Based Microparticles for the Sustained Release of BMP-2," *Polymers (Basel).*, vol. 3, no. 4, pp. 571–586, 2011.

[139] J. M. Curran, S. Fawcett, L. Hamilton, N. P. Rhodes, C. V Rahman, M. Alexander, K. Shakesheff, and J. a Hunt, "The osteogenic response of mesenchymal stem cells to an injectable PLGA bone regeneration system.," *Biomaterials*, vol. 34, no. 37, pp. 9352–9364, 2013.

[140] C. V Rahman, D. Ben-david, A. Dhillon, G. Kuhn, T. W. A. Gould, R. Müller, F. R. A. J. Rose, K. M. Shakesheff, and E. Livne, "Controlled release of BMP-2 from a sintered polymer scaffold enhances bone repair in a mouse calvarial defect model," *J. Tissue Eng. Regen. Med.*, vol. 8, no. 1, pp. 59–66, 2012.

[141] O. Jeon, M. Krebs, and E. Alsberg, "Controlled and sustained gene delivery from injectable, porous PLGA scaffolds.," *J. Biomed. Mater. Res. A*, vol. 98, no. 1, pp. 72–79, 2011.

[142] O. Qutachi, J. R. Vetsch, D. Gill, H. Cox, D. J. Scurr, S. Hofmann, R. Müller, R. a Quirk, K. M. Shakesheff, and C. V Rahman, "Injectable and porous PLGA microspheres that form highly porous scaffolds at body temperature," *Acta Biomater.*, vol. 10, no. 12, pp. 5090–5098, 2014.

[143] H. Shen, X. Hu, F. Yang, J. Bei, and S. Wang, "An injectable scaffold: rhBMP-2-loaded poly(lactide-co-glycolide)/hydroxyapatite composite microspheres," *Acta Biomater.*, vol. 6, no. 2, pp. 455–465, 2010.

[144] S. D. Nath, S. Son, A. Sadiasa, Y. K. Min, and B. T. Lee, "Preparation and characterization of PLGA microspheres by the electrospraying method for delivering simvastatin for bone regeneration.," *Int. J. Pharm.*, vol. 443, no. 1–2, pp. 87–94, 2013.

[145] N. V. S. Madhav and S. Kala, "Review on microparticulate drug delivery system," *Int. J. PharmTech Res.*, vol. 3, no. 3, pp. 1242–1254, 2011.

[146] K. Andreas, R. Zehbe, M. Kazubek, K. Grzeschik, N. Sternberg, H. Bäumler, H. Schubert, M. Sittinger, and J. Ringe, "Biodegradable insulin-loaded PLGA microspheres fabricated by three different emulsification techniques: investigation for cartilage tissue engineering.," *Acta Biomater.*, vol. 7, no. 4, pp. 1485–1495, 2011.

[147] T. K. Giri, C. Choudhary, A. Alexander, H. Badwaik, and D. K. Tripathi, "Prospects of pharmaceuticals and biopharmaceuticals loaded microparticles prepared by double emulsion technique for controlled delivery," *Saudi Pharm. J.*, vol. 21, no. 2, pp. 125–141, 2013.

[148] H. C. Cox, "A biodegradable system for the tailored delivery of growth factors and its application to bone morphogenetic protein-2 protein 2 delivery for bone repair," The University of Nottingham, 2013.

[149] G. J. S. Dawes, L. E. Fratila-Apachitei, B. S. Necula, I. Apachitei, G. J. Witkamp, and J. Duszczyk, "Release of PLGA-encapsulated dexamethasone from microsphere loaded porous surfaces," *J. Mater. Sci. Mater. Med.*, vol. 21, no. 1, pp. 215–221, 2010.

[150] G. J. S. Dawes, L. E. Fratila-Apachitei, K. Mulia, I. Apachitei, G. J. Witkamp, and J. Duszczyk, "Size effect of PLGA spheres on drug loading efficiency and release

profiles," *J. Mater. Sci. Mater. Med.*, vol. 20, no. 5, pp. 1089–1094, 2009.

[151] A. Paillard-Giteau, V. T. Tran, O. Thomas, X. Garric, J. Coudane, S. Marchal, I. Chourpa, J. P. Benoît, C. N. Montero-Menei, and M. C. Venier-Julienne, "Effect of various additives and polymers on lysozyme release from PLGA microspheres prepared by an s/o/w emulsion technique," *Eur. J. Pharm. Biopharm.*, vol. 75, no. 2, pp. 128–136, 2010.

[152] T.-J. Cho, L. C. Gerstenfeld, and T. A. Einhorn, "Differential Temporal Expression of Members of the Transforming Growth Factor β Superfamily During Murine Fracture Healing," *J. Bone Miner. Res.*, vol. 17, no. 3, pp. 513–520, 2002.

[153] M. T. Poldervaart, H. Wang, J. van der Stok, H. Weinans, S. C. G. Leeuwenburgh, F. C. Oner, W. J. A. Dhert, and J. Alblas, "Sustained release of BMP-2 in bioprinted alginate for osteogenicity in mice and rats," *PLoS One*, vol. 8, no. 8, pp. 1–9, 2013.

[154] A. Dhillon, P. Schneider, G. Kuhn, Y. Reinwald, L. J. White, A. Levchuk, F. R. A. J. Rose, R. Müller, K. M. Shakesheff, and C. V. Rahman, "Analysis of sintered polymer scaffolds using concomitant synchrotron computed tomography and in situ mechanical testing," *J. Mater. Sci. Mater. Med.*, vol. 22, no. 12, pp. 2599–2605, 2011.

[155] T. Jiang, W. I. Abdel-Fattah, and C. T. Laurencin, "In vitro evaluation of chitosan/poly(lactic acid-glycolic acid) sintered microsphere scaffolds for bone tissue engineering," *Biomaterials*, vol. 27, no. 28, pp. 4894–4903, 2006.

[156] A. Jaklenec, E. Wan, M. E. Murray, and E. Mathiowitz, "Novel scaffolds fabricated from protein-loaded microspheres for tissue engineering," *Biomaterials*, vol. 29, no. 2, pp. 185–192, 2008.

[157] A. Jaklenec, A. Hinckfuss, B. Bilgen, D. M. Ciombor, R. Aaron, and E. Mathiowitz, "Sequential release of bioactive IGF-I and TGF-β1 from PLGA microsphere-based scaffolds," *Biomaterials*, vol. 29, no. 10, pp. 1518–1525, 2008.

[158] M. F. Pittenger, A. M. Mackay, S. C. Beck, R. K. Jaiswal, R. Douglas, J. D. Mosca, M. A. Moorman, D. W. Simonetti, S. Craig, and D. R. Marshak, "Multilineage potential of adult human mesenchymal stem cells," *Science.*, vol. 284, pp. 143–146, 1999.

[159] K. Sudo, M. Kanno, K. Miharada, S. Ogawa, T. Hiroyama, K. Saijo, and Y. Nakamura, "Mesenchymal progenitors able to differentiate into osteogenic, chondrogenic, and/or adipogenic cells in vitro are present in most primary fibroblast-like cell populations," *Stem Cells*, vol. 25, pp. 1610–1617, 2007.

[160] A. I. Caplan, "Adult Mesenchymal Stem Cells for Tissue Engineering Versus Regenerative Medicine," *J. Cell. Physiol.*, vol. 213, pp. 341–347, 2007.

[161] N. W. Marion and J. J. Mao, "Mesenchymal Stem Cells and Tissue Engineering," *Methods Enzymol.*, vol. 420, no. 6, pp. 339–361, 2006.

[162] L. Vernon, L. Kaplan, and C.-Y. C. Huang, "Stem cell based bone tissue engineering," in *Bone Regeneration*, 2012, pp. 11–32.

[163] P. Bianco and P. G. Robey, "Stem cells in tissue engineering.," *Nature*, vol. 414, no. 6859, pp. 118–121, 2001.

[164] A. Uccelli, L. Moretta, and V. Pistoia, "Mesenchymal stem cells in health and disease.," *Nat. Rev. Immunol.*, vol. 8, no. 9, pp. 726–736, 2008.

[165] D. Marolt, M. Knezevic, and G. V. Novakovic, "Bone tissue engineering with human stem cells.," *Stem Cell Res. Ther.*, vol. 1, no. 2, pp. 1–10, 2010.

[166] P. Nooeaid, V. Salih, J. P. Beier, and A. R. Boccaccini, “Osteochondral tissue engineering: Scaffolds, stem cells and applications,” *J. Cell. Mol. Med.*, vol. 16, no. 10, pp. 2247–2270, 2012.

[167] S. H. Lee and H. Shin, “Matrices and scaffolds for delivery of bioactive molecules in bone and cartilage tissue engineering,” *Adv. Drug Deliv. Rev.*, vol. 59, no. 4–5, pp. 339–359, 2007.

[168] S. W. Kang, W. G. La, and B. S. Kim, “Open Macroporous Poly(lactic-co-glycolic Acid) Microspheres as an Injectable Scaffold for Cartilage Tissue Engineering.,” *J. Biomater. Sci. Polym. Ed.*, vol. 20, no. 3, pp. 399–409, 2009.

[169] K. K. Taek, J. Y. Jun, S. L. Doo, and T. G. Park, “Gas foamed open porous biodegradable polymeric microspheres,” *Biomaterials*, vol. 27, no. 2, pp. 152–159, 2006.

[170] Y. Yang, N. Bajaj, P. Xu, K. Ohn, M. D. Tsifansky, and Y. Yeo, “Development of highly porous large PLGA microparticles for pulmonary drug delivery,” *Biomaterials*, vol. 30, no. 10, pp. 1947–1953, 2009.

[171] N. Y. Yoo, Y. S. Youn, N. M. Oh, K. T. Oh, D.-K. Lee, K.-H. Cha, Y. T. Oh, and E. S. Lee, “Antioxidant encapsulated porous poly(lactide-co-glycolide) microparticles for developing long acting inhalation system.,” *Colloids Surf. B. Biointerfaces*, vol. 88, no. 1, pp. 419–424, 2011.

[172] A. Mittal, P. Negi, K. Garkhal, S. Verma, and N. Kumar, “Integration of porosity and bio-functionalization to form a 3D scaffold: cell culture studies and in vitro degradation.,” *Biomed. Mater.*, vol. 5, no. 4, pp. 1–16, 2010.

[173] S. E. Bae, J. S. Son, K. Park, and D. K. Han, “Fabrication of covered porous PLGA microspheres using hydrogen peroxide for controlled drug delivery and regenerative medicine.,” *J. Control. Release*, vol. 133, no. 1, pp. 37–43, 2009.

[174] L. Sun, S. Zhou, W. Wang, X. Li, J. Wang, and J. Weng, “Preparation and characterization of porous biodegradable microspheres used for controlled protein delivery,” *Colloids Surfaces A Physicochem. Eng. Asp.*, vol. 345, no. 1–3, pp. 173–181, 2009.

[175] A. R. Ahmed and R. Bodmeier, “Preparation of preformed porous PLGA microparticles and antisense oligonucleotides loading.,” *Eur. J. Pharm. Biopharm.*, vol. 71, no. 2, pp. 264–270, 2009.

[176] H. K. Kim, H. J. Chung, and T. G. Park, “Biodegradable polymeric microspheres with ‘open/closed’ pores for sustained release of human growth hormone.,” *J. Control. Release*, vol. 112, no. 2, pp. 167–174, 2006.

[177] H. J. Chung, H. K. Kim, J. J. Yoon, and T. G. Park, “Heparin immobilized porous PLGA microspheres for angiogenic growth factor delivery,” *Pharm. Res.*, vol. 23, no. 8, pp. 1835–1841, 2006.

[178] X. Luan, M. Skupin, J. Siepmann, and R. Bodmeier, “Key parameters affecting the initial release (burst) and encapsulation efficiency of peptide-containing poly(lactide-co-glycolide) microparticles.,” *Int. J. Pharm.*, vol. 324, no. 2, pp. 168–175, 2006.

[179] A. Mittal, P. Negi, K. Garkhal, S. Verma, and N. Kumar, “Integration of porosity and bio-functionalization to form a 3D scaffold: cell culture studies and in vitro degradation.,” *Biomed. Mater.*, vol. 5, no. 4, pp. 1–16, 2010.

[180] R. T. Tran, E. Naseri, A. Kolasnikov, X. Bai, and J. Yang, “A new generation of

sodium chloride porogen for tissue engineering.," *Biotechnol. Appl. Biochem.*, vol. 58, no. 5, pp. 335–344, 2011.

[181] M. J. O'Neil, *The Merck Index - An Encyclopedia of Chemicals, Drugs, and Biologicals*. Cambridge: Royal Society of Chemistry, 2013.

[182] Y. Y. Yang, H. H. Chia, and T. S. Chung, "Effect of preparation temperature on the characteristics and release profiles of PLGA microspheres containing protein fabricated by double-emulsion solvent extraction/evaporation method," *J. Control. Release*, vol. 69, no. 1, pp. 81–96, 2000.

[183] R. C. Mehta, R. Jeyanthi, S. Calls, B. C. Thanoo, K. W. Burton, and P. P. DeLuca, "Biodegradable microspheres as depot system for patenteral delivery of peptide drugs," *J. Control. Release*, vol. 29, no. 3, pp. 375–384, 1994.

[184] M. Nasr, G. A. S. Awad, S. Mansour, A. Al Shamy, and N. D. Mortada, "Hydrophilic versus hydrophobic porogens for engineering of poly(lactide-co-glycolide) microparticles containing risedronate sodium.," *Pharm. Dev. Technol.*, vol. 18, no. 5, pp. 1078–1088, 2013.

[185] M. Nasr, G. A. S. Awad, S. Mansour, I. Taha, A. Al Shamy, and N. D. Mortada, "Different modalities of NaCl osmogen in biodegradable microspheres for bone deposition of risedronate sodium by alveolar targeting.," *Eur. J. Pharm. Biopharm.*, vol. 79, no. 3, pp. 601–611, 2011.

[186] Y. Cai, Y. Chen, X. Hong, Z. Liu, and W. Yuan, "Porous microsphere and its applications," *Int. J. Nanomedicine*, vol. 8, pp. 1111–1120, 2013.

[187] M. Rumyantsev, "Influences of co-solvent on hydrogen bond reorganization in ternary poly(vinyl alcohol) solutions," *Eur. Polym. J.*, vol. 49, no. 8, pp. 2257–2266, 2013.

[188] H. Takeuchi and M. Kobayashi, "Influence of the degrees of hydrolyzation and polymerization of poly (vinylalcohol) on the preparation and properties of poly (DL-lactide-co-glycolide) nanoparticle," *Int. J. Pharm.*, vol. 149, pp. 43–49, 1997.

[189] Y. Y. Yang, T. S. Chung, and N. P. Ng, "Morphology, drug distribution, and in vitro release profiles of biodegradable polymeric microspheres containing protein fabricated by double-emulsion solvent extraction/evaporation method.," *Biomaterials*, vol. 22, no. 3, pp. 231–41, 2001.

[190] H. Zhao, J. Gagnon, and U. O. Häfeli, "Process and formulation variables in the preparation of injectable and biodegradable magnetic microspheres," *Biomagn. Res. Technol.*, vol. 5, p. 2, 2007.

[191] N. Zafar, A. Bitar, J. P. Valour, H. Fessi, and A. Elaissari, "Elaboration of ammonio methacrylate copolymer based spongy cationic particles via double emulsion solvent evaporation process," *Mater. Sci. Eng. C*, vol. 61, pp. 85–96, 2016.

[192] O. Qutachi, K. M. Shakesheff, and L. D. K. Buttery, "Delivery of definable number of drug or growth factor loaded poly(dl-lactic acid-co-glycolic acid) microparticles within human embryonic stem cell derived aggregates," *J. Control. Release*, vol. 168, no. 1, pp. 18–27, 2013.

[193] R. Edelman, R. G. Russell, G. Losonsky, B. D. Tall, C. O. Tacket, M. M. Levine, and D. H. Lewis, "Immunization of rabbits with enterotoxigenic E.coli colonization factor antigen (CFA/I) encapsulated in biodegradable microspheres of poly (lactide-co-glycolide)," *Vaccine*, vol. 11, no. 2, pp. 155–158, 1993.

[194] E. Gavini, P. Chetoni, M. Cossu, M. G. Alvarez, M. F. Saettone, and P. Giunchedi,

"PLGA microspheres for the ocular delivery of a peptide drug, vancomycin using emulsification/spray-drying as the preparation method: in vitro/in vivo studies.," *Eur. J. Pharm. Biopharm.*, vol. 57, no. 2, pp. 207–212, 2004.

[195] T. Jiang, Y. Khan, L. S. Nair, W. I. Abdel-Fattah, and C. T. Laurencin, "Functionalization of chitosan/poly(lactic acid-glycolic acid) sintered microsphere scaffolds via surface heparinization for bone tissue engineering," *J. Biomed. Mater. Res. A*, vol. 93, no. 3, pp. 1193–1208, 2010.

[196] A. Rafati, A. Boussahel, K. M. Shakesheff, A. G. Shard, C. J. Roberts, X. Chen, D. J. Scurr, S. Rigby-Singleton, P. Whiteside, M. R. Alexander, and M. C. Davies, "Chemical and spatial analysis of protein loaded PLGA microspheres for drug delivery applications," *J. Control. Release*, vol. 162, no. 2, pp. 321–329, 2012.

[197] Y. Boukari, D. J. Scurr, O. Qutachi, A. P. Morris, S. P. Doughty, C. V Rahman, and N. Billa, "Physicomechanical properties of sintered scaffolds formed from porous and protein-loaded poly(DL-lactic-co-glycolic acid) microspheres for potential use in bone tissue engineering," *J. Biomater. Sci. Polym. Ed.*, vol. 26, no. 12, pp. 796–811, 2015.

[198] P. Kocbek, S. Baumgartner, and J. Kristl, "Preparation and evaluation of nanosuspensions for enhancing the dissolution of poorly soluble drugs," *Int. J. Pharm.*, vol. 312, no. 1–2, pp. 179–186, 2006.

[199] H. Yuan, L. L. Wang, Y. Z. Du, J. You, F. Q. Hu, and S. Zeng, "Preparation and characteristics of nanostructured lipid carriers for control-releasing progesterone by melt-emulsification," *Colloids Surf. B. Biointerfaces*, vol. 60, no. 2, pp. 174–179, 2007.

[200] G. Mittal, D. K. Sahana, V. Bhardwaj, and M. N. V Ravi Kumar, "Estradiol loaded PLGA nanoparticles for oral administration: effect of polymer molecular weight and copolymer composition on release behavior in vitro and in vivo," *J. Control. Release*, vol. 119, no. 1, pp. 77–85, 2007.

[201] V. Karageorgiou and D. Kaplan, "Porosity of 3D biomaterial scaffolds and osteogenesis," *Biomaterials*, vol. 26, no. 27, pp. 5474–5491, 2005.

[202] Y. Yeo and K. Park, "Control of encapsulation efficiency and initial burst in polymeric microparticle systems," *Arch. Pharm. Res.*, vol. 27, no. 1, pp. 1–12, 2004.

[203] E. Misch, Z. Qu, and M. W. Bidez, "Mechanical properties of trabecular bone in the human mandible: implications for dental implant treatment planning and surgical placement," *J. Oral Maxillofac. Surg.*, vol. 57, pp. 700–706, 1999.

[204] M. Van De Weert, R. Van 't Hof, J. Van Der Weerd, R. M. Heeren, G. Posthuma, W. E. Hennink, and D. J. Crommelin, "Lysozyme distribution and conformation in a biodegradable polymer matrix as determined by FTIR techniques," *J. Control. Release*, vol. 68, no. 1, pp. 31–40, 2000.

[205] M. Igartua, R. Hernandez, A. Esquisabel, A. Gascon, M. Calvo, and J. Pedraz, "Influence of formulation variables on the in-vitro release of albumin from biodegradable microparticulate systems," *J. Microencapsul. Micro Nano Carriers*, vol. 14, no. 3, pp. 349–356, 1997.

[206] A. L. Pérez, R. Spears, J. L. Gutmann, and L. A. Opperman, "Osteoblasts and MG-63 osteosarcoma cells behave differently when in contact with ProRoot MTA and White MTA.," *Int. Endod. J.*, vol. 36, no. 8, pp. 564–570, 2003.

[207] W. S. Koegler and L. G. Griffith, "Osteoblast response to PLGA tissue engineering

scaffolds with PEO modified surface chemistries and demonstration of patterned cell response.," *Biomaterials*, vol. 25, no. 14, pp. 2819–2830, 2004.

[208] M. J. Santander-Ortega, A. B. Jódar-Reyes, N. Csaba, D. Bastos-González, and J. L. Ortega-Vinuesa, "Colloidal stability of pluronic F68-coated PLGA nanoparticles: a variety of stabilisation mechanisms.," *J. Colloid Interface Sci.*, vol. 302, no. 2, pp. 522–529, 2006.

[209] D. L. Sellers, T. H. Kim, C. W. Mount, S. H. Pun, and P. J. Horner, "Poly(lactic-co-glycolic) acid microspheres encapsulated in Pluronic F-127 prolong hirudin delivery and improve functional recovery from a demyelination lesion.," *Biomaterials*, vol. 35, no. 31, pp. 8895–8902, 2014.

[210] J. H. Lee, G. Khang, J. W. Lee, and H. B. Lee, "Interaction of Different Types of Cells on Polymer Surfaces with Wettability Gradient," *J. Colloid Interface Sci.*, vol. 205, pp. 323–330, 1998.

[211] M. Thomas, A. Arora, and D. S. Katti, "Surface hydrophilicity of PLGA fibers governs in vitro mineralization and osteogenic differentiation.," *Mater. Sci. Eng. C. Mater. Biol. Appl.*, vol. 45, pp. 320–332, 2014.

[212] M. D. Darrabie, W. F. Kendall, and E. C. Opara, "Characteristics of Poly-L-Ornithine-coated alginate microcapsules.," *Biomaterials*, vol. 26, no. 34, pp. 6846–6852, 2005.

[213] S.-A. Abbah, J. Liu, R. W. M. Lam, J. C. H. Goh, and H.-K. Wong, "In vivo bioactivity of rhBMP-2 delivered with novel polyelectrolyte complexation shells assembled on an alginate microbead core template.," *J. Control. Release*, vol. 162, no. 2, pp. 364–372, 2012.

[214] L. Liu, Y. J. Won, P. H. Cooke, D. R. Coffin, M. L. Fishman, K. B. Hicks, and P. X. Ma, "Pectin/poly(lactide-co-glycolide) composite matrices for biomedical applications," *Biomaterials*, vol. 25, no. 16, pp. 3201–3210, 2004.

[215] J. V. Araujo, N. Davidenko, M. Danner, R. E. Cameron, and S. M. Best, "Novel porous scaffolds of pH responsive chitosan/carrageenan-based polyelectrolyte complexes for tissue engineering," *J. Biomed. Mater. Res. Part A*, vol. 102, no. 12, pp. 4415–4426, 2014.

[216] Y. Hou, J. Hu, H. Park, and M. Lee, "Chitosan based nanoparticles as a sustained protein release carrier for tissue engineering applications," *J Biomed Mater Res Part A*, vol. 100, no. 4, pp. 939–947, 2012.

[217] A. Di Martino, M. Sittinger, and M. V. Risbud, "Chitosan: A versatile biopolymer for orthopaedic tissue-engineering," *Biomaterials*, vol. 26, no. 30, pp. 5983–5990, 2005.

[218] W. Zeng, J. Huang, X. Hu, W. Xiao, M. Rong, Z. Yuan, and Z. Luo, "Ionically cross-linked chitosan microspheres for controlled release of bioactive nerve growth factor," *Int. J. Pharm.*, vol. 421, no. 2, pp. 283–290, 2011.

[219] L. Qian and H. Zhang, "One-step synthesis of protein-encapsulated microspheres in a porous scaffold by freeze-drying double emulsions and tuneable protein release," *Chem. Commun.*, vol. 49, no. 78, pp. 8833–8835, 2013.

[220] K. Song, Y. Liu, H. M. Macedo, L. Jiang, C. Li, G. Mei, and T. Liu, "Fabrication and evaluation of a sustained-release chitosan-based scaffold embedded with PLGA microspheres," *Mater. Sci. Eng. C*, vol. 33, no. 3, pp. 1506–1513, 2013.

[221] Y. Fu, L. Du, Q. Wang, W. Liao, Y. Jin, A. Dong, C. Chen, and Z. Li, "In vitro sustained release of recombinant human bone morphogenetic protein-2 microspheres

embedded in thermosensitive hydrogels," *Pharmazie*, vol. 67, no. 4, pp. 299–303, 2012.

[222] X. Hu, J. Zhou, N. Zhang, H. Tan, and C. Gao, "Preparation and properties of an injectable scaffold of poly(lactic-co-glycolic acid) microparticles/chitosan hydrogel," *J. Mech. Behav. Biomed. Mater.*, vol. 1, no. 4, pp. 352–359, 2008.

[223] L. Casettari, E. Castagnino, S. Stolnik, A. Lewis, S. M. Howdle, and L. Illum, "Surface characterisation of bioadhesive PLGA/chitosan microparticles produced by supercritical fluid technology," *Pharm. Res.*, vol. 28, no. 7, pp. 1668–1682, 2011.

[224] F. Han, F. Zhou, X. Yang, J. Zhao, Y. Zhao, and X. Yuan, "Facile Preparation of PLGA Microspheres With Diverse Internal Structure by Modified Double-Emulsion Method for Controlled Release," *Polym. Eng. Sci.*, vol. 55, no. 4, pp. 896–906, 2015.

[225] C. M. Pandey, A. Sharma, G. Sumana, I. Tiwari, and B. D. Malhotra, "Cationic poly(lactic-co-glycolic acid) iron oxide microspheres for nucleic acid detection," *Nanoscale*, vol. 5, no. 9, pp. 3800–3807, 2013.

[226] D. H. Choi, R. Subbiah, I. H. Kim, D. K. Han, and K. Park, "Dual growth factor delivery using biocompatible core-shell microcapsules for angiogenesis," *Small*, vol. 9, no. 20, pp. 3468–3476, 2013.

[227] S. S. Chakravarthi and D. H. Robinson, "Enhanced cellular association of paclitaxel delivered in chitosan-PLGA particles," *Int. J. Pharm.*, vol. 409, no. 1–2, pp. 111–120, 2011.

[228] Y. Yu, J. Chen, R. Chen, L. Cao, W. Tang, D. Lin, J. Wang, and C. Liu, "Enhancement of VEGF-Mediated Angiogenesis by 2- *N* ,6- *O* -Sulfated Chitosan-Coated Hierarchical PLGA Scaffolds," *ACS Appl. Mater. Interfaces*, vol. 7, no. 18, pp. 9982–9990, 2015.

[229] C. Tao, J. Huang, Y. Lu, H. Zou, X. He, Y. Chen, and Y. Zhong, "Development and characterization of GRGDSPC-modified poly(lactide-co-glycolide acid) porous microspheres incorporated with protein-loaded chitosan microspheres for bone tissue engineering," *Colloids Surfaces B Biointerfaces*, vol. 122, pp. 439–446, 2014.

[230] C. M. Mahoney, J. Yu, A. Fahey, and J. A. Gardella, "SIMS depth profiling of polymer blends with protein based drugs," *Appl. Surf. Sci.*, vol. 252, no. 19, pp. 6609–6614, 2006.

[231] P. K. Sharma and S. R. Bhatia, "Effect of anti-inflammatories on Pluronic F127: micellar assembly, gelation and partitioning.," *Int. J. Pharm.*, vol. 278, no. 2, pp. 361–377, 2004.

[232] J. Duan, J. Du, and Y. Zheng, "Synthesis and Characterization of a Novel Biodegradable Polymer Poly (lactic acid – glycolic acid-4-hydroxyproline)," *J. Appl. Polym. Sci.*, vol. 103, pp. 3585–3590, 2006.

[233] G. Ratzinger, U. Länger, L. Neutsch, F. Pittner, M. Wirth, and F. Gabor, "Surface modification of PLGA particles: the interplay between stabilizer, ligand size, and hydrophobic interactions.," *Langmuir*, vol. 26, no. 3, pp. 1855–1859, 2010.

[234] Q. Gao, Q. Liang, F. Yu, J. Xu, Q. Zhao, and B. Sun, "Synthesis and characterization of novel amphiphilic copolymer stearic acid-coupled F127 nanoparticles for nano-technology based drug delivery system.," *Colloids Surf. B. Biointerfaces*, vol. 88, no. 2, pp. 741–748, 2011.

[235] N. B. Shelke, A. P. Rokhade, and T. M. Aminabhavi, "Preparation and Evaluation of

Novel Blend Microspheres of Poly (lactic- co -glycolic) acid and Pluronic F68 / 127 for Controlled Release of Repaglinide," *J. Appl. Polym. Sci.*, vol. 116, pp. 366–372, 2010.

[236] A. Seth and D. S. Katti, "A one-step electrospray-based technique for modulating morphology and surface properties of poly (lactide- co -glycolide) microparticles using Pluronics ®," *Int. J. Nanomedicine*, vol. 7, pp. 5129–5136, 2012.

[237] C.-J. Chang, S. Hsu, F. Lin, H. Chang, and C.-S. Chang, "Low-intensity-ultrasound-accelerated nerve regeneration using cell-seeded poly(D,L-lactic acid-co-glycolic acid) conduits: Anin vivo andin vitro study," *J. Biomed. Mater. Res. Part B Appl. Biomater.*, vol. 75B, no. 1, pp. 99–107, 2005.

[238] D. Kweon and S. Lim, "Preparation and Characteristics of a Water-Soluble Chitosan – Heparin Complex," *J. Appl. Polym. Sci.*, vol. 87, pp. 1784–1789, 2003.

[239] C. Kelco, *Genu Carrageenan Book*. 2001.

[240] R. K. Mishra, A. K. Banthia, and A. B. A. Majeed, "Pectin based formulations for biomedical applications: A review," *Asian J. Pharm. Clin. Res.*, vol. 5, no. 4, pp. 1–7, 2012.

[241] F. Ganji and M. J. Abdekhodaie, "Chitosan-g-PLGA copolymer as a thermosensitive membrane," *Carbohydr. Polym.*, vol. 80, no. 3, pp. 740–746, 2010.

[242] V. Boeris, B. Farruggia, and G. Pico, "Chitosan-bovine serum albumin complex formation: A model to design an enzyme isolation method by polyelectrolyte precipitation," *J. Chromatogr. B-Analytical Technol. Biomed. Life Sci.*, vol. 878, no. 19, pp. 1543–1548, 2010.

[243] C. H. Zheng and W. Liang, "A one-step modified method to reduce the burst initial release from PLGA microspheres," *Drug Deliv.*, vol. 17, no. 2, pp. 77–82, 2010.

[244] M. L. Manca, G. Loy, M. Zaru, A. M. Fadda, and S. G. Antimisiaris, "Release of rifampicin from chitosan, PLGA and chitosan-coated PLGA microparticles," *Colloids Surf. B. Biointerfaces*, vol. 67, no. 2, pp. 166–170, 2008.

[245] X. Li, X. Deng, and Z. Huang, "In Vitro Protein Release and Degradation of Poly-dl-lactide-poly(ethylene glycol) Microspheres with Entrapped Human Serum Albumin: Quantitative Evaluation of the Factors Involved in Protein Release Phases," *Pharm. Res.*, vol. 18, no. 1, pp. 117–124, 2001.

[246] M. H. Amer, L. J. White, and K. M. Shakesheff, "The effect of injection using narrow-bore needles on mammalian cells: Administration and formulation considerations for cell therapies," *J. Pharm. Pharmacol.*, vol. 67, no. 5, pp. 640–650, 2015.

[247] S. J. Lee, J. S. Choi, K. S. Park, G. Khang, Y. M. Lee, and H. B. Lee, "Response of MG63 osteoblast-like cells onto polycarbonate membrane surfaces with different micropore sizes.," *Biomaterials*, vol. 25, no. 19, pp. 4699–4707, 2004.

[248] L. Wang, C. Li, Y. Chen, S. Dong, X. Chen, and Y. Zhou, "Poly(lactic-co-glycolic) acid/nanohydroxyapatite scaffold containing chitosan microspheres with adrenomedullin delivery for modulation activity of osteoblasts and vascular endothelial cells," *Biomed Res. Int.*, vol. 2013, 2013.

[249] C. Vitale-Brovarone, E. Verné, L. Robiglio, P. Appendino, F. Bassi, G. Martinasso, G. Muzio, and R. Canuto, "Development of glass-ceramic scaffolds for bone tissue engineering: characterisation, proliferation of human osteoblasts and nodule formation.," *Acta Biomater.*, vol. 3, no. 2, pp. 199–208, 2007.

[250] W.-H. Lee, C.-Y. Loo, A. V. Zavgorodniy, M. Ghadiri, and R. Rohanizadeh, “A novel approach to enhance protein adsorption and cell proliferation on hydroxyapatite: citric acid treatment,” *RSC Adv.*, vol. 3, no. 12, pp. 4040–4051, 2013.

[251] M. Bächle and R. J. Kohal, “A systematic review of the influence of different titanium surfaces on proliferation, differentiation and protein synthesis of osteoblast-like MG63 cells,” *Clin. Oral Implants Res.*, vol. 15, no. 6, pp. 683–692, 2004.

[252] T. W. A. Gould, J. P. Birchall, A. S. Mallick, T. Alliston, L. R. Lustig, K. M. Shakesheff, and C. V Rahman, “Development of a porous poly(DL-lactic acid-co-glycolic acid)-based scaffold for mastoid air-cell regeneration.,” *Laryngoscope*, vol. 123, no. 12, pp. 3156–3161, 2013.

[253] Human Tissue Authority, “Research FAQs.” [Online]. Available: https://www.hta.gov.uk/faqs/research-faqs. [Accessed: 30-May-2016].

[254] J. R. Azevedo, R. H. Sizilio, M. B. Brito, A. M. B. Costa, M. R. Serafini, A. A. S. Araújo, M. R. V Santos, A. A. M. Lira, and R. S. Nunes, “Physical and chemical characterization insulin-loaded chitosan-TPP nanoparticles,” *J. Therm. Anal. Calorim.*, vol. 106, no. 3, pp. 685–689, 2011.

[255] S. C. Balmert, A. C. Zmolek, A. J. Glowacki, T. D. Knab, S. N. Rothstein, J. M. Wokpetah, M. V. Fedorchak, and S. R. Little, “Positive charge of ‘sticky’ peptides and proteins impedes release from negatively charged PLGA matrices,” *J. Mater. Chem. B*, vol. 3, no. 23, pp. 4723–4734, 2015.

[256] I. F. Amaral, M. Lamghari, S. R. Sousa, P. Sampaio, and M. A. Barbosa, “Rat bone marrow stromal cell osteogenic differentiation and fibronectin adsorption on chitosan membranes: the effect of the degree of acetylation.,” *J. Biomed. Mater. Res. A*, vol. 75, no. 2, pp. 387–397, 2005.

[257] Y. C. Wu, S. Y. Shaw, H. R. Lin, T. M. Lee, and C. Y. Yang, “Bone tissue engineering evaluation based on rat calvaria stromal cells cultured on modified PLGA scaffolds,” *Biomaterials*, vol. 27, no. 6, pp. 896–904, 2006.

[258] B. Jung and P. Theato, “Chitosan-based biomaterials for tissue repair and regeneration,” in *Advances in Polymer Science*, vol. 244, no. May 2012, 2012, pp. 1–34.

[259] L. F. Bonewald, S. E. Harris, J. Rosser, M. R. Dallas, S. L. Dallas, N. P. Camacho, B. Boyan, and A. Boskey, “Von kossa staining alone is not sufficient to confirm that mineralization in vitro represents bone formation,” *Calcif. Tissue Int.*, vol. 72, no. 5, pp. 537–547, 2003.

[260] G. S. Stein, J. B. Lian, and T. A. Owen, “Relationship of cell growth to the regulation of tissue-specific gene expression during oseoblast differentiation,” *FASEB journal*, vol. 4, no. 13. pp. 3111–3123, 1990.

[261] L. H. Chuah, N. Billa, C. J. Roberts, J. C. Burley, and S. Manickam, “Curcumin-containing chitosan nanoparticles as a potential mucoadhesive delivery system to the colon,” *Pharm. Dev. Technol.*, vol. 18, no. 3, pp. 591–599, 2011.

[262] S. Verrier, S. Pallu, R. Bareille, A. Jonczyk, J. Meyer, M. Dard, and J. Amedee, “Function of linear and cyclic RGD-containing peptides in osteoprogenitor cells adhesion process,” *Biomaterials*, vol. 23, no. 2, pp. 585–596, 2002.

[263] V. Viateau, D. Logeart-Avramoglou, G. Guillemin, and H. Petite, “Animal models for bone tissue engineering purposes,” in *Models for Biomedical Research*, M. Conn, Ed.

Springer, 2008, pp. 725–736.

[264] M. A. K. Liebschner, “Biomechanical considerations of animal models used in tissue engineering of bone,” *Biomaterials*, vol. 25, no. 9, pp. 1697–1714, 2004.